

**SYNTHESIS OF COPPER BASED METAL
ORGANIC FRAMEWORK FOR SEPARATION OF
CO₂/H₂ AT HIGH PRESSURE**

**A Thesis Submitted to
the Graduate School of Engineering and Sciences of
İzmir Institute of Technology
in Partial Fulfillment of the Requirements for the Degree of**

MASTER OF SCIENCE

in Chemical Engineering

**by
Ahmet Uğur ÇİÇEK**

**December 2014
İZMİR**

We approve the thesis of **Ahmet Uğur ÇİÇEK**

Examining Committee Members:

Prof. Dr. Fehime ÇAKICIOĞLU ÖZKAN

Department of Chemical Engineering, İzmir Institute of Technology

Prof. Dr. Semra ÜLKÜ

Department of Chemical Engineering, İzmir Institute of Technology

Assist. Prof. Dr. Güler NARİN

Department of Chemical Engineering, Uşak University

19 December 2014

Prof. Dr. Fehime ÇAKICIOĞLU ÖZKAN

Supervisor, Department of Chemical
Engineering
İzmir Institute of Technology

Prof. Dr. Fehime ÇAKICIOĞLU ÖZKAN

Head of the Department of Chemical
Engineering

Prof. Dr. R. Tuğrul SENGER

Dean of the Graduate School of
Engineering and Sciences

ACKNOWLEDGMENTS

Foremost, I would like to express my appreciation to my supervisor Prof. Dr. Fehime AKICIOĐLU ZKAN for the continuous support and guidance through my M.Sc. study. Furthermore, I would like to thank to Prof. Dr. Őerife Őeref HELVACI for her academic support during the project.

I want to thank my friend TuĐba UGRANLI for her unflagging support in this endeavor. My gratitude also goes to my labmate and best friend zgn DELİİSMAİL for his help, support, and friendship. Additionally, I am so indebted to my dear friends Elif GNGRMŐŐ, İmran ZER, and Burak Muhammet KAMA for their friendships. Thanks to Center for Materials Research personnel and Chemical Engineering Department personnel for their helps during the analyses of my samples.

At last but most important special thanks go to my family. I am also so grateful and appreciate to my family for their infinite support, love, and encouragement.

This thesis was supported financially by TUBİTAK (112M294) and İzmir Institute of Technology Scientific Research Project (2014İYTE09).

ABSTRACT

SYNTHESIS OF COPPER BASED METAL ORGANIC FRAMEWORK FOR SEPARATION OF CO₂/H₂ AT HIGH PRESSURE

In this study, synthesis of Copper based metal organic framework (CuTPA) was achieved. Terephthalic acids were used as an organic linkers supplied from PETKİM A.Ş. Synthesis procedure was carried out in three steps; crystallization, purification and activation with different parameters. Crystallization time and temperature, purification method and solvent type, thermal activation rate are studied. MOFs were characterized by using SEM (Scanning Electron Microscopy), Fourier Transformer Infrared (FTIR), Thermal Gravimetric Analyzer (TGA), X-ray Diffractometer (XRD), and Volumetric Adsorption Instrument (ASAP 2010). The CuTPA with the highest specific surface area ($S_{Lang}=776 \text{ m}^2/\text{g}$) was synthesized after purification with methanol by soxhlet method in a schott bottle for 24 hours at crystallization temperature of 110 °C.

Copper based MOF synthesized ($S_{Lang}=776 \text{ m}^2/\text{g}$) and Commercial NaX zeolite ($S_{Lang}= 1359 \text{ m}^2/\text{g}$) were packed in the column. Dynamic adsorption behavior of adsorbents was also studied; breakthrough of CO₂/H₂ and gases from the packed bed were carried out under total molar flow rate of 10, 20, and 30 mL/min gas mixture at 1, 5, and, 10 bars. It was conclude that the adsorption data results obtained from our system is reliable. As a result of breakthrough experiment both adsorbents (CuTPA and 13X zeolite) did not adsorbed H₂. The break points are increased with increasing pressure and decreasing total flow rate. The amount to be adsorbed by the adsorbent in the column is increased indicating that the adsorption mechanism, controlling mechanism is changed with decreasing total flow rate.

ÖZET

YÜKSEK BASINÇTA CO₂/H₂ AYIRIMI İÇİN BAKIR BAZLI METAL ORGANİK AĞ YAPISININ SENTEZLENMEZİ

Bu çalışmada, bakır temelli mikrogözenekli metal ağ yapılarının sentezi gerçekleştirilmiştir. PETKİM A.Ş. ve Aldrich'ten tedarik edilen tereftalik asitler organik bağlayıcı olarak kullanılmıştır. Sentez prosedürü üç basamak halinde; kristalizasyon, saflaştırma ve aktivasyon basamaklarında farklı parametrelerin incelenmesiyle yürütülmüştür. Kristalizasyon basamağında zaman ve sıcaklık, saflaştırma basamağında yöntem ve çözücü, aktivasyon basamağında ise sıcaklık artış hızları parametrik olarak çalışılmıştır. Adsorpsiyon basamağında önce; taramalı elektron mikroskobu, X ışını kırınımı ve volumetrik adsorpsiyon cihazı ile sentezlenen ağ yapılarının karakterizasyonu yapılmıştır. En yüksek yüzey alanı, 776 m²/g (S_{Lang}), 110 °C de 24 saat boyunca shot şişesinde gerçekleştirilen reaksiyon ve metanol ile soklet yöntemi sonucunda saflaştırılan örnekte elde edilmiştir.

Kolon sentezlenen metal organik ağ yapıları veya ticari olarak kullanılan NaX zeolitleri (13X) ile doldurulmuştur. Adsorbentlerin dinamik adsorpsiyon davranışları da bu çalışma kapsamında incelenmiştir. Adsorpsiyon çalışmaları toplam 10, 20 ve 30 mL/dk olacak şekilde ikili (CO₂/H₂) gaz karışımının 1, 5 ve 10 bar basınç ve sabit sıcaklıktaki dolgulu kolana gönderilmesiyle gerçekleştirilmiştir. Sonuç olarak her iki adsorbentine H₂ tutmadığı görülmüştür. Gazların salınım yapma zamanları basınç artışıyla ve gaz akış hızı azalmasıyla artmıştır. Elde edilen salınım eğrileri ve ilgili denklemler ile yüzeye tutunan miktarlar hesaplanmıştır. Kolonda adsorbent tarafından adsorplanan miktarın akış hızının azalmasıyla artması, adsorpsiyon control mekanizmasının değiştiğini göstermektedir.

TABLE OF CONTENTS

LIST OF FIGURES	viii
LIST OF TABLES	xii
CHAPTER 1. INTRODUCTION	1
CHAPTER 2. ADSORBENTS	3
2.1. NaX Zeolite (13X)	3
2.2. Metal Organic Frameworks (MOFs)	4
2.2.1. Copper Based Metal Organic Frameworks (Cu TPAs)	6
2.2.1.1. Hydro/Solvothermal Synthesis Method	7
2.2.1.2. Slow Evaporation Synthesis Method.....	8
2.2.1.3. Microwave Assisted Synthesis Method.....	9
2.2.1.4. Electrochemical Synthesis Method	9
2.2.1.5. Mechanochemical Synthesis Method	10
2.2.1.6. Sonochemical Synthesis Method.....	10
2.2.2. Applications of MOFs.....	10
2.2.2.1. Gas Storage in MOFs	11
2.2.2.2. MOFs in Catalysis	11
2.2.2.3. Magnetic Properties of MOFs	12
2.2.2.4. MOFs in Sensors	12
2.2.2.5. MOFs in Drug Delivery.....	12
CHAPTER 3. GAS SEPARATION VIA ADSORPTION	14
3.1. Adsorption.....	14
3.1.1. Physical Adsorption	16
3.1.2. Chemical Adsorption	16
3.2. Adsorption in Porous Solids	17
3.2.1. Adsorption in Micropores	17
3.2.2. Adsorption in Mesopores	17
3.3. Pore Size and Surface Area Calculations.....	18

3.4. Model Equations for Gas Adsorption	19
3.5. Cyclic Adsorptive Separation Processes.....	21
3.5.1. Pressure/Vacuum Swing Adsorption	22
3.5.2. Temperature Swing Adsorption	24
CHAPTER 4. EXPERIMENTAL STUDIES	25
4.1. Materials	25
4.2. Synthesis of CuTPA.....	25
4.2.1. Crystallization	25
4.2.2. Purification.....	27
4.2.3. Activation.....	28
4.3. Characterization of Adsorbents.....	28
4.4. Adsorption Studies.....	28
CHAPTER 5. RESULTS AND DISCUSSIONS	32
5.1. CuTPA Synthesis	32
5.1.1. Crystallization Step.....	32
5.1.2. Purification Step.....	41
5.1.3. Activation Step.....	47
5.2. High Pressure Adsorption Studies	53
CHAPTER 6. CONCLUSIONS.....	68
REFERENCES	69

LIST OF FIGURES

<u>Figure</u>	<u>Page</u>
Figure 2.1. Structure of zeolite 13X	4
Figure 2.2. 1D, 2D, and 3D structures of MOFs which is constructed by molecular building units.....	5
Figure 2.3. The CuTPA framework	5
Figure 2.4. Examples of SBUs from carboxylate MOFs; O, red: N, green: C: black	6
Figure 2.5. (a) Synthesis methods commonly used for MOF production (b) percentage of MOF synthesized with different methods	7
Figure 2.6. Structure of copper terephthalate in the (001) plane to form porous structure which responsible for high surface area.....	8
Figure 3.1. Basic concept of adsorption phenomena	14
Figure 3.2. Pore geometries and schematic pores classification of zeolite; (a) closed pores, (b, f) pores open only at one end, (c, d, g) open pores, (e) open at two ends	15
Figure 3.3. General design and demonstration of PSA and TSA process	22
Figure 4.1. Synthesis procedure of CuTPA	26
Figure 4.2. Crystallization reactors: (a) Schott bottle (F), (b) Autoclave (A), (c) Parr (P).....	27
Figure 4.3. Soxhlet extraction method used in the purification step	27
Figure 4.4. Gas adsorption system; VTP1, VTP2, and VTP3: three way valves, MFC1 and MFC2: mass flow controllers, M1: manifold, F1: filter, BPR: back pressure regulator	29
Figure 5.1. SEM images of the CuTPAs obtained from schott (a) F48-MSx-R50, Parr (b) P48-MSx-R50 reactor	34
Figure 5.2. FTIR spectra of the synthesized CuTPAs in different reactors.....	34
Figure 5.3. TGA termographs for CuTPAs obtained from Schott bottle and Parr reactor.....	35
Figure 5.4. X-ray diffraction scans of synthesized CuTPAs with two different reactor.....	36
Figure 5.5. Synthesized CuTPAs with a difference in crystallization time in Schott bottle (F): (a) F36-MSx-R50, (b) F48-MSx-R50.....	36

Figure 5.6. FTIR spectra for synthesized under different conditions (36 h and 48 h)....	37
Figure 5.7. Thermal behavior of synthesized CuTPAs for 36 h and 48 h	38
Figure 5.8. XRD pattern of CuTPAs	38
Figure 5.9. SEM images of the CuTPAs synthesized under different crystallization temperature; (a) F36-MS _x -R50 (110°C), (b) F36-MS _x -R50 (50°C)	39
Figure 5.10. Infrared spectra of CuTPAs produced at 50 °C (F36-MS _x -R50 (50°C)) and 110 °C (F36-MS _x -R50 (110°C))	40
Figure 5.11. Change in thermal stability of the CuTPAs produced at 50 °C (F36-MS _x -R50 (50°C)) and 110 °C (F36-MS _x -R50 (110°C))	40
Figure 5.12. X-ray diffractometer pattern of synthesized CuTPAs under different crystallization temperatures	41
Figure 5.13. SEM micrographs of CuTPAs washed with DMF (F36-DS _x -R225) or MeOH (F36-MS _x -R225).....	42
Figure 5.14. FTIR spectra for the CuTPA samples washed with MeOH (F36-MS _x -R225) and DMF (F36-DS _x -R225).....	42
Figure 5.15. TGA curves for CuTPAs washed with different solvent	43
Figure 5.16. XRD pattern of CuTPAs synthesized.....	44
Figure 5.17. SEM micrographs of CuTPAs washed with MeOH under stirring (F36-MSt-R225) (a) after crystallization and (b) after washing.....	45
Figure 5.18. SEM micrographs of CuTPAs depending on the washing method: stirring (a) F36-MSt-R225 and soxhlet (b) F36-MS _x -R225	45
Figure 5.19. FTIR spectra for CuTPA washed with MeOH under stirring (F36-MSt-R225) and soxhlet extraction (F36-MS _x -R225)	46
Figure 5.20. TGA curves for CuTPAs washed with MeOH under stirring and soxhlet extraction	46
Figure 5.21. XRD pattern of synthesized CuTPAs obtained by string and soxhlet methods	47
Figure 5.22. SEM micrographs of CuTPAs synthesized by differently activated: (a) F36-MS _x -R50, (b) F36-MS _x -R225	48
Figure 5.23. FTIR spectra for differently activated CuTPAs	49
Figure 5.24. TGA curves for CuTPAs synthesized by different activation method.....	49
Figure 5.25. XRD pattern of CuTPAs	50
Figure 5.26. SEM images of activated CuTPA at 160 °C (F24-MS _x 3d-R160).....	51

Figure 5.27. Infrared spectra of CuTPA produced at 110 °C for 24 h (F24-MSx3d-R160).....	51
Figure 5.28. Thermal stability of the CuTPA produced at 110 °C (F24-MSx-R50) and activated at 160 °C (F24-MSx3d-R160).....	52
Figure 5.29. X-ray diffractometer pattern of synthesized CuTPA under different activation temperatures	53
Figure 5.30. Breakthrough curves of CO ₂ and H ₂ effluent over 13X.....	54
Figure 5.31. Effect of pressure on CO ₂ adsorption breakthrough curves in 13X zeolite (Total flow rate= 10 mL/min)	54
Figure 5.32. CO ₂ desorption curves with helium flow over 13X zeolite (Flow rate (He)= 20 mL/min).....	55
Figure 5.33. Effect of pressure on CO ₂ adsorption breakthrough curves in 13X zeolite (Total flow rate= 20 mL/min)	56
Figure 5.34. Effect of pressure on CO ₂ adsorption breakthrough curves in 13X zeolite (Total flow rate= 30 mL/min)	56
Figure 5.35. Effect of feed flow rate on CO ₂ adsorption breakthrough curves in 13X zeolite (P= 1 bar).....	57
Figure 5.36. Effect of feed flow rate on CO ₂ adsorption breakthrough curves in 13X zeolite (P= 5 bar).....	57
Figure 5.37. Effect of feed flow rate on CO ₂ adsorption breakthrough curves in 13X zeolite (P= 10 bar).....	58
Figure 5.38. Cumulative CO ₂ flow in feed versus CO ₂ fraction at out flow (P= 10 bar)	58
Figure 5.39. Adsorption isotherms of CO ₂ in 13X zeolite at different flow rates at 303 K.....	59
Figure 5.40. Breakthrough curves of CO ₂ and H ₂ effluent over CuTPA.....	61
Figure 5.41. Effect of pressure on CO ₂ adsorption breakthrough curves in CuTPA (Total flow rate= 10 mL/min)	61
Figure 5.42. CO ₂ desorption curves with helium flow over CuTPA (Flow rate (He)= 20 mL/min)	62
Figure 5.43. Effect of pressure on CO ₂ adsorption breakthrough curves in CuTPA (Total flow rate= 20 mL/min)	63
Figure 5.44. Effect of pressure on CO ₂ adsorption breakthrough curves in CuTPA (Total flow rate= 30 mL/min)	63

Figure 5.45. Effect of feed flow rate on CO ₂ adsorption breakthrough curves in CuTPA (P= 1 bar)	64
Figure 5.46. Effect of feed flow rate on CO ₂ adsorption breakthrough curves in CuTPA (P= 5 bar)	64
Figure 5.47. Effect of feed flow rate on CO ₂ adsorption breakthrough curves in CuTPA (P= 10 bar)	65
Figure 5.48. Cumulative CO ₂ flow in feed versus CO ₂ fraction at out flow (P= 10 bar)	65
Figure 5.49. Adsorption isotherms of CO ₂ in CuTPA for different flow rates at 303 K.....	66

LIST OF TABLES

<u>Table</u>	<u>Page</u>
Table 3.1. Typical characteristics of adsorption processes.....	16
Table 4.1. Column characteristics and properties of adsorbents	30
Table 5.1. Textural properties and experimental conditions of CuTPAs synthesized....	33
Table 5.2. Breakthrough, adsorption and, desorption times for CO ₂ over 13X.....	55
Table 5.3. CO ₂ amount adsorbed by 13X	60
Table 5.4. Breakthrough, adsorption and, desorption times for CO ₂ over CuTPA	62
Table 5.5. CO ₂ amount adsorbed by CuTPA.....	67
Table 5.6. Comparison of amount adsorbed and adsorption/desorption times of adsorbents	67

CHAPTER 1

INTRODUCTION

Besides to organic porous materials and polymeric foams, a large number of inorganic porous materials have been developed. Porous materials find application in gas separation and storage (Morris and Wheatley 2008), shape/size selective catalysis (Ranocchiari and Bokhoven 2011) and drug delivery (Keskin and Kızılel 2011), insulation (Eisenhardt et al. 2014), cushioning, impact protection and construction materials depending on pore sizes (from nanometer to millimeter), ordered or irregular arrangement of pores, various chemical compositions (metal, oxides...) and different preparative approaches. An extensive overview of the development of porous materials, starting with the discovery of natural zeolites, is dating back to 18th century. Metal Organic Frameworks (MOFs) also known as coordination polymers are porous materials. They are usually crystalline compounds built from metal cluster and organic linker with very high surface areas up to 6000 m²/g (Yaghi and Li 2009). Due to tunable pore size and shape, the synthesis of MOFs is generally conducted under relatively mild conditions in three steps; crystallization, purification, and activation. In the synthesis, metal clusters and organic linkers are mixed in solvent medium. Selection of the solvent plays important role in thermodynamics and activation energy for the crystallization. Major methods in the synthesis can be ordered as solvo/hydrothermal, slow evaporation, microwave-assisted, electrochemical, mechanochemical, and sonochemical.

Hydrogen is regarded as an important energy carrier with a fuel cell as its converter. In the world, H₂ can be produced from enrichment of steam methane reformer off gas with removal of CO₂. As other adsorbents, CO₂ adsorption capacity of MOFs is depend on pore size/volume and surface area. Therefore, selective CO₂ adsorption over H₂ rich gas mixture is targeted. The key component of separation methods based on adsorption such as pressure swing adsorption, vacuum swing adsorption, and temperature swing adsorption is the packed column.

Even mostly studied microporous adsorbent NaX zeolite gives very high CO₂ adsorption capacity. Recently, MOFs are evaluated as an alternative adsorbent due to their high pore volume and surface area. Their flexible pore structure makes them

different from the conventional rigid adsorbents such as zeolite, activated carbon and, silica gel. Thus adsorption capacity of these flexible materials is increased with increasing pressure (Peter et al. 2013).

Copper-based MOFs was chosen as an alternative adsorbent due to promising results and very limited number of studies present in the literature. In this study, Cu-based metal organic frameworks (CuTPAs) were synthesized and their CO₂ adsorption performance over H₂ was studied at different total pressures (1, 5 and, 10 bars) and flow rates (5, 10 and, 30 ml/min) of mixture. The results obtained were compared with the commercial NaX zeolite (13X).

CHAPTER 2

ADSORBENTS

Activated carbon, zeolites, silica gel, alumina, and recently coordinating polymers (metal organic frameworks, MOFs) are the adsorbents usually used in the form of spherical pellets, rods, moldings or monoliths with diameters between 0.5 and 10 mm for gas separation. High abrasion resistance, thermal stability and surface area are some of the important properties of these adsorbents (Ruthven 1984).

2.1. NaX Zeolite (13X)

Zeolites are three dimensional microporous crystalline aluminosilicates of the alkali and alkaline earth elements such as sodium, potassium and, calcium. The empirical formula was represented as $M_{2/n}O \cdot Al_2O_3 \cdot xSiO_2 \cdot yH_2O$ where n is the valence of the cation, x and y are integers. The structure of the zeolite is commonly identified on covalent bonded TO_4 tetrahedra in which T is silicon or aluminum. According to the Löwenstine rule Silicon/Aluminum ratio of zeolite should be at least 1. Framework was formed by tetrahedral blocks to form the cavities for the guest molecules. The hydrophilic nature of the zeolite increases with substitution of aluminum atoms resulting from increase in the negative charge on the framework. Metal ions such as Na^+ , K^+ , Ca^{2+} , Mg^{2+} was used to balance the charge of the framework.

As a member of synthetic zeolites (Fig. 2.1), NaX is used for different applications such as catalysis, adsorbent, etc. Commonly, zeolite X is synthesized from silica and alumina sources via hydrothermal reaction (Chen, Park, and Ahn 2014).

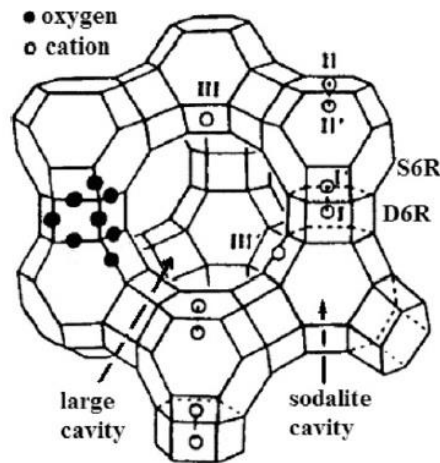


Figure 2.1. Structure of zeolite 13X
 (Source: Erten-Kaya and Cakicioglu-Ozkan 2012)

2.2. Metal Organic Frameworks (MOFs)

Metal organic frameworks (MOFs) are an emerging class of porous materials constructed from metal (Cu, Zn, Cr, Mn etc.) clusters and organic ligands such as carboxylic acid to form extended polymeric structures in one (1D), two (2D) and three (3D) dimensions. Thanks to pioneer studies of Hofmann and Küspert (1897) complex, now metal organic frameworks (MOFs) was produced (MacGillivray 2010). These materials are crystalline, highly porous and stable at high temperature. MOFs provide very high surface area (Ranocchiari and Bokhoven 2011) and controllable pore sizes due to multifunctionality of bridging organic ligands. Organic ligands and metal clusters which are secondary building units (SBUs), link to each other to form the extended framework (Figure 2.2). At the most basic definition, MOFs are polymeric crystal lattices which contain voids, possibly containing guest molecules, and those which do not. Materials which contain voids may be described as porous, but those porous materials which allow exchange of guest molecules are termed open-framework materials.

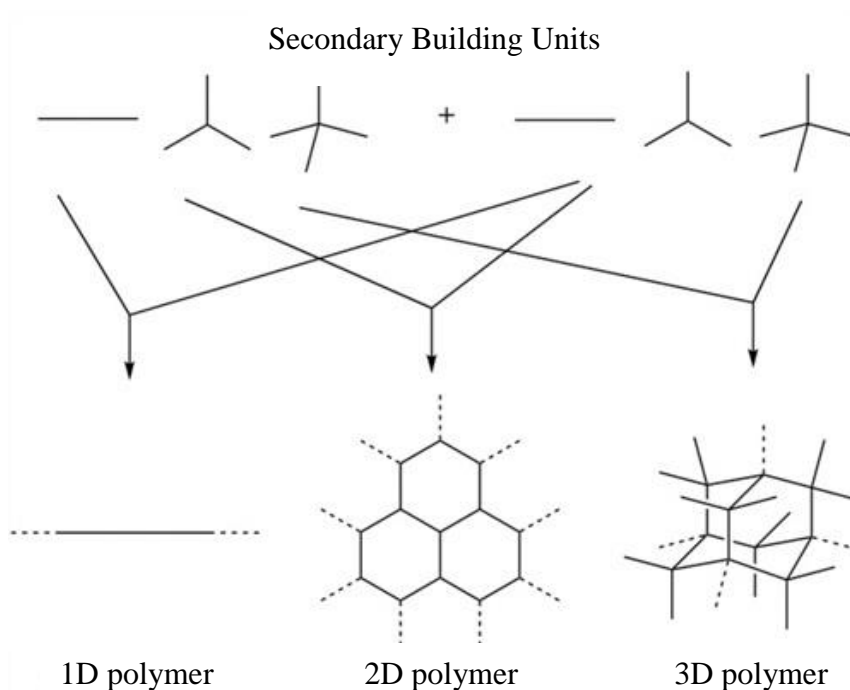


Figure 2.2. 1D, 2D, and 3D structures of MOFs which is constructed by molecular building units (Source: Yaghi et al. 2003)

As an example of 3D MOFs, Figure 2.3 and Figure 2.4 show framework structure of Cu-based terephthalate (CuTPA) and the general structure of secondary building units, respectively.

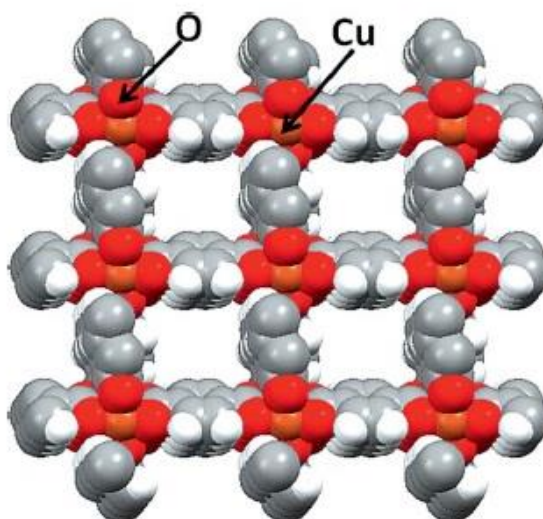


Figure 2.3. The CuTPA framework (Source: Carson et al. 2014)

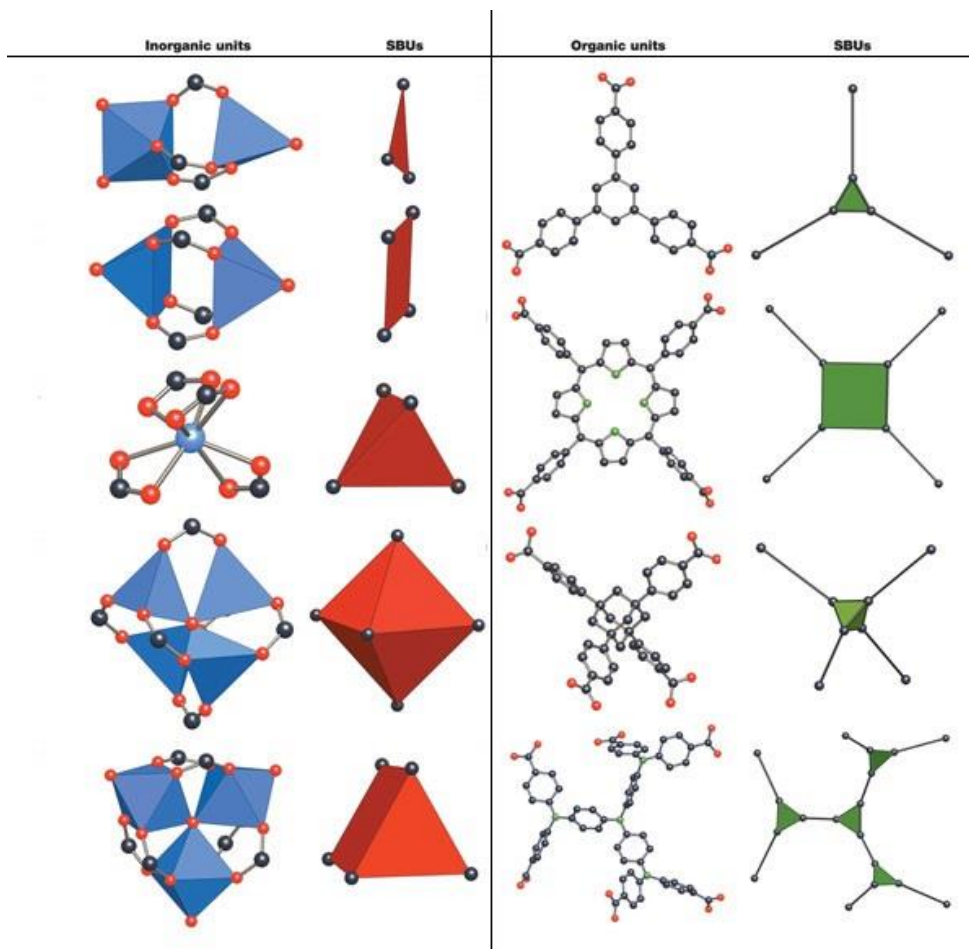


Figure 2.4. Examples of SBUs from carboxylate MOFs; O, red: N, green: C: black (Source: Yaghi et al. 2003)

MOFs also have wide range of potential applications such as gas adsorption and separation, catalysis, luminescence sensing, drug delivery and proton conduction (Zhou and Kitagawa 2014).

The crystallization of copper metal with terephthalate was first reported by Sherif (1970), but crystal structure was later elucidated by Cueto et al. (1991).

2.2.1. Copper Based Metal Organic Frameworks (Cu TPAs)

MOF syntheses generally occur in liquid medium in which the solutions are mixed together after metal cluster and organic linker solutions (in solvent medium) are mixed separately. For these type liquid-phase reactions, the solvent should be selected by considering the reactivity, solubility, redox potential and stability constant. Apart

from liquid-phase synthesis, solid-phase synthesis is another synthesis procedure due to its more quickness and easiness. However, beyond this advantage, solid phase synthesis has difficulties like determination of the crystal structure. Slow evaporation and solvo/hydrothermal methods are regular methods for synthesis of MOFs. Microwave-assisted, electrochemical, mechanochemical and sonochemical syntheses are used as the alternative methods (Fig. 2.5).

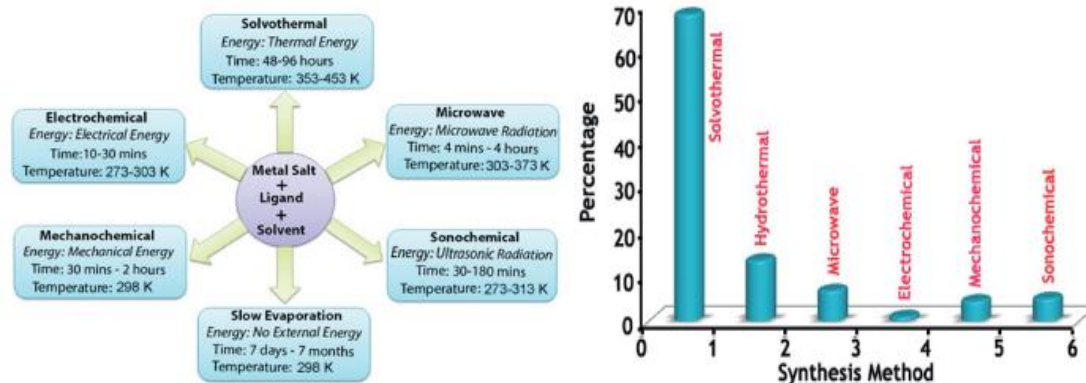


Figure 2.5. (a) Synthesis methods commonly used for MOF production (b) percentage of MOF synthesized with different methods (Source: Dey et al. 2014)

2.2.1.1. Hydro/Solvothermal Synthesis Method

Solvothermal and hydrothermal syntheses are generally performed in a closed vessel (autoclave, flask). For the best crystallization, the synthesis should be also carried out under autogenesis pressure above the boiling point of solvent. However, these methods typically require long crystallization times depending on solvent type, reaction temperature and reagent concentrations. Organic solvents that have high boiling temperature are used for solvothermal reactions such as dimethyl formamide and diethyl formamide; and water medium is used for hydrothermal reactions.

A survey of the literature reveals that there are many MOFs synthesized by using transition elements as the metal sources. Copper is the one of those metals which is potential applicant from selective gas separation to sensing (luminescent material) to catalysis to drug delivery. Copper-based carboxylate was firstly investigated by Cueto et al. (1991) which is about conductivity and magnetic susceptibility of material synthesized. However, Mori et al. (1997) reported the first copper terephthalate

synthesized which has large surface area and studied the adsorption capacity of the material synthesized. Mori et al. (2005) and Carson et al. (2009) conducted the studies to improve the magnetic susceptibility of copper terephthalate (Fig. 2.6) and solvothermal synthesis was achieved with a surface area of 625 m²/g.

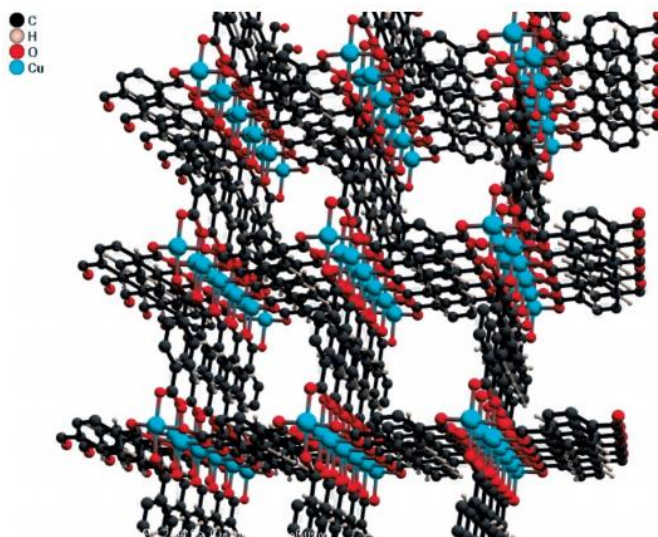


Figure 2.6. Structure of copper terephthalate in the (001) plane to form porous structure which responsible for high surface area (Source: Carson et al. 2009)

Copper terephthalate (MIL-53 (Cu) or copper (III) dicarboxylates) can also be synthesized under hydrothermal conditions. The adsorption capacity was found 8.52 mmol/g at 35 bars and 25 °C for methane adsorption. During the synthesis, hydrofluoric acid and terephthalic acid were used as organic linker (Anbia and Sheykhi 2012). Lincke et al. (2011) worked on highly adsorptive material which including copper acetate as metal salt and (4-(3,5-dimethyl-4H-1,2,4-triazol-4-yl)benzoate)/Me₂trzpba⁻ as the linker. Two different synthesis routes were studied with different solvent medium.

2.2.1.2. Slow Evaporation Synthesis Method

Slow evaporation method is commonly used to synthesize MOFs due to no need to external energy power in contrast to solvo/hydrothermal method. However, when compared to the methods that need energy (heating), this method takes a long time. Solution of the starting materials is concentrated by slow evaporation of the solvent at a

fixed temperature, mostly at room temperature. Mixture of different solvents can be used as solvent medium to faster reaction by using low-boiling solvents (Du, Li, and Zhao (2005), Halper et al. (2006))

2.2.1.3. Microwave Assisted Synthesis Method

Synthesis of MOFs requires many hours with conventional methods. Microwave assisted synthesis reduces this time almost 12 times with respect to the solvothermal method (Arunkumar et al. 2007). Firstly, Jhung et al. (2007) studied the chromium terephthalate under microwave irradiation. In particular, the optimum time was found to be 60 minutes. This method actually can be called microwave assisted solvo/hydrothermal method because just the heating medium is different from the conventional solvo/hydrothermal method. Zinc-based MOFs via microwave-assisted solvothermal method was reported by Ni and Masel (2006) who obtained microcrystals of IRMOF 1, IRMOF 2, and IRMOF 3. This method can also control the crystal size from near-millimeter to sub-micrometer by manipulating the temperature and the concentration of the reactants in the solution. Moreover, quality of the crystals are the same with the crystals obtained from solvo/hydrothermal method (Bux et al. (2009), Hindelang et al. (2012), Liang and D'Alessandro (2013), Zornoza et al. (2011), Klinowski et al. (2011).

2.2.1.4. Electrochemical Synthesis Method

In this method, large crystals and amounts of MOF can be produced with different solvent preference under mild conditions. Synthesis of MOFs via electrochemical method basically relies on supplying metal ions from anodic dissolution as follows the metal cluster is not supplied as salts but by oxidation of the electrode. Method is excludes unneeded anions during the synthesis, which contribute to the waste stream and can complicate the synthesis and purification (Martinez Joaristi et al. 2012). This is the major advantage of the method, especially for the industrial scale production. Basolite MOFs which are manufactured by BASF by using mentioned method are currently being marketed by Sigma-Aldrich (Mueller et al. 2006).

2.2.1.5. Mechanochemical Synthesis Method

Researchers have studied the synthesis method of MOFs to develop an environmentally friendly process under solvent-free condition. The mechanochemical synthesis method involves use of mechanical forces to drive the solventless reactions of reagents. Recently, Beldon et al. (2010) reported a study in which small amount of solvent has used for rapid synthesis of MOFs. Frišćić et al. (2013) have shown that by changing the added solvent, 1D, 2D, and 3D MOFs can be obtained from the same mixture. Copper based MOF was also studied by Pichon, Lazuen-Garay, and James (2006). A ball mill was used to grind copper acetate monohydrate and isonicotinic acid together.

2.2.1.6. Sonochemical Synthesis Method

MOFs can be synthesized by sonochemical method which exhibited rapid synthesis kinetics and excellent phase purity in inorganic material synthesis. The sonochemical method promotes homogeneous nucleation and reduces crystallization time. The sonication method allowed the use of 1-methyl-2-pyrrolidinone (NMP) as an alternative solvent to diethyl formamide (DEF) traditionally used in solution synthesis. MOFs are recently explored by Son et al. (2008) in the synthesis of MOF 5 from solutions of zinc nitrate and terephthalic acid. Arul Dhas, Raj, and Gedanken (1998) also reported that MOF-5 synthesis using sonochemical method in 1-methyl-2-pyrrolidinone can produce 5-25 mm crystals in 30 minutes, which is MOF 5 synthesized by solvothermal method with several hours.

2.2.2. Applications of MOFs

Recently, MOFs have been one of the most interesting materials due to their unique network and properties for potential applications such as gas/energy storage (Morris, 2008), catalysis (Ranocchiari, 2011), luminescent material, sensor, and drug delivery (Kuppler et al. 2009). In this topic, most important applications of MOFs are going to be mentioned.

2.2.2.1. Gas Storage in MOFs

The energy usage of World is increasing day by day, which is leading to consumption of fossil fuel reserves. Therefore, renewable ways to generate, store and deliver energy are being investigated. The ways of reducing CO₂ emission was also studied by researchers due to concerns about the implications of global warming.

Gas storage in MOFs is the most important application due to high surface area of these porous materials. MOFs are which have 3D structures incorporating uniform pores and a network of channels, often containing guest species. If these guest molecules removed from the structure without losing porosity, hydrogen, methane or nitrogen can be stored in to the network. Many adsorbents such as activated carbon, zeolites have been studied for gas storage (Morris and Wheatley 2008). However the MOFs have received more attention than others due to their flexible framework (adjustable pore size), pore geometries and high surface areas. In 1997, the first methane storage (Kondo et al. 1997); in 2003, the first hydrogen storage (Rosi et al. 2003) studies was reported. After that many MOF were studied for methane and hydrogen storage (Langmi et al. (2014), Panella and Hirscher (2013), Zhao, Yuan, and Zhou (2008)).

2.2.2.2. MOFs in Catalysis

The well-defined pores which can be tailored or modified different chemical groups in MOFs enable them to be used as a catalyst. Including high metal content is another advantage of these materials. Unsaturated active sites can be found in two parts either metal parts or organic linkers. Size and shape selective catalysis is also important application of such materials. First study of MOF as a catalyst was reported by Fujita et al. (1994) which is synthesis of 2D [Cd(4,4-Bpy)₂](NO₃)₂ for cyanosilylation of aldehydes. Horike et al. (2008) synthesized manganese based MOF (Mn₃[(Mn₄Cl)₃(BTT)₈(CH₃OH)₁₀]₂) which is show similar catalytic property with previous study mentioned above. Recently, Farha et al. (2011) reported a successful synthesis of MOFs with different metals (Al, Zn, Pd, Mn, and Fe) that are effective catalysts for the oxidation of alkenes and alkanes.

2.2.2.3. Magnetic Properties of MOFs

Magnetic materials are becoming important with increasing number of usage of magnets. Magnetic properties (ferromagnetism, anti-ferromagnetism, ferrimagnetism) of MOFs result of exchange coupling between unpaired spins on transition metal centers were investigated by many researchers. Copper (Abdelouhab et al. 2005), Nickel (Carton et al. 2007) and Cobalt (Huang et al. 2000) based metal organic frameworks was reported in the literature and cobalt received more attention than others.

2.2.2.4. MOFs in Sensors

The potential usage of MOFs as sensing devices is based on their luminescence properties which is coming luminescent metal ion or organic linker. These luminescent materials can be used in small-molecule sensors (Lu et al. (2011), Sun et al. (2013)), pH sensors (Harbuzaru et al. 2009), light concentrators for photovoltaic devices, and high technology optics. There are two basic types of luminescence material. One is fluorescence which is spinning allowed. Another is phosphorescence which is spinning forbidden. The most common way to synthesize the luminescent MOF is use of lanthanide ions (especially Eu-Europium and Tb-Terbium) as metal sources due to strong visible luminescence of these ions. ZMOF type luminescent material was synthesized by Liu et al. (2006) which can serve as sensor unit. Tb(BTC) terbium based MOF reported by Chen et al. (2008) and showed that material was able to recognize and sense anions.

2.2.2.5. MOFs in Drug Delivery

In developing MOFs for drug delivery, the scope is to design carriers that show lower toxicity in human body. While some of metals that construct the MOF structure exist in acceptable amounts in the human body, there are also highly toxic ones like chromium. As a potential drug delivery, first MOFs that are group of MIL (Materials of Institut Lavoisier) family were investigated by Ferey et al. (2005). In this study,

synthesized MOFs are constructed by trivalent metal centers and carboxylic acid linkers with large pores (25-34 Å) and high surface area (3100-5900 m²/g). Another study was conducted by the same group concerning controlled drug release of ibuprofen using MIL-53(Cr/Fe) which has loading of 0.220 g ibuprofen/g MOF (Horcajada et al. 2008).

CHAPTER 3

GAS SEPARATION VIA ADSORPTION

3.1. Adsorption

Adsorption can be simply defined as the concentration of a solute, which may be molecules in a gas stream or a dissolved or suspended substance in a liquid stream, on the surface of the solid material. It includes the capture of gaseous or liquid components of mixtures from the external and/or internal surface of porous solids (Inglezakis and Pouloupoulos 2006). Gas vapor or liquid molecules may become bound to the surface if they approach sufficiently close to interact. The solid material is called as adsorbent; the gas or vapor molecule prior to being adsorbed is called as adsorptive and while bound to the solid surface as the adsorbate. In an adsorption process, molecules or atoms or ions in a gas or liquid diffuse to the surface of the solid, where they bond with solid surface or are held there by weak inter molecular forces.

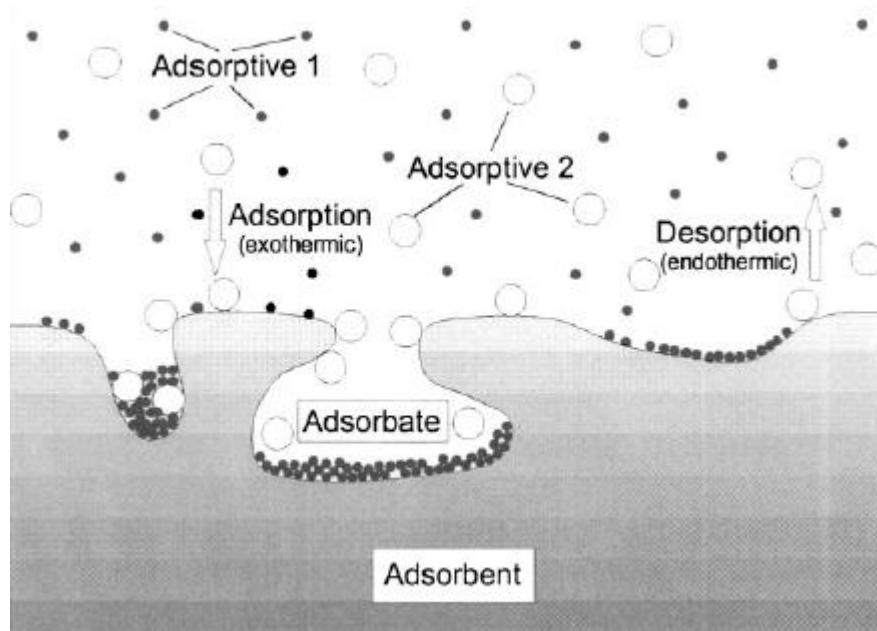


Figure 3.1. Basic concept of adsorption phenomena
(Source: Keller and Staudt 2005)

Similar to surface tension, adsorption is a consequence of surface energy. In a bulk material, all the bonding requirements of the constituent atoms of the material are filled. However, atoms on the surface experience a bond deficiency, because they are not wholly surrounded by other atoms. Thus, it is energetically favorable for them to bond with whatever happens to be available. The exact nature of the bonding depends on the details of the species involved, but the adsorption is generally classified as physical and chemical adsorption.

Adsorption and absorption terms express two different phenomena which is adherence of molecules to the free surfaces called adsorption and penetration of the molecules to the surfaces called absorption. These terms should not consider as a same case.

Classification (Fig. 3.1) of pores and geometries (Fig. 3.2) are important parameters for the solid materials especially in adsorption. Adsorptive molecules are adsorbed through the macropores to mesopores and finally enter the micropores. Thus, total pore volume and pore size distribution determine the adsorption capacity of the adsorbents. According to The International Union of Pure and Applied Chemistry (IUPAC), porous materials are classified into the following groups: macropores (>50 nm), mesopores (2-50 nm), micropores (<2 nm), supermicroporous (0.7-2 nm), and ultramicropores (<0.7 nm) in diameter (Everett 1972).

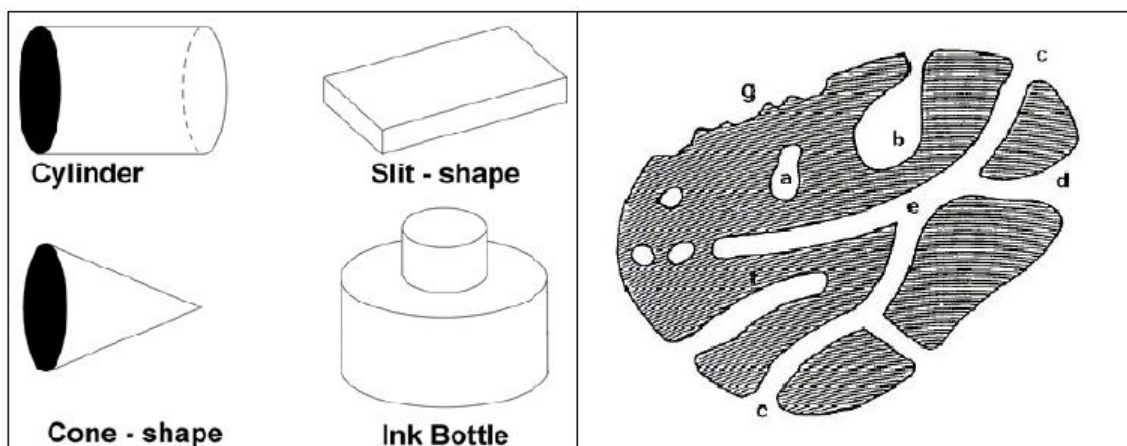


Figure 3.2. Pore geometries and schematic pores classification of zeolite; (a) closed pores, (b, f) pores open only at one end, (c, d, g) open pores, (e) open at two ends (Source: Zdravkov et al. 2007)

3.1.1. Physical Adsorption

Physical adsorption is the result of a relatively weak solid-gas interaction and takes place on all surfaces provided that temperature and pressure conditions are favorable. In this interaction, exchange of electrons is not observed. It is therefore physical attraction resulting from nonspecific, relatively weak Van der Waal's forces. The heat of adsorption is generally not exceeding 80 kJ/mole, with typical energies being considerably less (Webb 2003). Physically adsorbed molecules can diffuse along the surface of the adsorbent and typically are not bound to a specific location on the surface. Being only weakly bound, physical adsorption is easily reversed.

3.1.2. Chemical Adsorption

Adsorption also can result in a surface complex, a union much stronger than a physical bond with heat of adsorption up to about 600 kJ/mole for C-H bond and 800 kJ/mole for chemical bonds. These bonds involve sharing of electrons between the adsorbate and the adsorbent. Generally, only a single molecular layer can be adsorbed. Due to the strength of the bond, chemical adsorption is difficult to reverse.

Both physical and chemical adsorption may occur on the surface at the same time; a layer of molecules can be physically adsorbed over chemically adsorbed one (Table 3.1). Therefore, the same surface can display two different sorption temperatures (Inglezakis and Poulopoulos 2006).

Table 3.1. Typical characteristics of adsorption processes
(Source: Inglezakis and Poulopoulos 2006)

	Chemical Adsorption	Physical Adsorption
Material Specificity (variation between substrates of different chemical composition)	Substantial variation between materials	Slight dependence upon substrate composition
Crystallographic Specificity (variation between different surface planes of the same crystal)	Marked variation between crystal planes	Virtually independent of surface atomic geometry

(cont. on next page)

Table 3.1. (cont.)

Temperature Range	Unlimited	Near or below the condensation point of the adsorbate
Adsorption Enthalpy	Wide range (related to the chemical bond strength) (40-800 kJ/mole)	Related to factors like molecular mass and polarity (5-40 kJ/mole)
Nature of Adsorption	Often dissociative	Non-dissociative
Saturation Uptake	Monolayer	Multilayer

3.2. Adsorption in Porous Solids

Porous solids are known by a long time and are very familiar in practice. In spite of this, modeling adsorption on porous surfaces is a very difficult task because of different possibilities which porosity can be showed. Surface of adsorbent or complex topography can be imagined distribution of enormous of voids. These voids called as pores which are defined in Fig. 3.2.

3.2.1. Adsorption in Micropores

The description of adsorption in micropores on adsorbents with pore size below 2 nm (Fig. 3.2) is expected to require both the volume available for adsorption and the special nature of the adsorption potential inside the pore.

3.2.2. Adsorption in Mesopores

Multilayer type isotherms are usually exhibited by adsorbates below their critical temperature. When the pore size is higher than 2 nm, the adsorption at high relative pressure produces, therefore the formation of films which can, with a good deal of approximation, be regarded as liquid.

Adsorption in mesopores is always associated with the existence of hysteresis loop in adsorption-desorption cycles. This hysteresis can be explained in terms of capillary condensation. For any assumed geometrical model of pores and for any

mechanism supposedly responsible for the hysteresis, one can calculate the pore size distribution from the isotherms describing the complete adsorption-desorption cycle.

3.3. Pore Size and Surface Area Calculations

The BET (Brunauer, Emmett, and Teller (1938)) theory assumes that there is no limitation in the number of layers on the surface of the adsorbent. BET can be also thought as generalized form of Langmuir theory which involves the multilayer adsorption. Hence, the same assumptions which are energetically homogeneous surface and no interaction among the adsorbed molecules were accepted as those used in the Langmuir theory (Do 1998). BET is expressed by the equation given below,

$$\frac{V}{V_m} = \frac{C \cdot P}{(P_o - P) \left[1 + (C - 1) \left(\frac{P}{P_o} \right) \right]} \quad (3.1)$$

or in linear form (Eq. 3.2);

$$\frac{P}{V(P_o - P)} = \frac{1}{V_m \cdot C} + \frac{C - 1}{V_m \cdot C} \left(\frac{P}{P_o} \right) \quad (3.2)$$

where V is the amount adsorbed, V_m is the monolayer capacity, C is a constant and P/P_o is the relative pressure which is restricted in the relative pressure (P/P_o) range of 0.05 – 0.35 BET surface (m^2/g) can easily calculated by using monolayer capacity as (Eq. 3.3);

$$S_{BET} = V_m \cdot N_a \cdot a_m \quad (3.3)$$

where N_a is the Avogadro's number and a_m is the molecular projected area of adsorptive (N_2 (nitrogen)). Horvath-Kawazoe (H-K) is the method that is originating from model of Everett and Powl to calculate the pore size distribution. This method is based on thermodynamic behavior of adsorbent using average potential which is related to the free energy change between filling pressure and pore width. It assumes that the pores are either completely empty or completely full according to whether filling pressure is low or not (Do 1998). The Horvath-Kawazoe (H-K) equation given as follows (Eq. 3.4):

$$R_g \cdot T \cdot \ln \left(\frac{P}{P_0} \right) = N_a \cdot \frac{N_1 \cdot A_1 + N_2 \cdot A_2}{\sigma^4 [2d - (\sigma_1 + \sigma_2)]} \chi \left[\frac{\sigma^{10}}{9 \cdot \left(\frac{\sigma_1 + \sigma_2}{2} \right)^9} - \frac{\sigma^4}{3 \cdot \left(\frac{\sigma_1 + \sigma_2}{2} \right)^3} - \frac{\sigma^{10}}{9 \cdot \left(2d - \frac{\sigma_1 + \sigma_2}{2} \right)^9} + \frac{\sigma^4}{3 \cdot \left(2d - \frac{\sigma_1 + \sigma_2}{2} \right)^3} \right] \quad (3.4)$$

where, N_a is the Avogadro's number, N_1 is the number of molecules per unit area of the adsorbate, N_2 is the number of atoms per unit area of surface, A_1 and A_2 are the Kirkwood-Muller dispersion constants, σ is the distance between the gas molecule and the surface, $2d$ is the distance between the two nuclei of the two parallel layers.

3.4. Model Equations for Gas Adsorption

In this part of chapter, general model equations will be given and these equations than fitted to experimental data to investigate the data-model fitting. Several isotherms are presented in the literature which is generalizations of well-known isotherms (Langmuir, BET, etc.) to multicomponent adsorbates on heterogeneous surfaces.

The first and still the most used adsorption model was published by Langmuir (1918). This model especially used for monolayer adsorption. Original derivation of the Langmuir isotherm was kinetic in character, but right after statistico-mechanical derivation was soon found. This derivation is based on following assumptions (Eq. 3.5) (Do (1998), Ruthven (1984)):

- Surface is homogeneous, that is adsorption energy is constant over all sites
- Surface is localized, that is adsorbed molecules or atoms are adsorbed at definite, localized sites
- Each site can accommodate only one molecule or atom
- Molecules or atoms does not interact with each other

$$\theta = \frac{b \cdot p}{1 + b \cdot p} \quad (3.5)$$

$$\frac{q}{q_s} = \frac{b \cdot p}{1 + b \cdot p} \quad (3.6)$$

where $\theta=q/q_s$ is the fractional coverage, the parameter b (k_a/k_d , affinity constant) is the ratio of adsorption to desorption and p is the pressure.

Extending the classical Langmuir adsorption isotherm because of needed from monolayer adsorption to multilayer is first proposed by Brunauer, Emmett, and Teller (1938) (BET method, Eq. 3.2). So from the original derivation of the Langmuir Eq. 3.7 was derived for multilayer adsorption isotherm. The BET theory (Cerofolini and Rudziński 1997) assumes that,

- The gas is perfect
- Adsorbed molecules are classical objects localized on their adsorption sites
- Adsorption takes place either on surface or on the top of molecules already adsorbed
- Only first layer interact with the surface, the others have interparticle interaction
- Adsorbed molecules do not interact laterally

$$\frac{q}{q_m} = \frac{b \cdot \left(\frac{p}{p_s}\right)}{\left(1 - \frac{p}{p_s}\right) \cdot \left(1 - \frac{p}{p_s} + \frac{b \cdot p}{p_s}\right)} \quad (3.7)$$

where p_s is the saturation vapor pressure of adsorbate, q_m is amount adsorbed monolayer, b is affinity constant.

The Freundlich isotherm has both historical importance, because of the oldest report data and a practical importance because of still largely using in real system. The model has a limitation that is not working at high pressure. Equation does not also account for Henry's law behavior at low surface coverage and for the saturation of the adsorbed phase (Eq. 3.8).

$$q = k_f \cdot c^n \quad (3.8)$$

where n and k_f are the specific constants of model, q is amount adsorbed at equilibrium. c also represents the adsorbate concentration.

The problem of Freundlich equation which is uncontrollable adsorbed amount with increasing pressure (Do 1998) was achieved with Sips model equation (Eq. 3.9) by Sips (1948). Equation also resembles the Langmuir equation. Therefore, this equation

sometimes called the Langmuir-Freundlich equation because of combination of Langmuir and Freundlich equations. .

$$q = q_m \cdot \frac{(b \cdot p)^{1/n}}{(1+(b \cdot p)^{1/n})} \quad (3.9)$$

where, q is the adsorbed amount at a given pressure (p), b and n are constants. N is usually called as heterogeneity factor. Sips equation is used as more appropriate for high pressure studies than standard Langmuir or Freundlich equations. Presented model equation is generally used in dynamic gas separation processes.

Toth model equation was originally proposed for monolayer adsorption which is extension of Langmuir and Freundlich model when applied to Type I isotherms for porous adsorbents by Toth (1971). This model is another empirical equation (Eq. 3.10) level open to improve Langmuir isotherm fittings and useful in describing heterogeneous adsorption systems, which satisfying both low and high end boundary concentration (Tedds et al. 2011).

$$q = q_m \cdot \frac{b \cdot p}{[1+(b \cdot p)^t]^{1/t}} \quad (3.10)$$

where t is the Toth parameter and b is the Langmuir constant. The parameter t takes a value of 0.233 (well deviated from unity) indicates a strong degree of heterogeneity of the system (Do 1998).

3.5. Cyclic Adsorptive Separation Processes

Main methods for adsorption, depending on regeneration methods, are pressure swing adsorption (PSA), vacuum swing adsorption (VSA) and temperature swing adsorption (TSA). In all three cases adsorption rates depend on partial pressure of adsorbate, temperature, pore size or surface area and surface interaction.

3.5.1. Pressure/Vacuum Swing Adsorption

Pressure swing adsorption is defined as the performing regeneration of the adsorbent by reducing the pressure from high pressure in feed to low pressure in regeneration. Like all adsorption separation processes, pressure swing adsorption consists of two principal steps: adsorption and desorption.

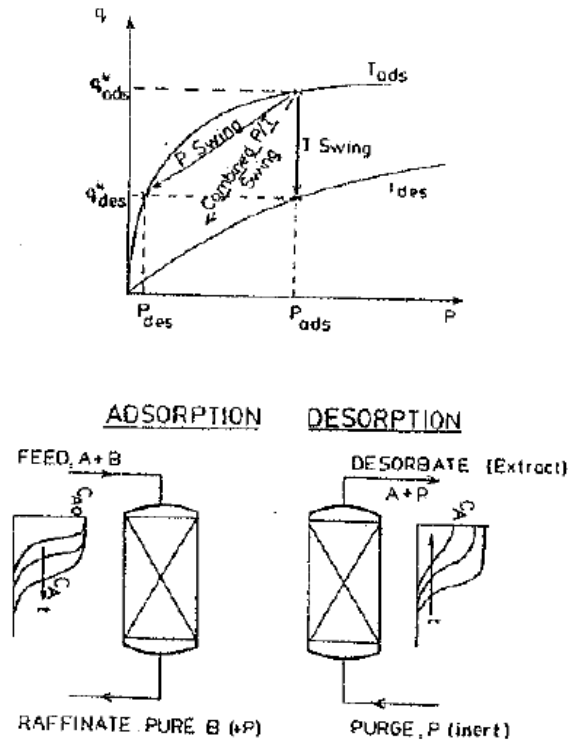


Figure 3.3. General design and demonstration of PSA and TSA process
(Source: Ruthven, Farooq, and Knaebel 1993)

Pioneer study on pressure swing adsorption to develop an adsorption separation process was conducted by Daniel and De (1964). Skarstrom (1966) was also accepted as the first researcher of present process. In this process, the steps are feed, pressurization, blowdown, depressurization and, regeneration, respectively. General process is schematically given in Figure 3.3. Isothermal conditions are commonly applying to this process to save the isotherm both in feed and regeneration pressures. The feed step is terminated before strongly adsorbed molecules break through the column, while regeneration is terminated before all the molecules are desorbed from the column.

The PSA system is well suited to rapid cycling and generally operates at relatively low adsorbent loadings since selectivity is greatest in the Henry's law region (Ruthven 1984). One of the most important advantages of PSA process is that the pressure can be easily controllable so this makes possible faster than conventional processes such as close ended, temperature controllable etc. However, adsorbed components should not be strongly adsorbed. When it occurs, expensive process is needed such as vacuum swing adsorption.

Microporous Zinc based MOF (MOF-508b) was reported by Bastin et al. (2008). Binary (CO_2/N_2 , CO_2/CH_4) and ternary ($\text{CO}_2/\text{CH}_4/\text{N}_2$) gas mixtures were studied in a column by using PSA system and adsorption capacity (5.5 mmol/g) and selectivity of material was calculated from equilibrium and dynamic adsorption results.

Silva, Schumann, and Rodrigues (2012) were studied adsorption kinetics of CO_2 and CH_4 on 13X zeolite by using zero length column (ZLC) technique. Later than, same group also studied H_2 purification and separation of CO_2 from steam methane reforming by pressure swing adsorption using Cu based MOF (CuBTC). CuBTC showed high adsorption. The experiments was carried out in a fixed bed column at 2 bars, 303 K (Silva et al. 2013).

Finsky et al. (2009) synthesized the aluminum-based MOF (MIL 53(Al)) to separate the CO_2/CH_4 mixture in a packed adsorbent column loaded with pellet form of MIL 53 (Al). Separation factor of the column was changed from 4 to 7 with change in the feed pressure from 1 to 8 bars at 303 K for mixture compositions and maximum CO_2 adsorption was found 3.2 mmol/g at 8 bars.

Recently Ribeiro et al. (2013) used iron based MOF as an adsorbent to separate nitrogen and propylene. Selectivity of propylene over nitrogen in fixed bed column, packed with iron-based MOF was found 40 for 30 % propylene at 2.5 bars, 70 °C.

Adsorption of CO_2 , CH_4 , N_2 , and CO on chromium based MOF (MIL 101(Cr)) was investigated by Munusamy et al. (2012). It was observed that inlet column flow rates and concentration of CO_2 was effective on dynamic adsorption capacity (1.68 mmol/g). Other group from Material from Institut Lavoisier (MIL) was reported the different type of chromium based MOF (MIL 53(Cr)) for separation of CO_2/CH_4 mixture. Study showed that the using of MIL 53(Cr) in PSA system is more suitable at intermediate pressures (0.2-1 MPa) (Hamon et al. 2009).

Dasgupta et al. (2012) investigated the CO_2 recovery from mixtures with nitrogen by vacuum swing adsorption (VSA). CuBTC and Zeolite X adsorbents were

provided by commercially and selectivity of CO₂ was found 3.6 in CuBTC and 120.3 in zeolite X.

3.5.2. Temperature Swing Adsorption

Temperature swing adsorption (TSA) is another type of adsorption separation process (Fig. 3.3) which involves the release of adsorbed gases from the adsorption column with heating while pressure swing adsorption (PSA) is taken advantage of changing in pressure. TSA systems are commercially used after 1960's for drying of compressed air, natural gas, and purification applications. Temperature swing adsorption employs a cyclic process where a number of connected column containing adsorbent with the target gas by heating and cooling step.

TSA was generally used for sequestration of an adsorbate (liquid or gas) from a mixture using various methods for temperature control of the adsorption column.

Mérel, Clausse, and Meunier (2006) investigated the CO₂ adsorption on zeolite 13X. Breakthrough experiment with a mixture of 10 % CO₂-90 % N₂ showed that, the adsorbent capacity unchanged and condition closed to isothermal adsorption. According to other result of this study, in desorption step almost 100 % recovery of CO₂ was achieved due to heating and no use of purge gas.

Kumar and Golden (1991) reported that trace impurities (chlorobenzene, dichloroethane, vinyl chloride, toluene, xylene, etc) adsorption from the multicomponent gas mixtures (Landfill gases (CO₂, CH₄, N₂, O₂, and etc.)) by TSA system which include changing different configurations on system. They revealed the 3 column has less regeneration gas than 2 column system.

CHAPTER 4

EXPERIMENTAL STUDIES

4.1. Materials

In this study, commercial zeolite zeolite (13X) (4-8 mesh, Aldrich, CAS#: 63213-69-6) copper nitrate trihydrate ($\text{Cu}(\text{NO}_3)_2 \cdot 3\text{H}_2\text{O}$), dimethylformamid ($(\text{CH}_3)_2\text{NCOH}$) and, methanol (CH_3OH) were used for synthesis. All chemicals are trade mark (merck). The terephthalic acid provided by Petkim and purchased from Aldrich was also used in synthesis of copper-based metal organic framework (copper terephthalate, CuTPA).

4.2. Synthesis of CuTPA

In the synthesis of CuTPA, the procedures proposed by Carson et al. (2009) and Carson et al. (2014) were studied. Effect of three main steps: crystallization, purification, and activation was investigated (Fig. 4.1).

4.2.1. Crystallization

Equimolar quantities (4 and 10 mmol) of $\text{Cu}(\text{NO}_3)_2 \cdot 3\text{H}_2\text{O}$ and terephthalic acid (TPA) were dissolved in dimethylformamide (DMF) under stirring at room temperature for 1 hour at 330 rpm and then taken into reactors: schott bottle (F), or autoclave (A) or parr reactor (P-model 4593 Parr). There is no mixing in the reactor F and A however stirring was only achieved in the reactor P (Fig. 4.2). Crystallization in the reactors was conducted at room temperature (24-26 °C), 50°C or 110°C for 24, 36, 48 or 72 hours. After the crystallization process, the reactors were taken out of oven (Binder ED 53 and Memmert 100-800) to cool down for 3.5 hours or overnight and it was observed that blue particles were precipitated. The precipitate, CuTPA was centrifuged (Hettich

Rotofix 32) at 3000 rpm for 25 minutes. The CuTPAs obtained were dried in the vacuum oven for overnight (P-Selecta Vaciotem-T) or overnight at room temperature.

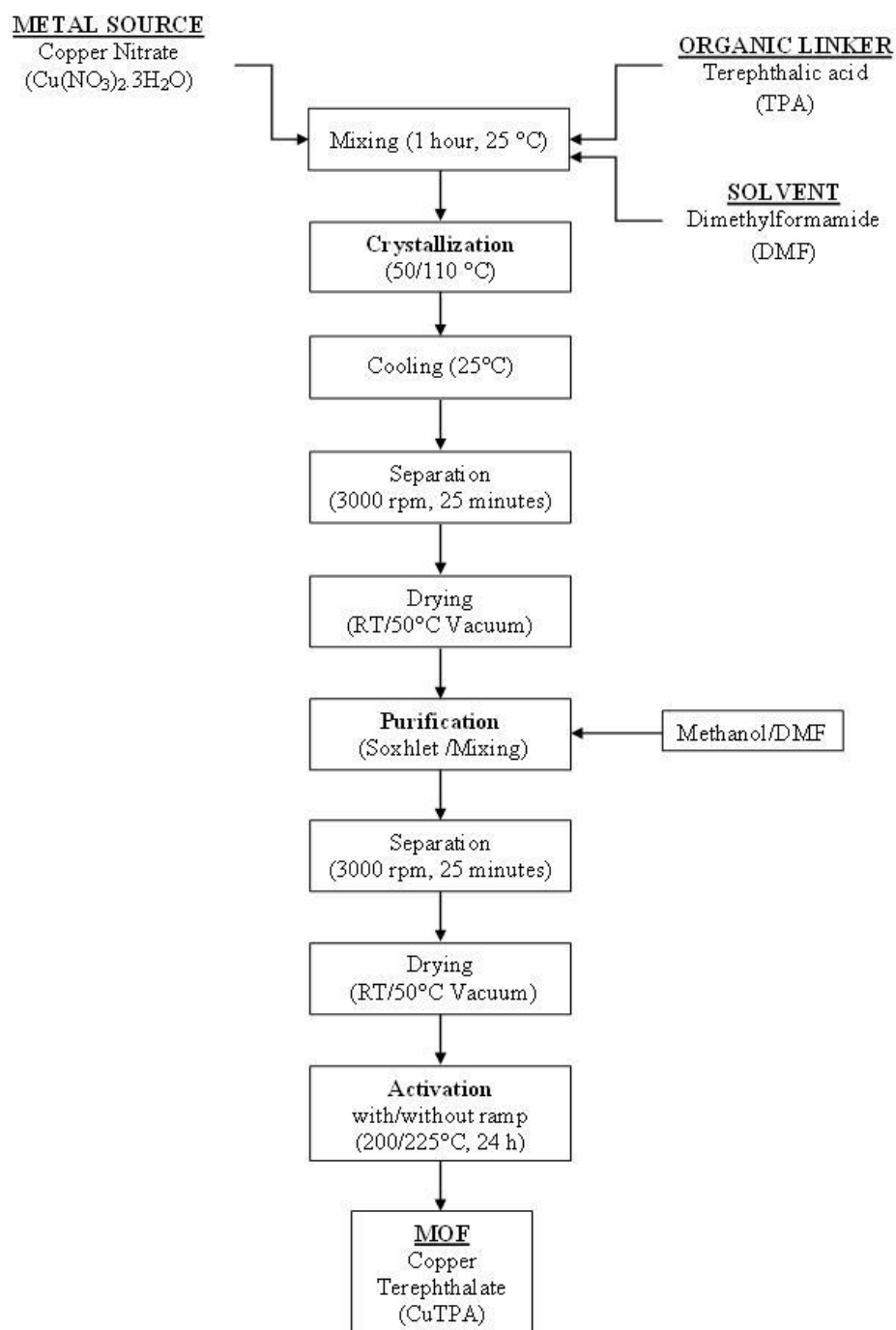


Figure 4.1. Synthesis procedure of CuTPA

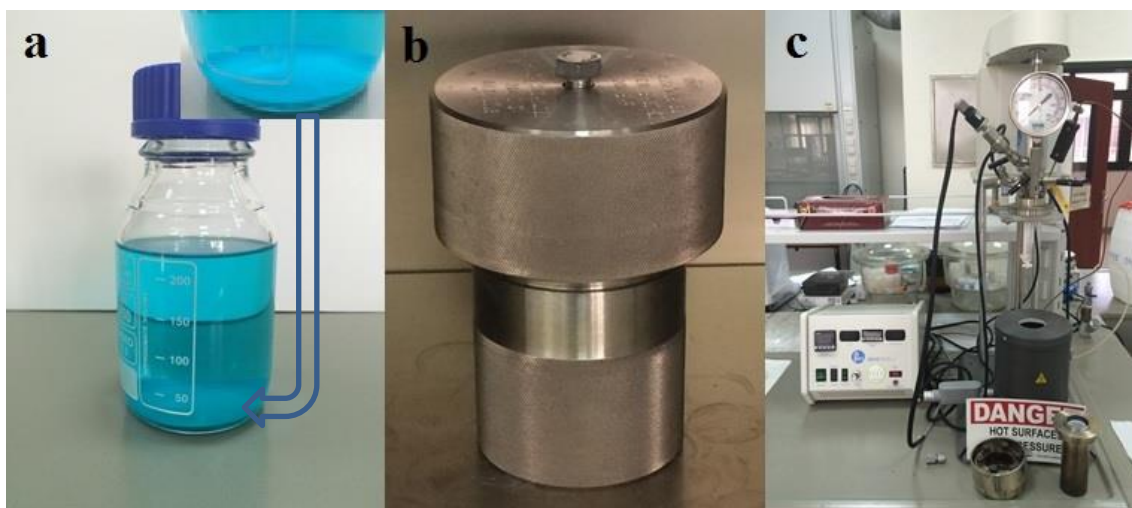


Figure 4.2. Crystallization reactors: (a) Schott bottle (F), (b) Autoclave (A), (c) Parr (P)

4.2.2. Purification

Purification step (solvent exchange) is the one of the most important step due to step of removal of unreacted terephthalic acid and solvent used in crystallization step by DMF or methanol that has the same role to purify material except for advantage of methanol which has a lower boiling point than DMF (Boiling point of methanol: 65 °C). For washing of the samples, either soxhlet extraction (Fig. 4.3) with 150 mL of solvent (5 cycles or 3 days) or mixing method was applied under agitation (150 mL for 24 h).

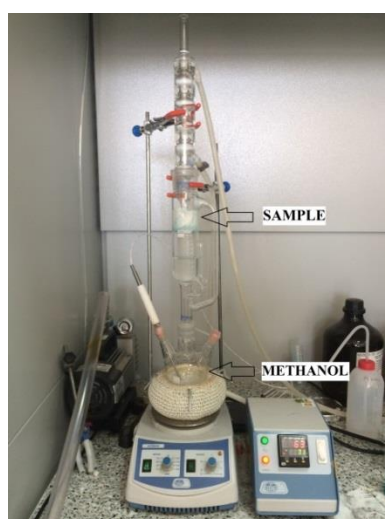


Figure 4.3. Soxhlet extraction method used in the purification step

4.2.3. Activation

Cu-TPA samples were kept under vacuum or room temperature for overnight prior to activation and activated at direct heating (heating up to 160°C under vacuum or 225 °C under air) or ramp heating (50 °C ramp and 32 min. soak up to 200 °C under vacuum) for 24 hours. In this step, heating rate and temperature are very effective on the crystal growth and framework structure. After the activation, it was expected that DMF, terephthalic acid and other solvent (methanol if used) are removed from the pores without any damage to the pore structure.

4.3. Characterization of Adsorbents

Morphologic structures of the synthesized CuTPA were investigated by scanning electron microscope (SEM, FEI QUANTA 250 FEG) with different magnifications under secondary electron (SE) and back scatter electron (BSE) detectors. Thermal stability of CuTPAs were determined by thermogravimetric analysis (Shimadzu TGA-51) with 10 °C/min heating rate under air flow at flow rate of 40 mL/min. Interaction between atoms and determination of bounded groups were found out by Fourier Transform Infrared spectrophotometer (FTIR, Shimadzu 8201). 1.5 mg of CuTPA was used with 148.5 mg of KBr for preparation of the pellet. Mineralogic and crystallographic structure was elucidated by X-ray diffraction (XRD, Philips X'Pert Pro Diffractometer) under CuK α radiation. Textural properties of the CuTPAs were measured by volumetric adsorption instrument (Micromeritics-ASAP2010M). Prior to the adsorption, the adsorbents were degassed at 160 and 210 °C for CuTPA and 250 °C for NaX zeolite with respect to their thermal stabilities.

4.4. Adsorption Studies

Adsorption studies were carried out in a home-made system (Fig. 4.4). The system involves gas (hydrogen, helium, and carbon dioxide) preparation part, containing three way valves (VTP1, VTP2, and VTP3, Ham-let), mass flow controllers

(MFC1 and MFC2) and manifold (M1), adsorbent column and gas analyzer (GC-Agilent 7890A).

In the binary gas adsorption, gases ($\text{CO}_2\text{-H}_2$) were regulated by high pressure regulators and sent to MFCs to measure and set the flow rates. Adsorbate gases were mixed in manifold (M1) after controllers then sent through the VTP1 to decide the selection of gases direction (bypass or reactor). Bypass line was used to prevent gases flow through reactor or adsorption column and stabilization of gases before starting to adsorption. Adsorption was started when the way of adsorbate gases were through column after gases were stabilized on bypass line. Finally, gases were analyzed by chromatographic method (GC) at outlet of the column. Gas chromatography has two thermal conductivity detectors: front and back (TCD) with two carrier gas (helium-front: 40 mL/min, nitrogen-back: 40 mL/min). Prior to each adsorption, adsorbent was regenerated under helium flow of 10, 20, and 30 mL/min (according to total flow rate of adsorbate gases) at 160 °C for CuTPA and 250 °C for 13X.

Adsorption column (Table 4.1) (24.8 cm in height and 0.675 cm in inner diameter) packed with adsorbents (4.6 g of zeolite 13X (granule) or 4 g of CuTPA (powder)) was placed before back pressure regulator (BPR, Bronkhorst) to be able to work at 1, 5 and 10 bars. The quartz wool was used at the both end of the packed adsorbent to prevent the sweep out of particles.

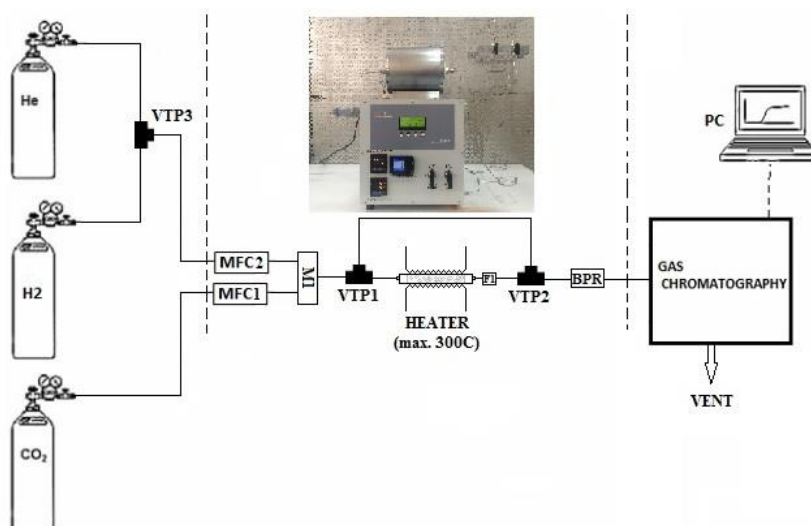


Figure 4.4. Gas adsorption system; VTP1, VTP2, and VTP3: three way valves, MFC1 and MFC2: mass flow controllers, M1: manifold, F1: filter, BPR: back pressure regulator

Table 4.1. Column characteristics and properties of adsorbents

	Zeolite 13X (granule)	CuTPA (powder)
Column length (cm)		24.80
Column diameter (cm)		0.67
Void volume ($V_{bed}-V_{solid}$, cm^3)	54.83	40.46
Mass of adsorbent (g)	4.6	4.0
Adsorbent layer length (cm)	18.80	10.80
Surface area (S_{Lang} , m^2/g)	1359 ($V_{mic}= 945$)	776 ($V_{mic}= 491$)
^a Micropore volume (cm^3/g)	0.49	0.26
^b Median pore diameter ($^{\circ}A$)	5.8	6.0

^aBJH method was used for calculation

^bHorvath-Kawazoe method was used for calculation

CO_2/H_2 binary adsorption dynamics of 13X and CuTPA synthesized was studied at different pressures (1, 5, and 10 bars) and flow rates (10, 20, and 30 mL/min). Differential material balance around the adsorbent packed column is used (Eq. 5.1).

$$\frac{dn_a}{dt} = F_{a0} - F_a \quad (5.1)$$

to calculate amount adsorbed (mmol) , n_a

$$dn_a = F_{a0} \int_0^t \left(1 - \frac{F_a}{F_{a0}}\right) dt \quad (5.2)$$

where X_a ($F_a/F_{a0}=C/C_0$) is flow rate ratio. Integration of Eq. 5.2 from 0 to t gives the mean residence time (min), τ_a

$$\tau_a = \int_0^t \left(1 - \frac{C}{C_0}\right) dt \quad (5.3)$$

Equation 5.4 was used to calculate amount adsorbed by adsorbent, q_a (mmol/g)

$$q_a = \frac{(F_{a0} \cdot \tau_a - \frac{(V_b - V_s) \times P_b \times X_a}{R \cdot T_b})}{m_{ads}} \quad (5.4)$$

where, V_b is the bed volume (mL) and V_s is the solid volume (mL); C is the concentration of CO_2 at time t , C_0 is the CO_2 concentration at bed inlet; P_b is the pressure in the bed (bar); F_a is the CO_2 flow rate at time t (mmol CO_2/min); F_{a0} is the CO_2 flow rate in feed (mmol CO_2/min); T_b is the column temperature (K); R is the ideal gas constant (0.0831 ml.bar/mmol.K).

CHAPTER 5

RESULTS AND DISCUSSIONS

The copper based terephthalates (CuTPAs) were synthesized; its performance in separation of CO₂/H₂ binary mixture at 1, 5, and, 10 bars was studied. In the separation, not only CuTPA, but also commercial NaX zeolite (13X) was used for separation of CO₂/H₂ in the adsorbent column as the packed material.

5.1. CuTPA Synthesis

The optimum conditions in each step (crystallization, purification and thermal activation) of the CuTPA synthesis were studied to obtain the adsorbent with high surface area, desired crystal structure and, high thermal stability. All surface area results obtained syntheses and conditions were summarized in Table 5.1.

5.1.1. Crystallization Step

In crystallization step, the first step of the synthesis, reactor type, crystallization time and temperature were investigated. Three different reactors (schott bottle: F, autoclave: A, and Parr: P) were used for the crystallization. These reactors with different void volume and heating rate (void %: 87 % (2.89 °C/min), 50 % (2.89 °C/min), and 50 % (5.5 °C/min), for F, A and P reactor, respectively) resulted in the crystals with different morphology and size (Fig. 5.1). Crystals of the CuTPA produced in the schott bottle are bigger (2-5 μ) than those produced in the Parr reactor's (0.5-2 μ).

Table 5.1. Textural properties and experimental conditions of CuTPAs synthesized

	MOFs		Crystallization		Separation		Purification		Activation			Textural Properties		
	CuTPA	Reactant amount mmol	Reactor type (F, A, P)	Decant (D)	Centrifuge (C)	Solvent (M, D)	Washing type (St or Sx)	R225	R160	R50	S _{BET}	S _{Lang}	S _{micro}	
Adrich TPA	F36-MSt-R225	4,36	F		√	M	St	√			66	95	25	
	F36-MSx-R225	4,36	F		√	M	Sx	√			86	123	7	
	F36-DSx-R225	4,36	F		√	D	Sx	√			32	46	5	
Petkim TPA	F36-DSx-R50	4,36	F		√	D	Sx			√	80	118	70	
	F36-DSx-R225-C (WW)	4,36	F		√	D	Sx	√			31	45	6	
	F36-DSx-R225-D (WW)	4,36	F	√		D	Sx	√			27	39	21	
	F36-MSx-R50 (50°C)	4,36	F		√	D	Sx			√	217	319	198	
	F36-MSx-R50	4,36	F		√	M	Sx			√	156	228	121	
	F48-MSx-R50	4,36	F		√	M	Sx			√	167	245	111	
	F24-MSx(3d)-R160	10	F		√	M	Sx		√		529	776	491	
	A24-MSx-R50	4,36	A		√	M	Sx			√	124	176	104	
	A48-MSx-R50	4,36	A		√	M	Sx			√	81	119	77	
	A72-MSx-R50	4,36	A		√	M	Sx			√	107	157	74	
	P24-MSx-R50	4,36	P		√	M	Sx			√	62	94	26	
P48-MSx-R50	4,36	P		√	M	Sx			√	106	157	96		

*Abbreviations	Crystallization	Separation	Washing	Activation
	F : Scintillation Flask	D: decant	M: Methanol (150 ml methanol is used for 5 loop at the soxlet extraction method)	R50 : by starting 50°C to ramp until 200°C under vacuum (50°C/h for 24 hour: 3+21 h)
	A: Autoclave Reactor	C: centrifuge		
	P: Parr Reactor		D: DMF (Dimethylformamide)	R160: increasing the temperature from room temp. to 160°C in 23 mins under vacuum. (for 24 hour)
			St: Stirring	R225: increasing the temperature from room temp. to 225°C in 32 mins under vacuum. (for 24 hour)
			Sx: Soxhlet Extraction	

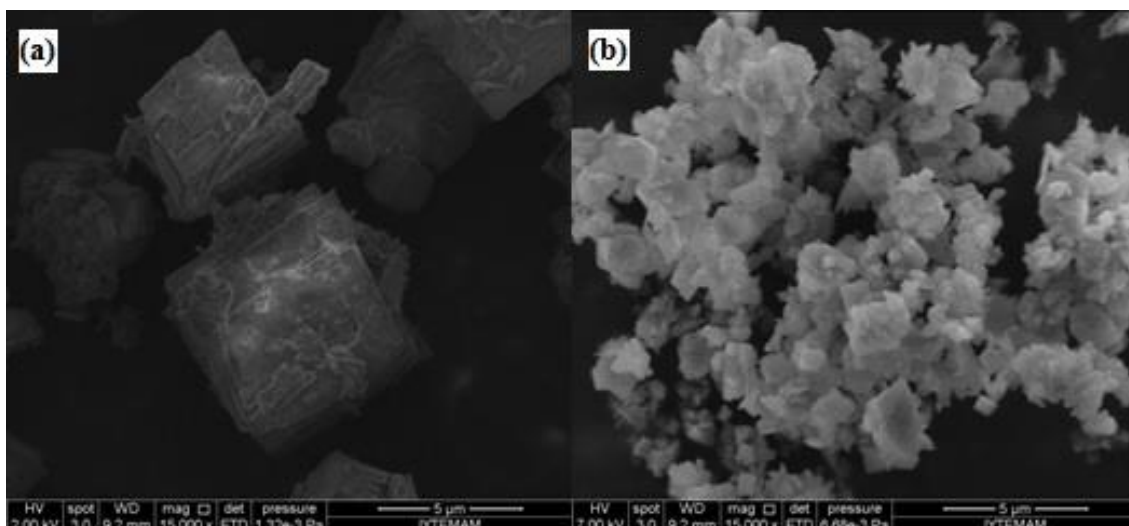


Figure 5.1. SEM images of the CuTPAs obtained from schott (a) F48-MSx-R50, Parr (b) P48-MSx-R50 reactor

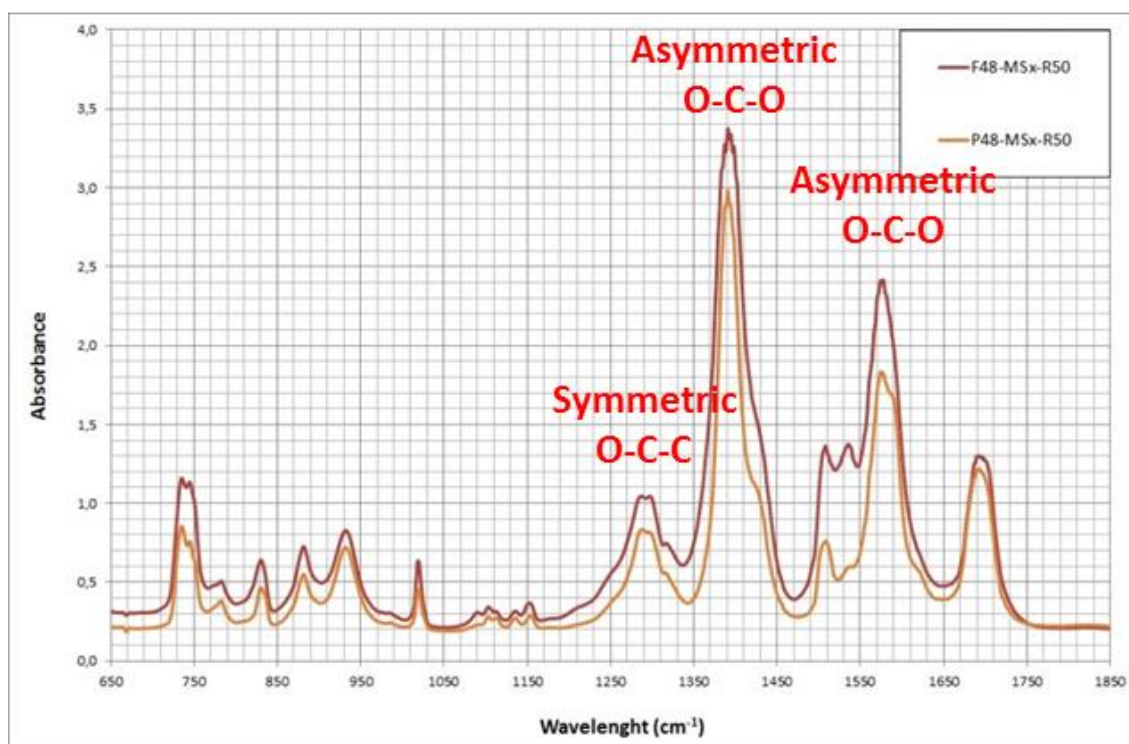


Figure 5.2. FTIR spectra of the synthesized CuTPAs in different reactors

Characteristic peaks for CuTPAs were seen at around 1280 cm^{-1} , 1390 cm^{-1} , and 1570 cm^{-1} which assigns the symmetric and asymmetric stretching of carboxylate groups (COO^-) even if reactors accordingly crystals are different (Fig. 5.2).

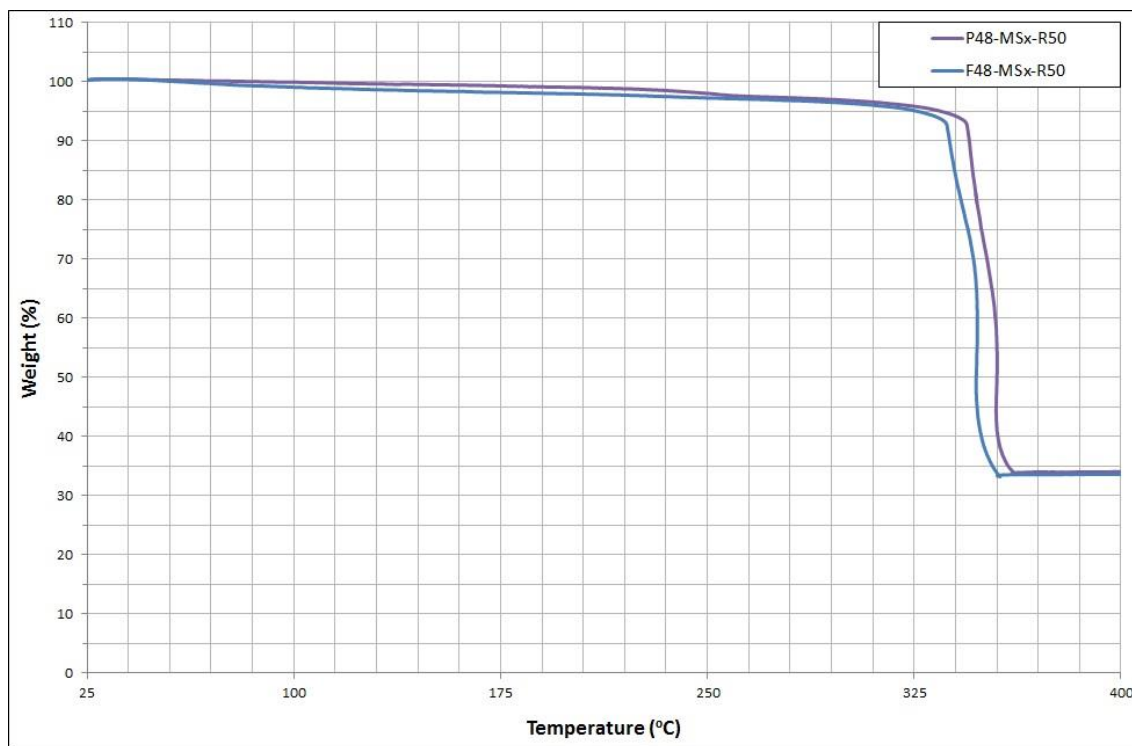


Figure 5.3. TGA thermographs for CuTPAs obtained from Schott bottle and Parr reactor

As seen from figure 5.2, crystal's shapes and sizes are different. However, both CuTPAs produced from Parr and Schott bottle have almost same thermal stability. As can be seen Figure 5.3, up to 334 °C (schott bottle) and 341 °C (Parr) only 7 % weight loss representing removal of DMF was observed. After that decomposition, in other word structural collapse was seen. XRD pattern of these CuTPAs (Fig. 5.4) are not identical as SEM images.

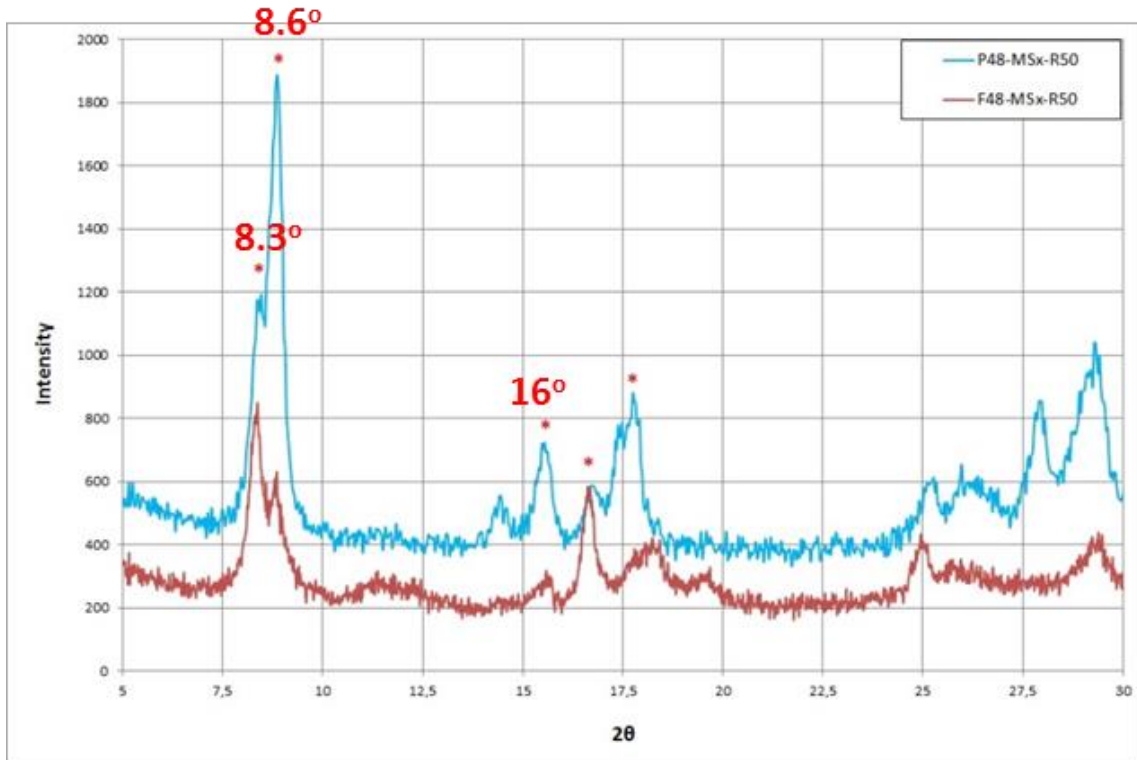


Figure 5.4. X-ray diffraction scans of synthesized CuTPAs with two different reactor

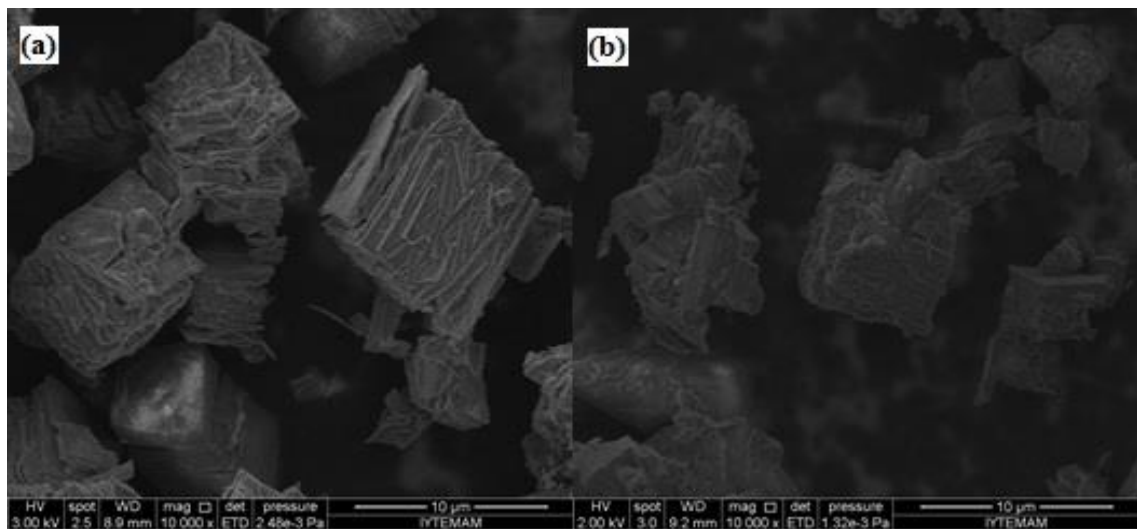


Figure 5.5. Synthesized CuTPAs with a difference in crystallization time in Schott bottle (F): (a) F36-MSx-R50, (b) F48-MSx-R50

Effect of time in crystallization of CuTPAs was studied in Schott bottle (F) for 36 and 48 h. There is no considerable difference in shape of crystals (Fig. 5.5); however, layers in cubic structures are looking irregular in the synthesis for 48 h.

Crystal sizes are also changed with crystallization time: range of crystal size: 2-10 μ scales for 36 h; 1-5 μ for 48 h syntheses.

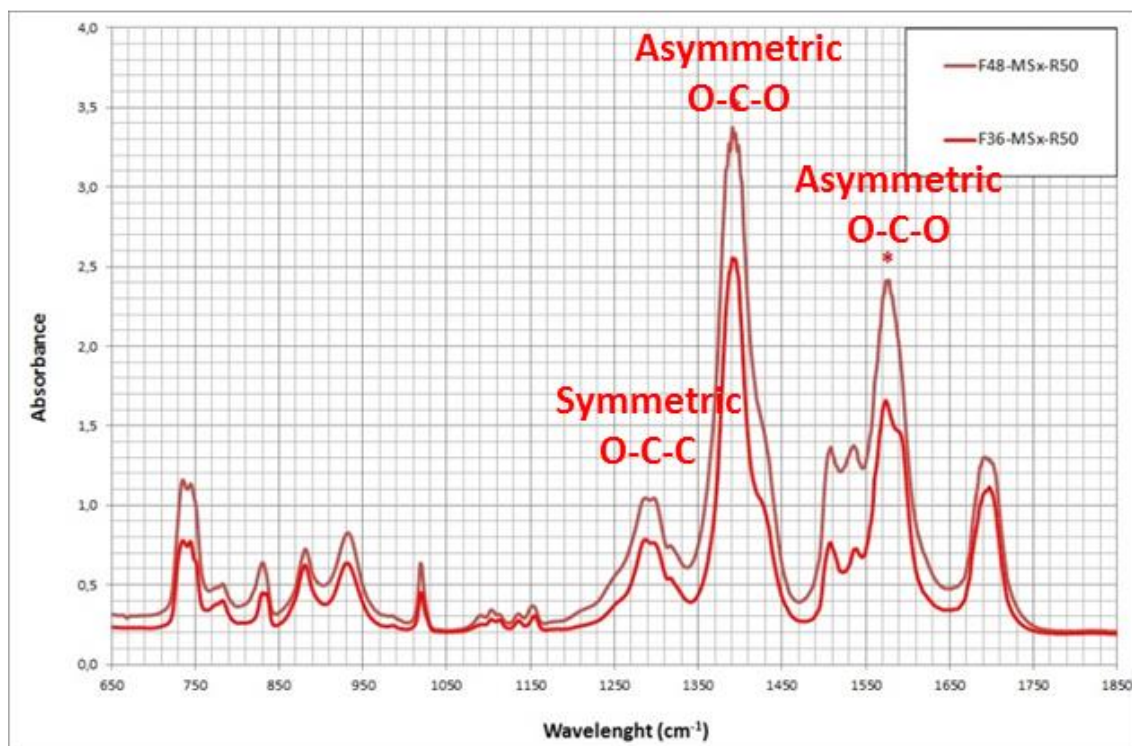


Figure 5.6. FTIR spectra for synthesized under different conditions (36 h and 48 h)

As seen in given Figure 5.6, similar spectra assigning carboxylate (COO^-) groups of CuTPA with 1390 and, 1573 cm^{-1} bands were observed. Similar thermal behavior with one step weight loss which is attributed to decomposition of CuTPA structures at about 330 $^\circ\text{C}$ with 62 % weight loss for both CuTPA metal organic frameworks was observed (Fig. 5.7). As seen from Figure 5.8, characteristic peaks, at 8.3 $^\circ$ (intense) and 8.6 $^\circ$ (less intense) have higher intensity (bigger crystal) for 36 h.

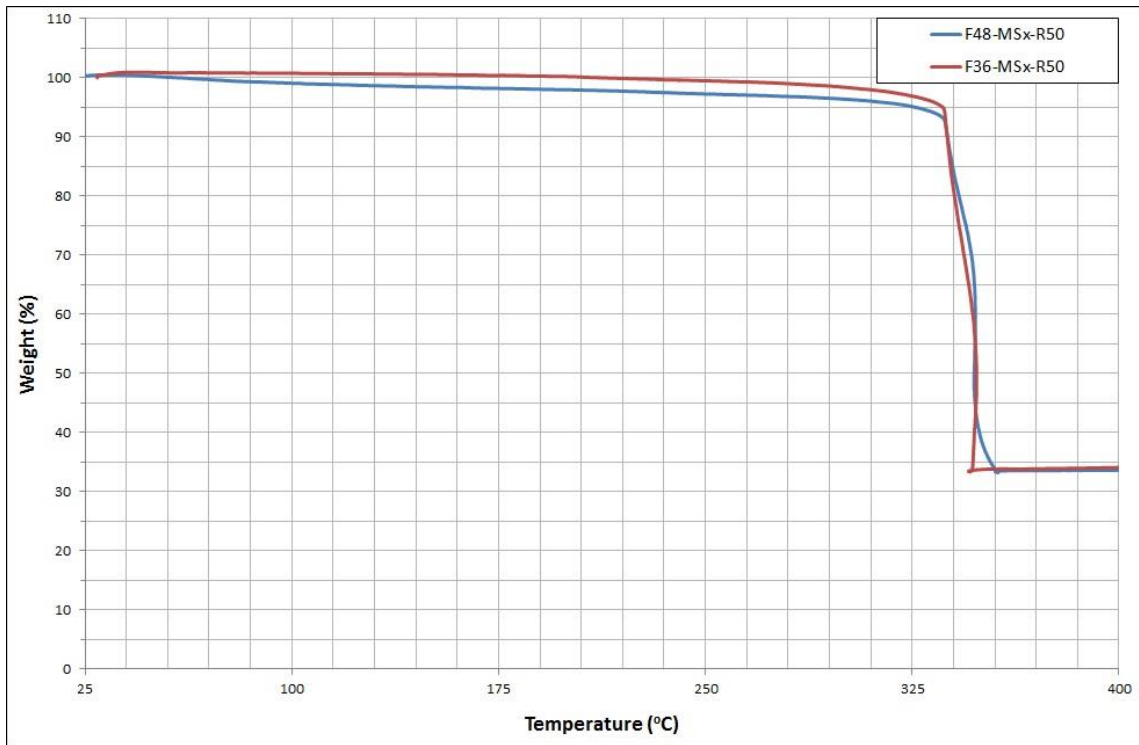


Figure 5.7. Thermal behavior of synthesized CuTPAs for 36 h and 48 h

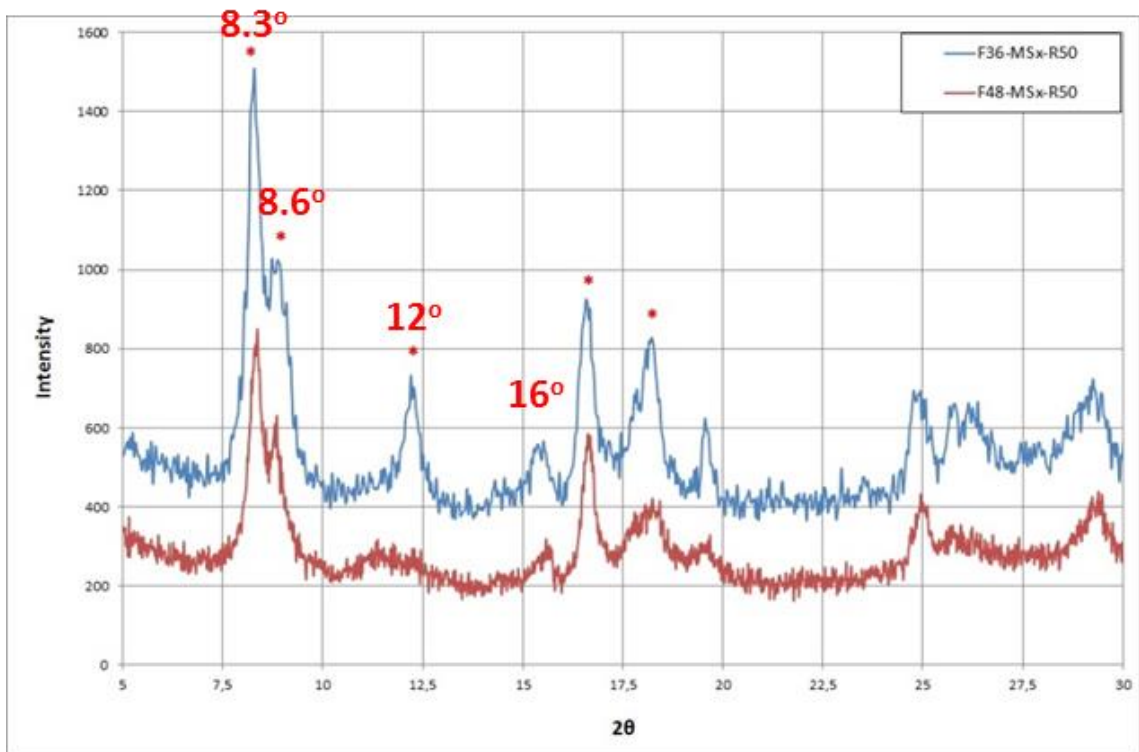


Figure 5.8. XRD pattern of CuTPAs

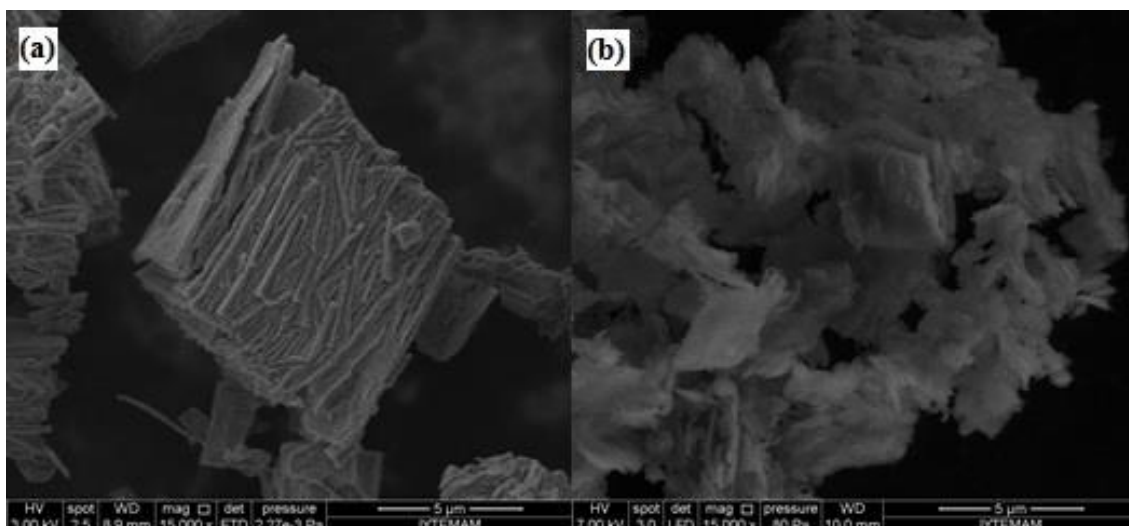


Figure 5.9. SEM images of the CuTPAs synthesized under different crystallization temperature; (a) F36-MSx-R50 (110°C), (b) F36-MSx-R50 (50°C)

According to literature, temperature of crystallization is the most effective parameter on the crystal growth (Carson et al. 2009). Therefore, the procedure followed was modified and synthesis was carried out at 50 °C and 110 °C. As seen from SEM images (Fig. 5.9) when temperature was decreased to 50 °C sheet like crystals with size of 2-5 μ was obtained. From Figure 5.10, carboxylate peaks (1280 cm^{-1} , 1390 cm^{-1} , and 1570 cm^{-1}), phenyl vibration (around 1506 cm^{-1}), and C=O stretching band of TPA (1685 cm^{-1}) can be seen clearly. Thermogravimetric profiles (Fig. 5.11) of the synthesized CuTPAs have one step weight loss. Both CuTPAs decomposed at around 345 °C with 63 % weight loss.

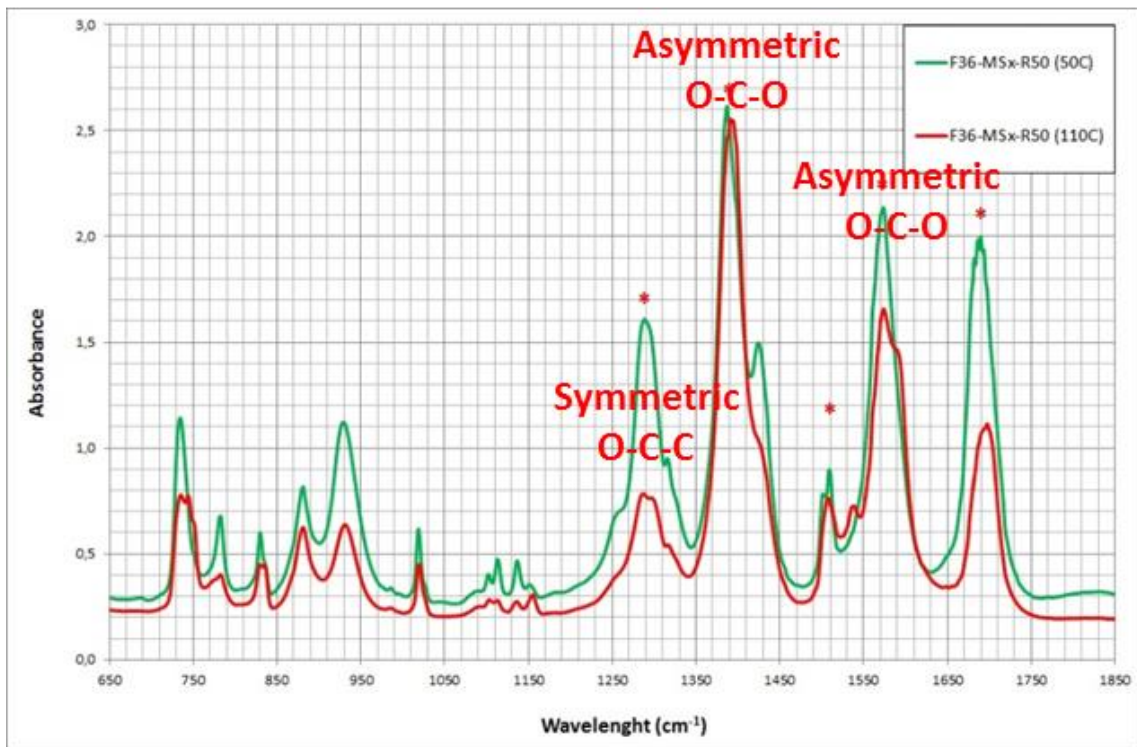


Figure 5.10. Infrared spectra of CuTPAs produced at 50 °C (F36-MS_x-R50 (50°C)) and 110 °C (F36-MS_x-R50 (110°C))

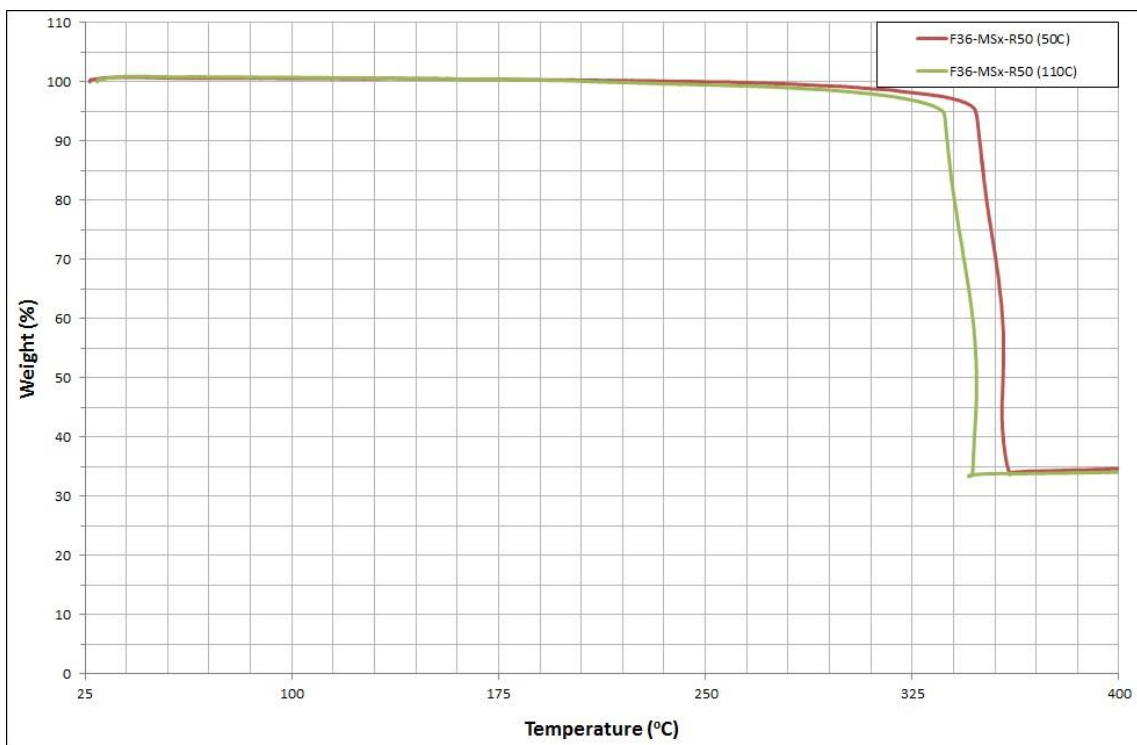


Figure 5.11. Change in thermal stability of the CuTPAs produced at 50 °C (F36-MS_x-R50 (50°C)) and 110 °C (F36-MS_x-R50 (110°C))

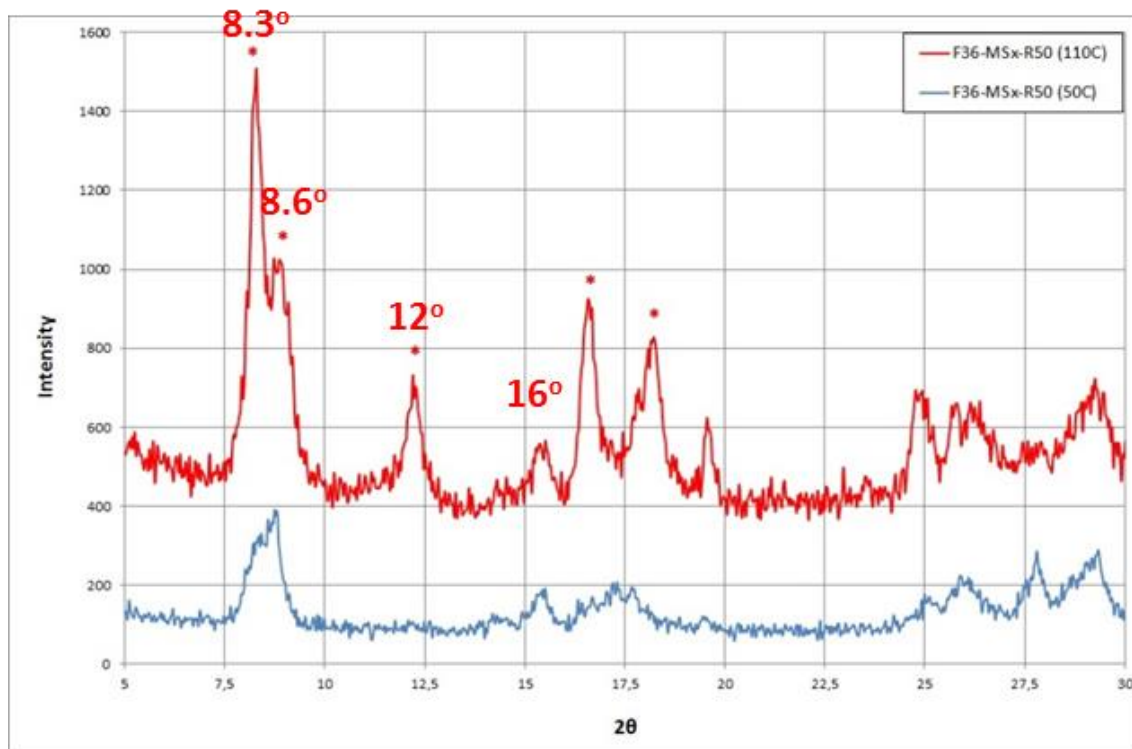


Figure 5.12. X-ray diffractometer pattern of synthesized CuTPAs under different crystallization temperatures

Even they have similar thermal behavior and bond vibrations, the crystals have different shape (sheet like) and size ($2\text{-}5\mu$) for $50\text{ }^{\circ}\text{C}$ and $100\text{ }^{\circ}\text{C}$ synthesis. The main patterns (8.3° , 8.6° , 12° and, 16°) for CuTPA were observed. Only the pattern at 8.6° was observed for $50\text{ }^{\circ}\text{C}$ (Fig. 5.12).

5.1.2. Purification Step

After crystallization, the purification step was applied to remove the unreacted reagents. In purification step, solvent (Dimethylformamide (DMF) or methanol (MeOH)) and purification method (stirring or soxhlet) were examined.

CuTPA obtained from crystallization for 36 h in schott bottle was washed with DMF or MeOH (F36-DSx-R225 and F36-MSx-R225, respectively) by soxhlet extraction to remove the unreacted TPA, copper nitrate and, solvent (DMF). Cubic crystals in the range of $2\text{-}10\mu$ can be seen clearly from the scanning electron microscope images of the CuTPAs (Fig. 5.13). More impurities were observed when CuTPA was

washed with DMF; therefore, MeOH was thought to be more appropriate solvent for removal of impurities (unreacted reagents).

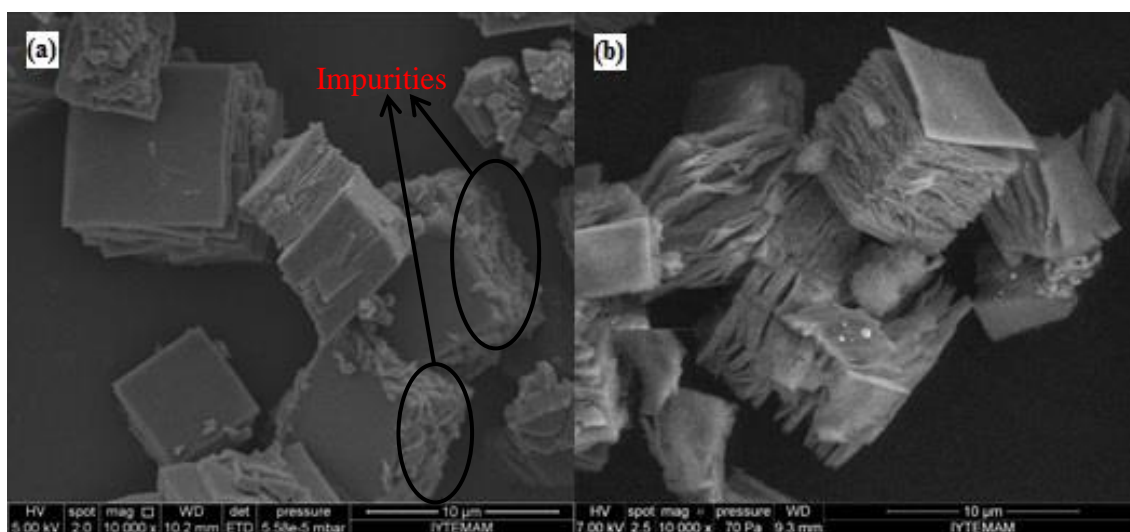


Figure 5.13. SEM micrographs of CuTPAs washed with DMF (F36-DSx-R225) or MeOH (F36-MSx-R225)

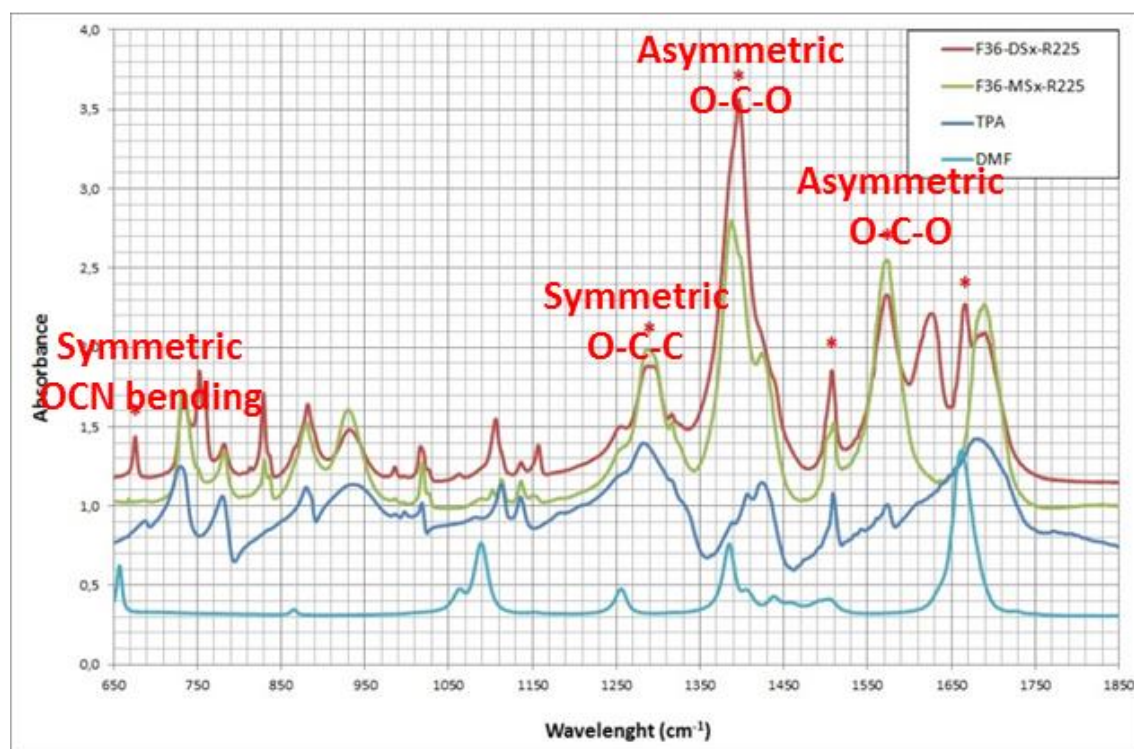


Figure 5.14. FTIR spectra for the CuTPA samples washed with MeOH (F36-MSx-R225) and DMF (F36-DSx-R225)

Figure 5.14 compares the infrared spectrums of CuTPAs, DMF, and TPA to determination of efficiency of solvent in purification step. Characteristic DMF peaks at 675 cm^{-1} (OCN bending) and 1663 cm^{-1} (CO stretching) were observed only in the CuTPA washed with DMF (F36-DSx-R225) as accepted by the SEM images. Presence of these peaks shows that DMF is still in the structure was not removed with thermal activation. Besides, characteristic peaks for CuTPA were observed at around 1280 cm^{-1} , 1390 cm^{-1} , and 1570 cm^{-1} which are assigned to the symmetric and asymmetric stretching of carboxylate groups (COO^-). The peaks assigned to phenyl vibrations, according to Wilson notations 11 and 19a, were also found at around 828 cm^{-1} and 1506 cm^{-1} (Carson et al. 2009).

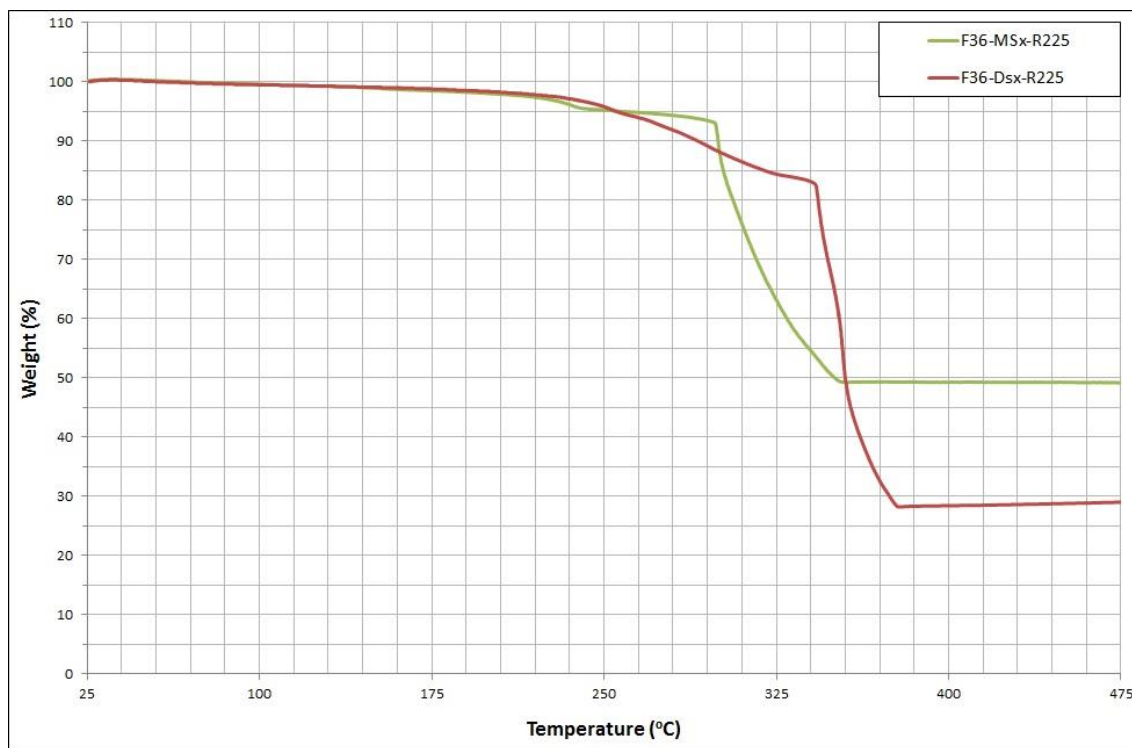


Figure 5.15. TGA curves for CuTPAs washed with different solvent

As shown in Figure 5.15, there are two weight loss steps for the CuTPAs. First step observed in the range of $216\text{--}240\text{ }^{\circ}\text{C}$ and $295\text{--}337\text{ }^{\circ}\text{C}$ for CuTPA washed with MeOH and DMF (2 % and 10 % weight loss, respectively). This weight loss results from the removal of DMF from the structure. This high weight loss observed for the DMF washed sample indicate that high amount of DMF molecules which is coming

from both crystallization and purification steps. Second step observed in the range of 295 - 337 °C and 342 - 387 °C indicates the structural collapse of CuTPAs.

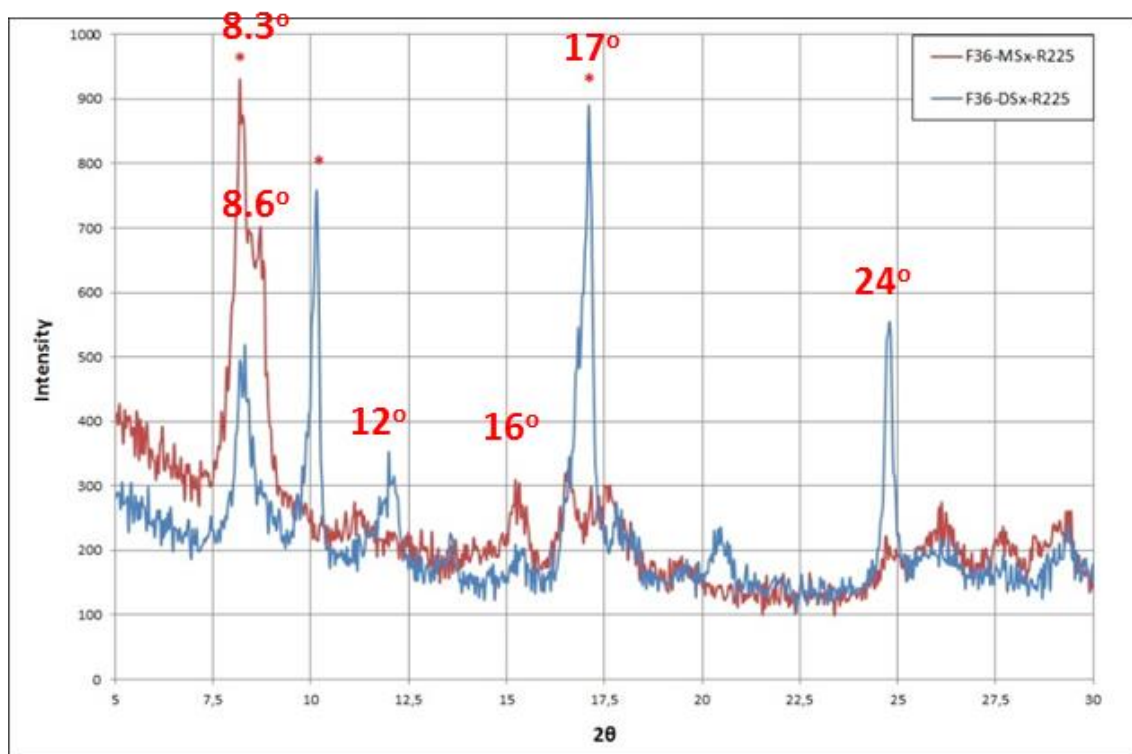


Figure 5.16. XRD pattern of CuTPAs synthesized

Figure 5.16 shows the different X-ray patterns for CuTPA washed with DMF and MeOH as crystal images of SEM. Difference in crystal directions show that thermal activation followed by purification was not effective to remove DMF completely from the structure (Carson et al. 2009). Therefore this difference was elucidated with crystal growth in the activation depending on solvent removal.

Besides to solvent, purification methods (soxhlet or stirring) were studied as parameter. Purification with MeOH by stirring was not effective because layers were splitted out (Fig. 5.17) and looking irregular when compared to soxhlet extraction (Fig. 5.18).

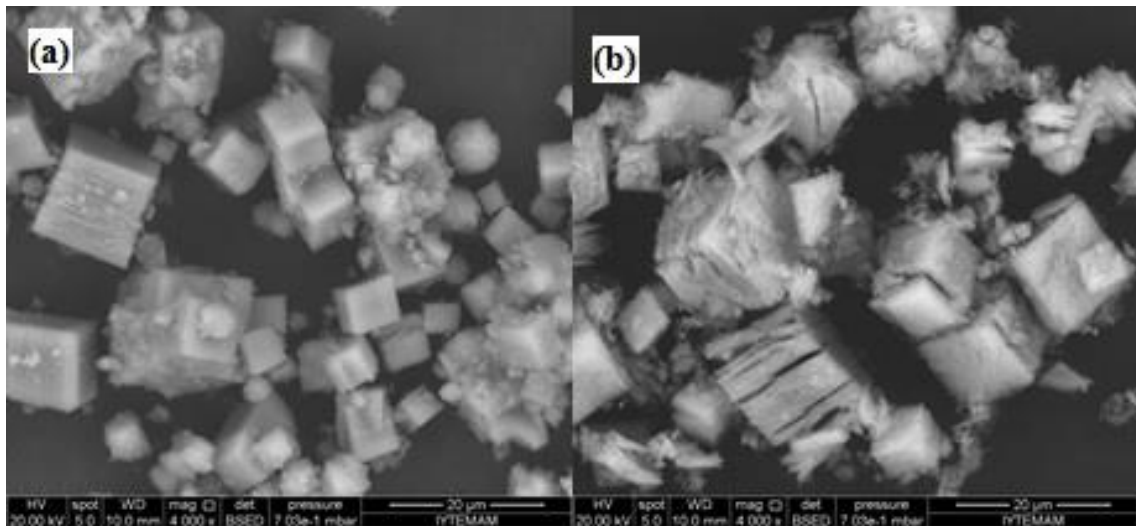


Figure 5.17. SEM micrographs of CuTPAs washed with MeOH under stirring (F36-MSt-R225) (a) after crystallization and (b) after washing

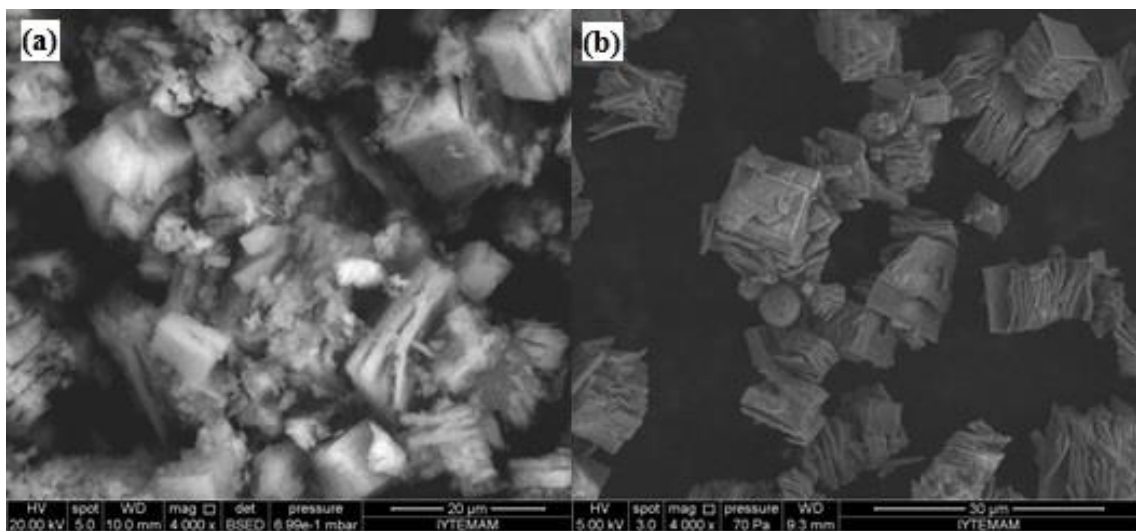


Figure 5.18. SEM micrographs of CuTPAs depending on the washing method: stirring (a) F36-MSt-R225 and soxhlet (b) F36-MSx-R225

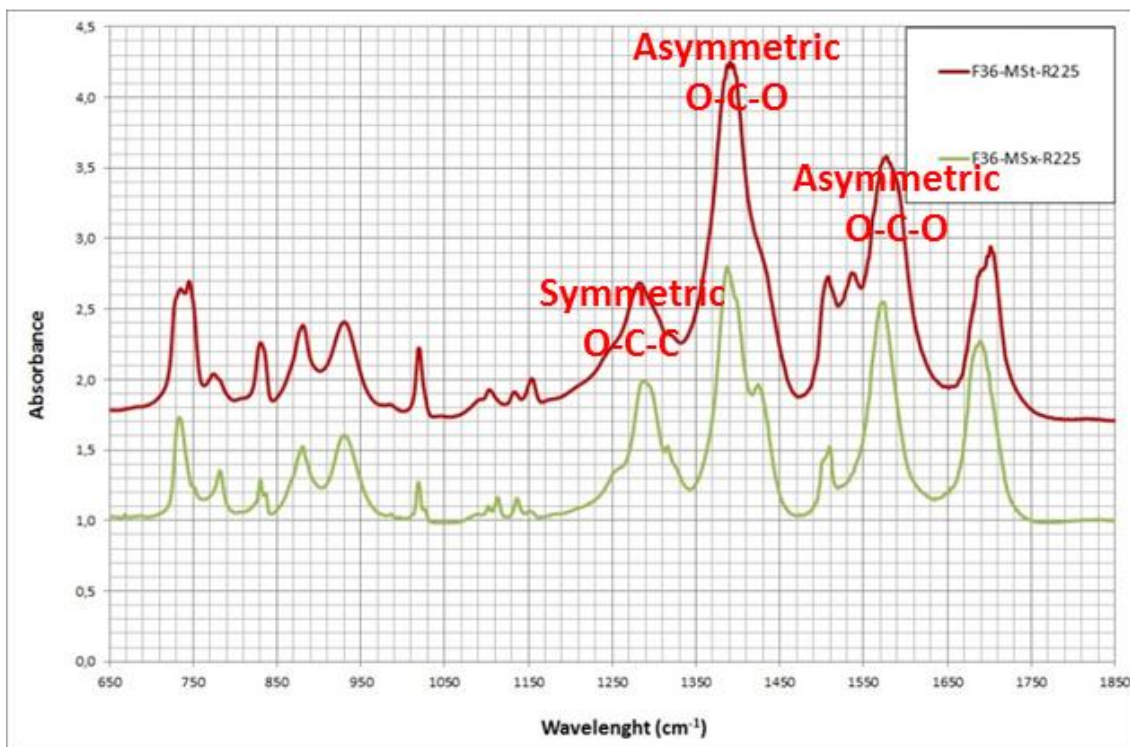


Figure 5.19. FTIR spectra for CuTPA washed with MeOH under stirring (F36-MSt-R225) and soxhlet extraction (F36-MSx-R225)

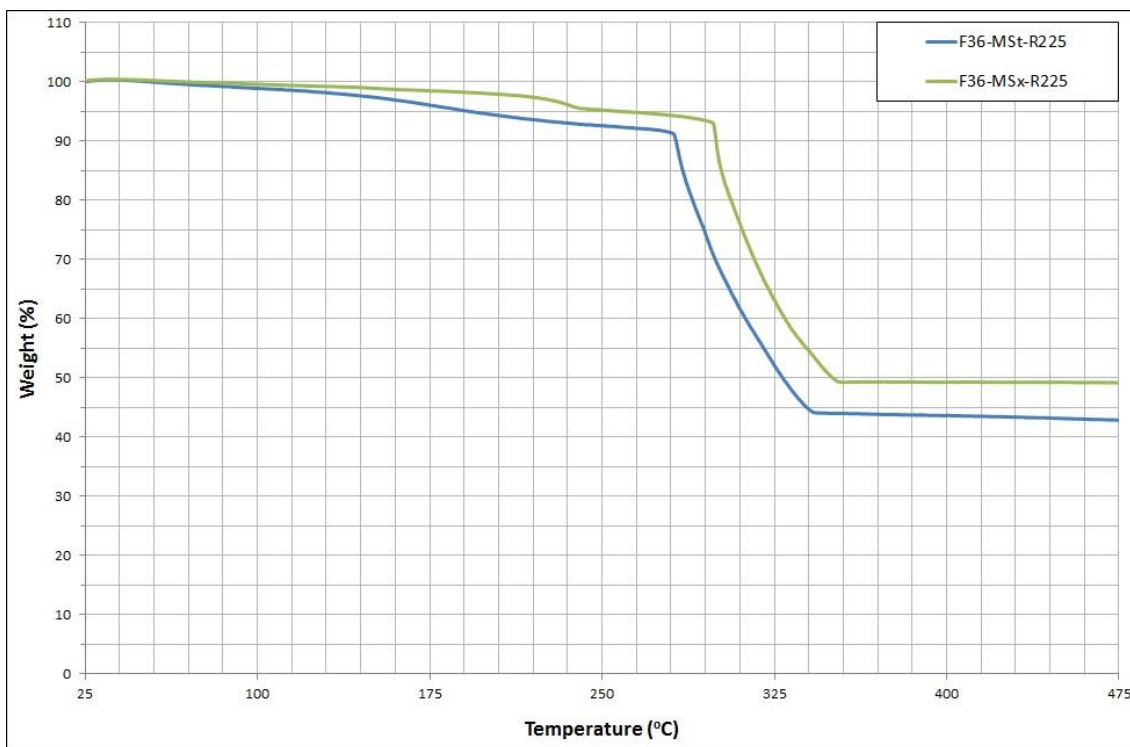


Figure 5.20. TGA curves for CuTPAs washed with MeOH under stirring and soxhlet extraction

FTIR spectra of both sample, washed under stirring and soxhlet extraction, was observed as expected. Characteristic carboxylate peaks of CuTPAs appeared at around 1280 cm^{-1} , 1390 cm^{-1} , and 1570 cm^{-1} (Fig. 5.19).

As can be seen in Figure 5.20, there is no remarkable change between two purification methods. First step observed up to $277\text{ }^{\circ}\text{C}$ and $295\text{ }^{\circ}\text{C}$ was attributed to loss of DMF molecules whereas second step up to $330\text{ }^{\circ}\text{C}$ and $335\text{ }^{\circ}\text{C}$ collapses of the structure for stirring and soxhlet extraction, respectively. Similar XRD patterns were observed for these TPAs (Fig. 5.21).

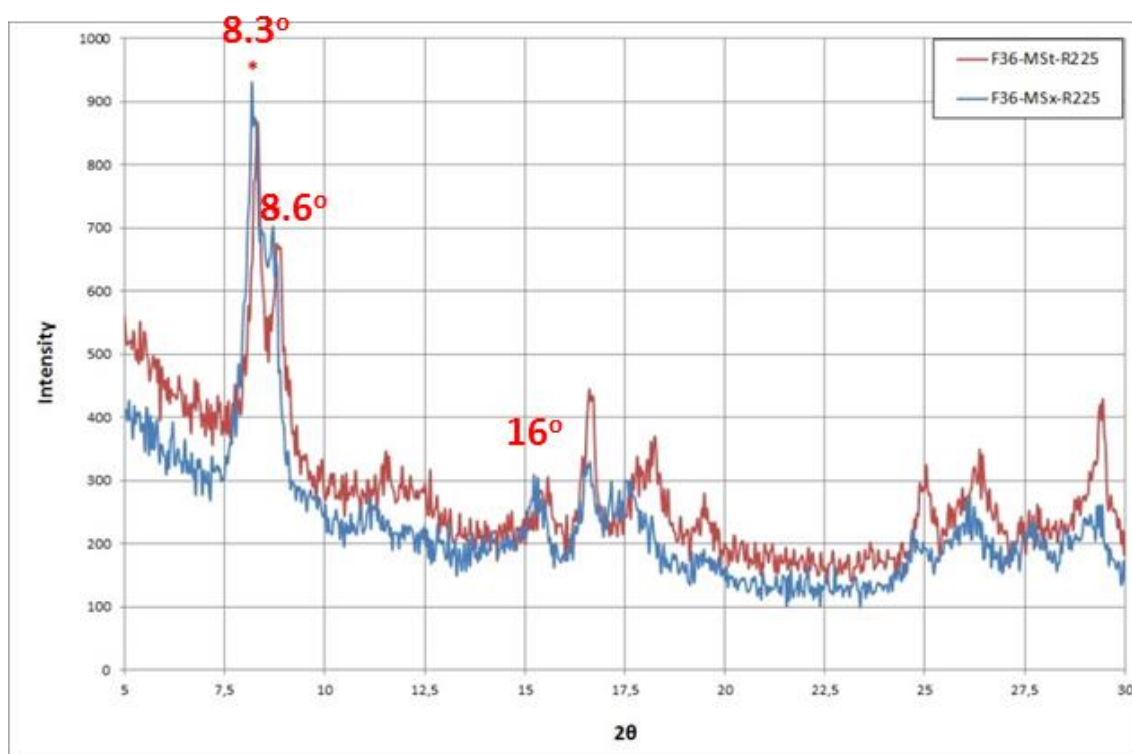


Figure 5.21. XRD pattern of synthesized CuTPAs obtained by string and soxhlet methods

5.1.3. Activation Step

Activation was applied as the last step to the purified CuTPAs for removal of the washing solvent and crystallization solvent (used as solvation medium) to obtain microporous material. Thermal activation was used for this aim. One of the methods was applied with $50\text{ }^{\circ}\text{C}$ step size per hour up to $200\text{ }^{\circ}\text{C}$ (R50) and another was directly

heated from room temperature to 160 °C (R160) under vacuum for 24 h. As the investigation of activation medium CuTPA was directly heated from room temperature to 225 °C (R225) in an oven (7 °C/min) under air. In the literature, it was emphasized that temperature affects the crystal growth in the activation (Carson et al. 2009).

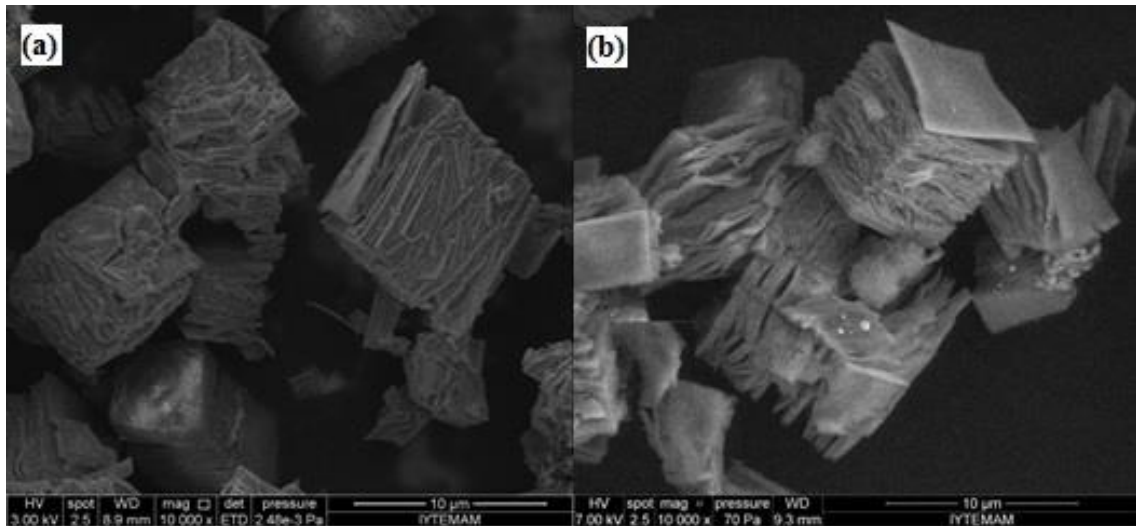


Figure 5.22. SEM micrographs of CuTPAs synthesized by differently activated: (a) F36-MSx-R50, (b) F36-MSx-R225

It can be clearly seen that crystal's shape affected from the heating rate in the activation. Crystals which have same size (2µ-10µ) and shape (cubic) are different when compared to voids between layers (Fig. 5.22). R50 activated crystals are more congested than R225. This is also seen from Figure 5.25 intensity of peaks in the diffractogram.

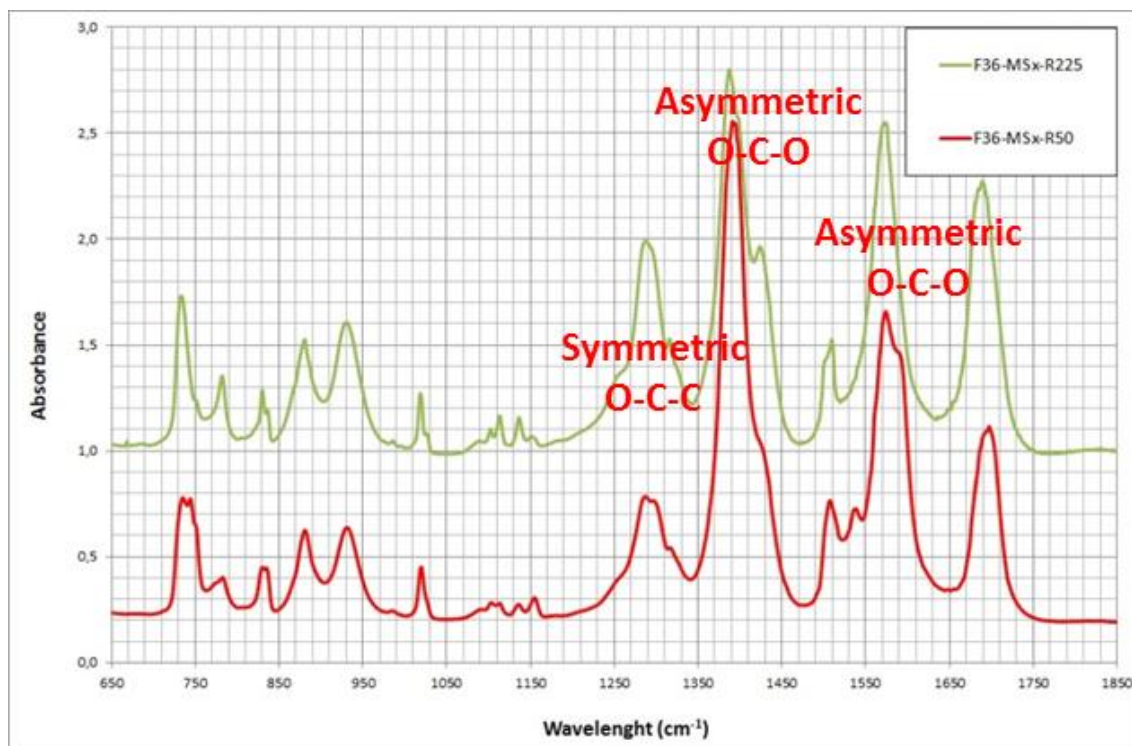


Figure 5.23. FTIR spectra for differently activated CuTPAs

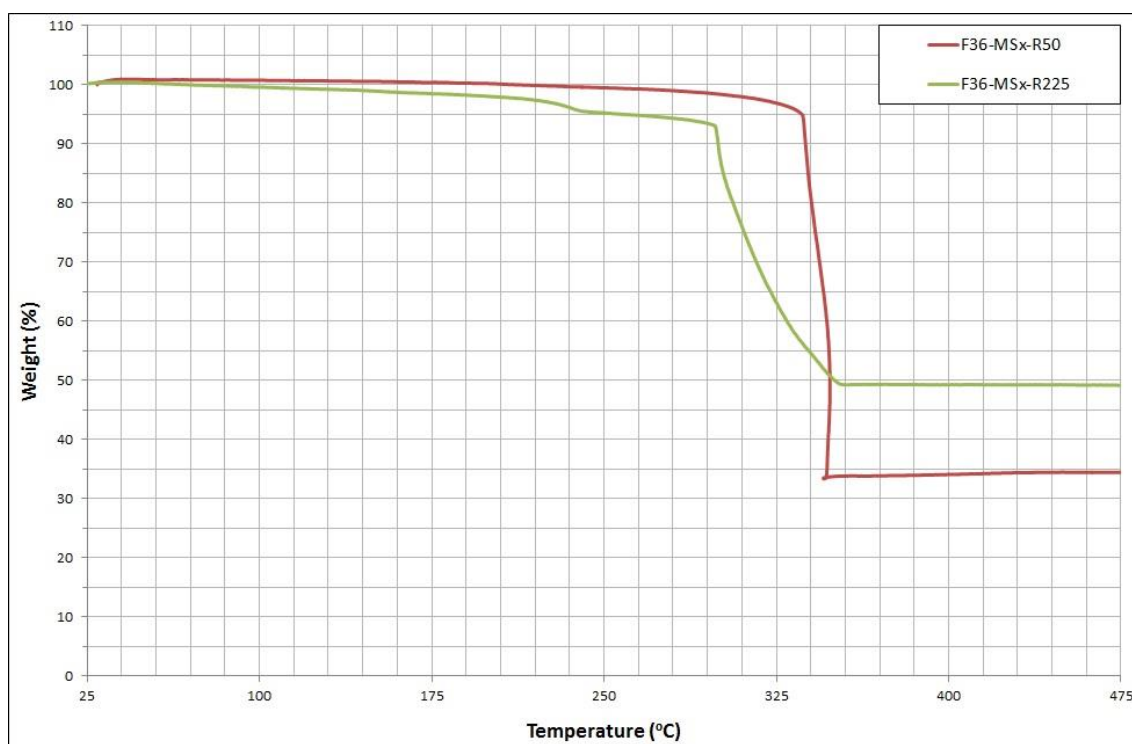


Figure 5.24. TGA curves for CuTPAs synthesized by different activation method

Infrared spectrum of differently activated CuTPAs showed the same absorption bands as expected (Fig. 5.23). In the range between 1250-1650 cm^{-1} , characteristic carboxylate (COO^-) and phenyl vibrational bands of Wilson notation were observed. As it is seen both XRD and TGA curves, absence of DMF in the structure was confirmed.

TGA curves showed the different regime, R225 has two steps (first: removal of DMF, second: structural collapse) weight losses while R50 has one step. This means that activation with ramp (R50) removed the DMF in the structure coming from the crystallization which is not removed with R225 (Fig. 5.24).

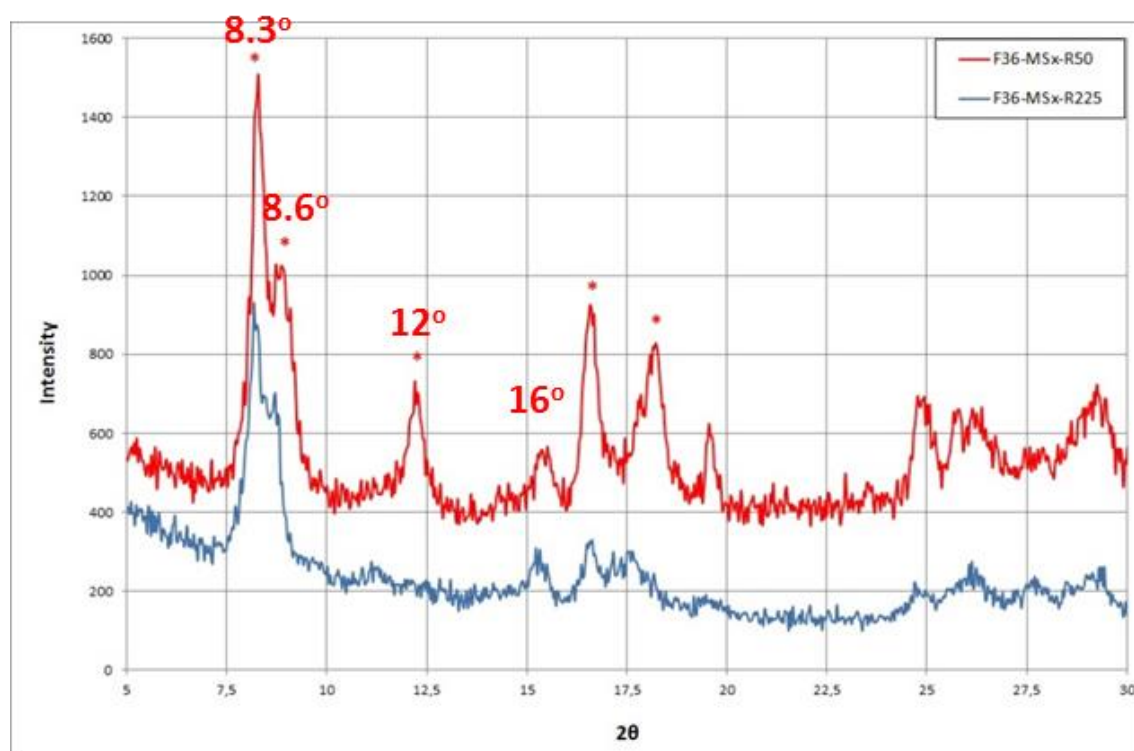


Figure 5.25. XRD pattern of CuTPAs

8.3, 8.6, 12 and 16° peaks are characteristic peaks for CuTPA, difference between methods were also observed in intensity of small peaks which is less intense with R225. Extra peak (18°) were clarified and new crystal direction was observed (Fig. 5.25). This is why SEM micrographs of synthesized CuTPAs activated R50 are looking more congested (Fig. 5.22).

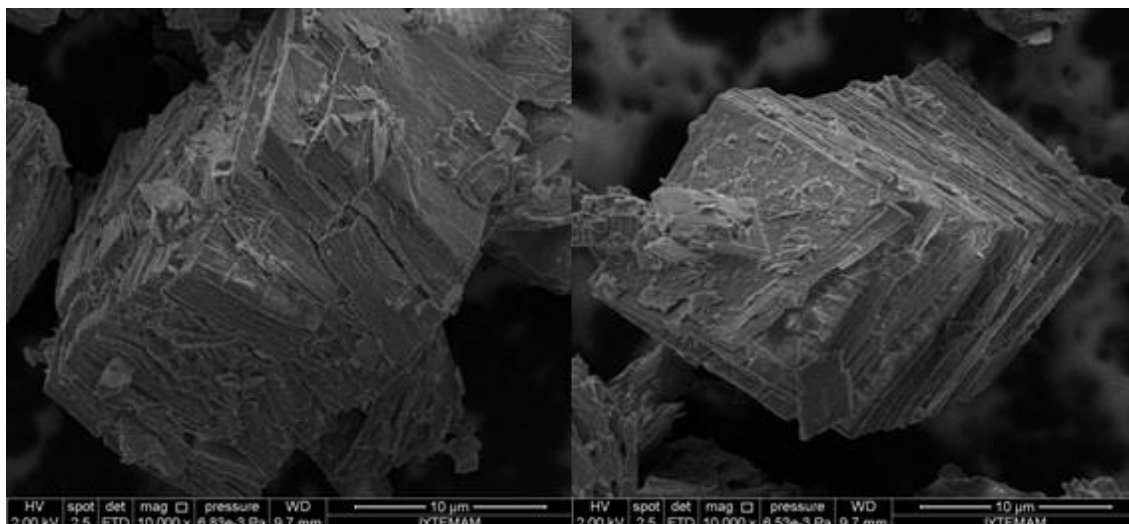


Figure 5.26. SEM images of activated CuTPA at 160 °C (F24-MSx3d-R160)

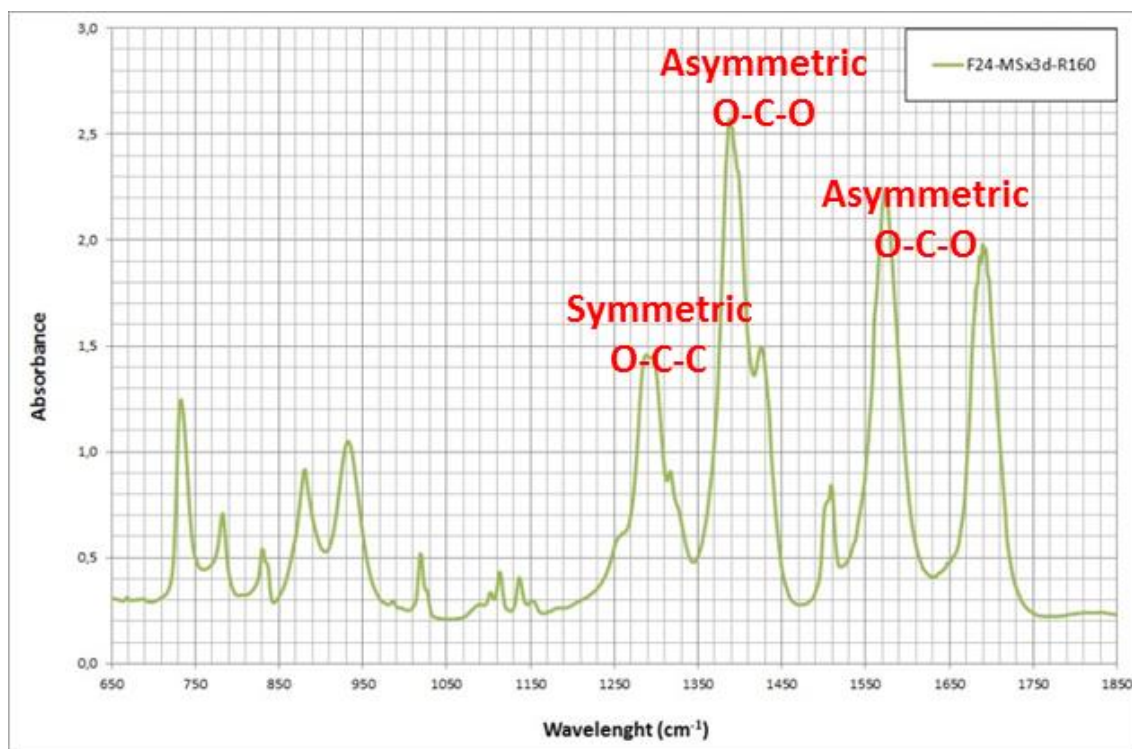


Figure 5.27. Infrared spectra of CuTPA produced at 110 °C for 24 h (F24-MSx3d-R160)

As seen from Figure 5.26, layers in the cubic structure were still appeared. These layers were seen other synthesis which is produced in schott bottle (F) as mentioned before. Bands at around 1280 cm^{-1} , 1390 cm^{-1} , and, 1570 cm^{-1} attributed to symmetric and asymmetric stretchings of carboxylate groups. Peak at 1508 cm^{-1} assigns

to phenyl vibration. C=O stretching band of terephthalic acid (1685 cm^{-1}) also seen (Fig. 5.27). Thermogravimetric profile given in Fig. 5.28 of synthesized CuTPA has one step weight loss. There is no important weight difference up to $336\text{ }^{\circ}\text{C}$ after that structure was collapsed after this temperature.

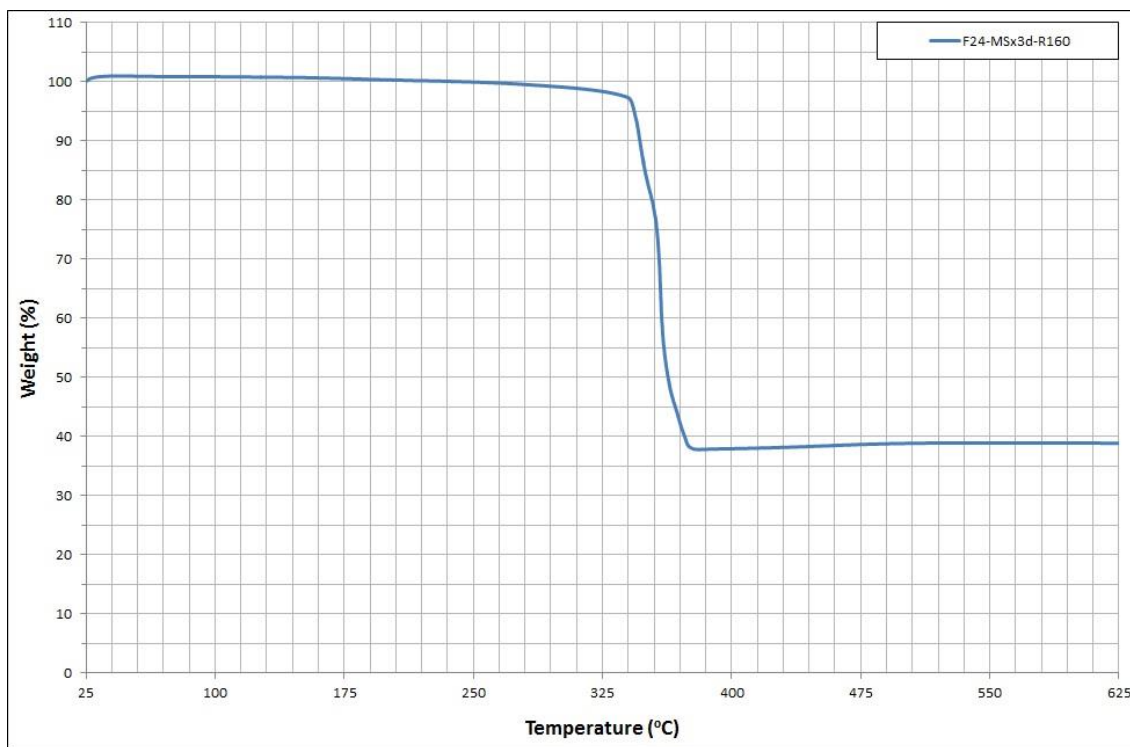


Figure 5.28. Thermal stability of the CuTPA produced at $110\text{ }^{\circ}\text{C}$ (F24-MSx-R50) and activated at $160\text{ }^{\circ}\text{C}$ (F24-MSx3d-R160)

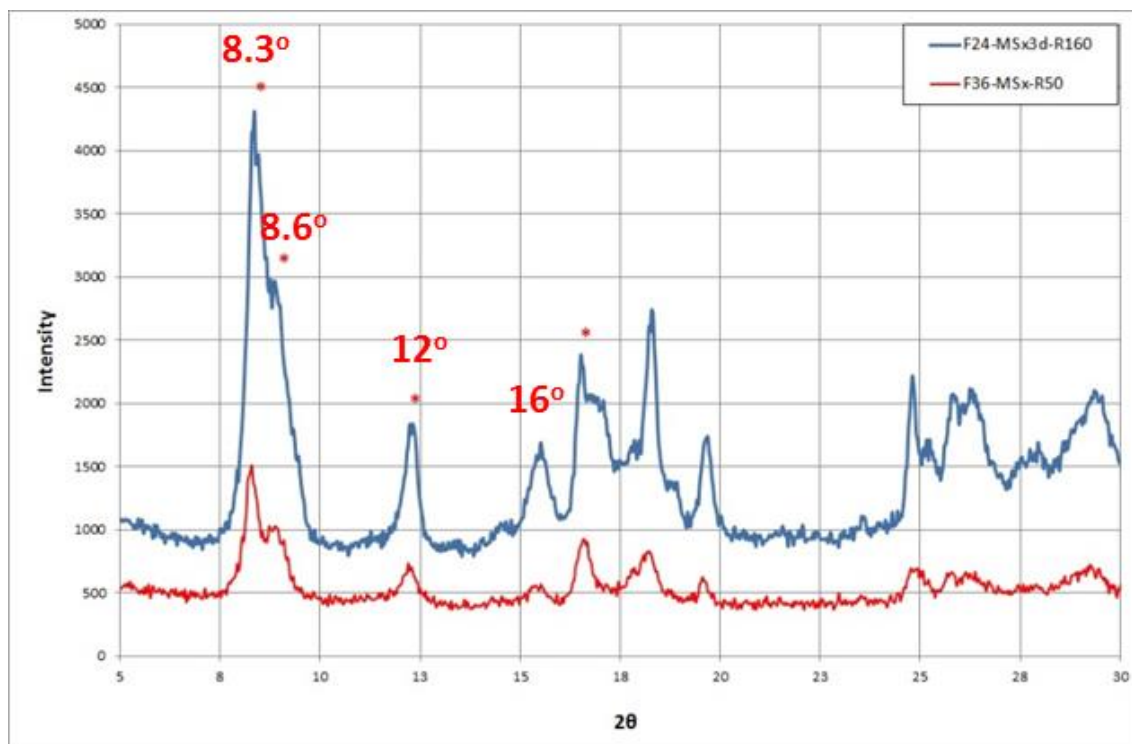


Figure 5.29. X-ray diffractometer pattern of synthesized CuTPA under different activation temperatures

Peaks at 8.3, 8.6, 12 and, 16° are the characteristic peaks. These peaks were seen more intense than other samples. As mentioned before activation time is the most important parameter with purification step. Higher activation cause damage on the pore structure. That is why surface area was found lower samples produced at activation temperature of 200 °C (Fig. 5.29).

5.2. High Pressure Adsorption Studies

CO₂ and H₂ mixture (50/50 %) breakthrough for 13X zeolite and CuTPA was studied for 1, 5 and, 10 bars and 10, 20 and, 30 mL/min total flow rate at 303 K. It was observed that both adsorbents did not adsorb H₂ until breakthrough times (Fig. 5.30 and Fig. 5.40). Figure 5.31-5.33-5.34 -5.35 -5.36 -5.37 show effect of pressure and total feed flow rate on the CO₂ breakthrough curves from equimolar CO₂/H₂ binary mixture. The amount to be adsorbed by the adsorbent in the column is increased with the increasing pressure. Thus the breakthrough times increased with the increasing pressure (Figures 5.35-5.37). As seen from the Fig.5.37, the breakthrough point is increased from

30 min to 87 min by the decreasing total flow rate from 30 to 10 mL/min at 10 bars. Desorption curves at 303 K for 10 mL/min total flow rate at 1, 5 and, 10 bars were given in figure 5.32. The highest desorption times were observed for 13X.

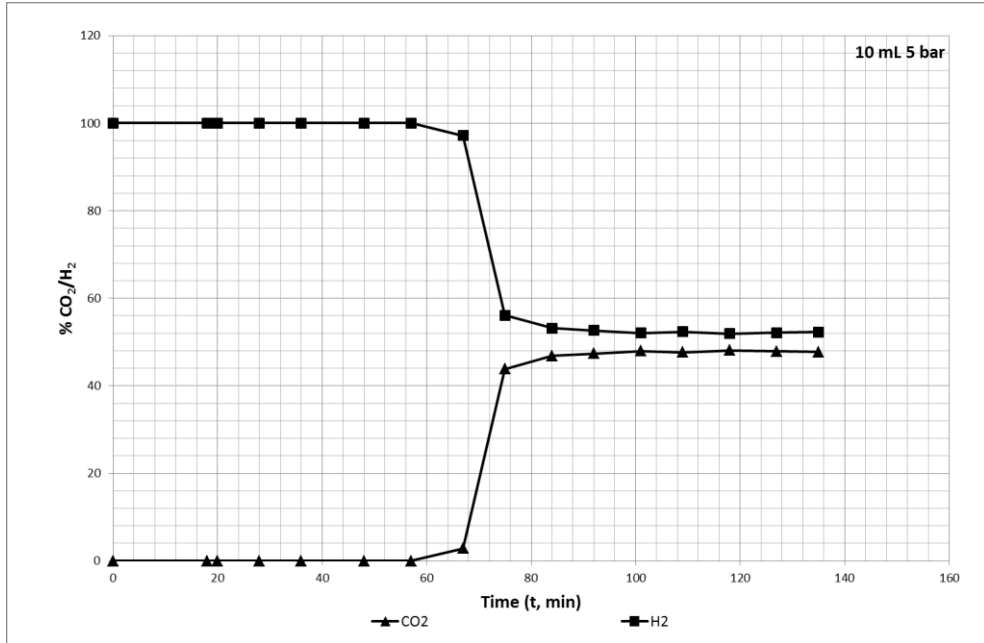


Figure 5.30. Breakthrough curves of CO₂ and H₂ effluent over 13X

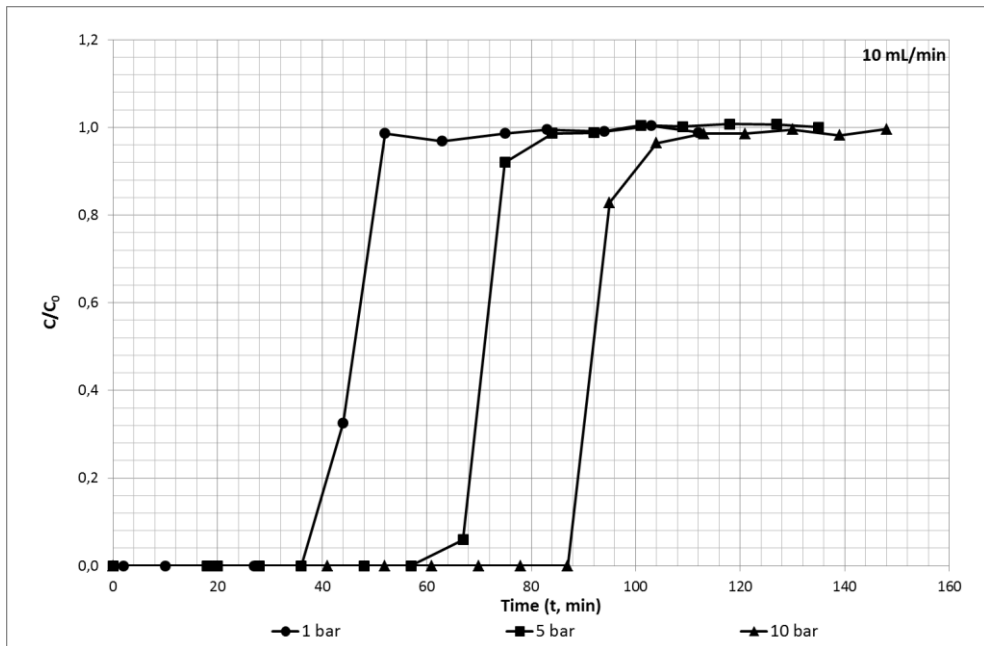


Figure 5.31. Effect of pressure on CO₂ adsorption breakthrough curves in 13X zeolite (Total flow rate= 10 mL/min)

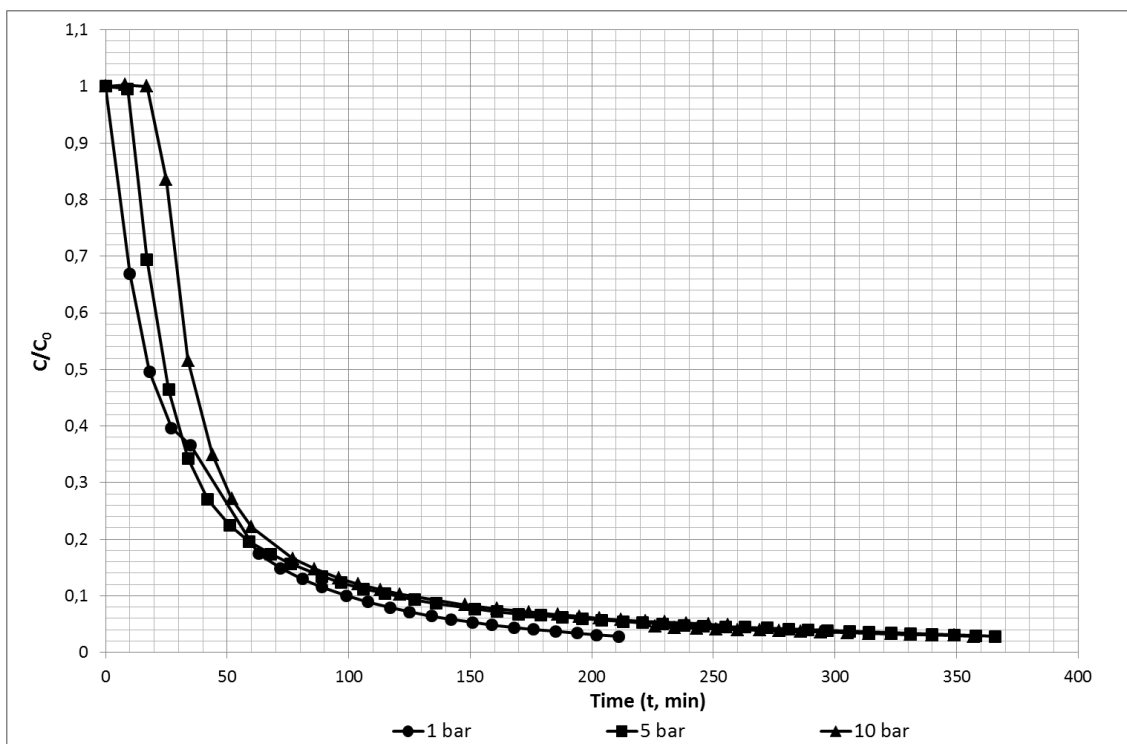


Figure 5.32. CO₂ desorption curves with helium flow over 13X zeolite (Flow rate (He)= 20 mL/min)

Table 5.2. Breakthrough, adsorption and, desorption times for CO₂ over 13X

		Breakthrough time (min)	Adsorption time (min)	Desorption time (min)
10 mL/min	1 bar	36	83	211
	5 bar	57	101	366
	10 bar	87	130	357

As can be seen from table 5.2, breakthrough times, adsorption times and, desorption times increased with the increasing pressure for 10 mL/min total flow rate of equimolar CO₂/H₂ mixture. Highly microporous structure and narrow pores causes this.

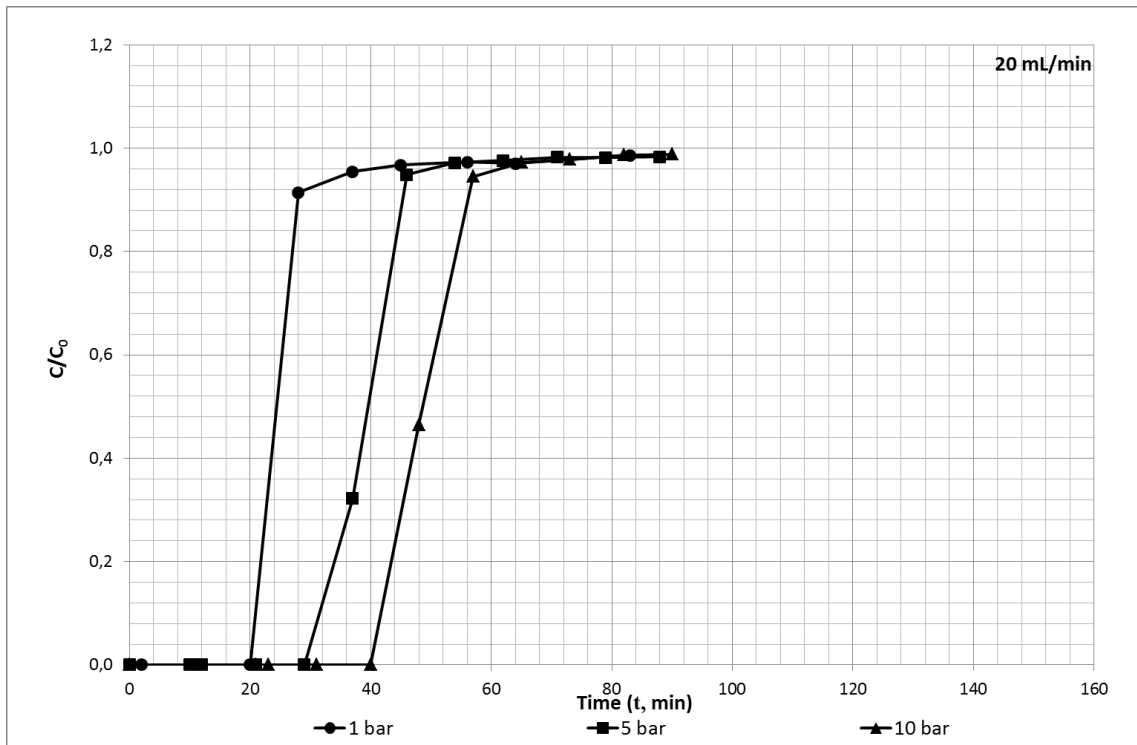


Figure 5.33. Effect of pressure on CO₂ adsorption breakthrough curves in 13X zeolite (Total flow rate= 20 mL/min)

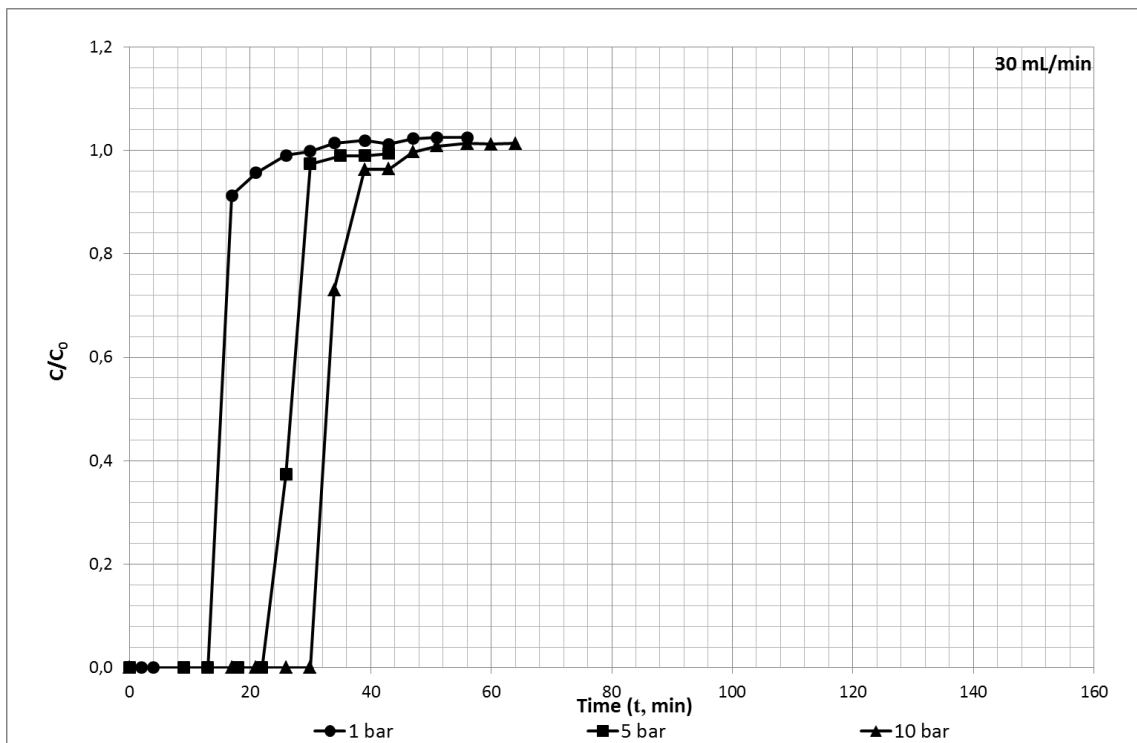


Figure 5.34. Effect of pressure on CO₂ adsorption breakthrough curves in 13X zeolite (Total flow rate= 30 mL/min)

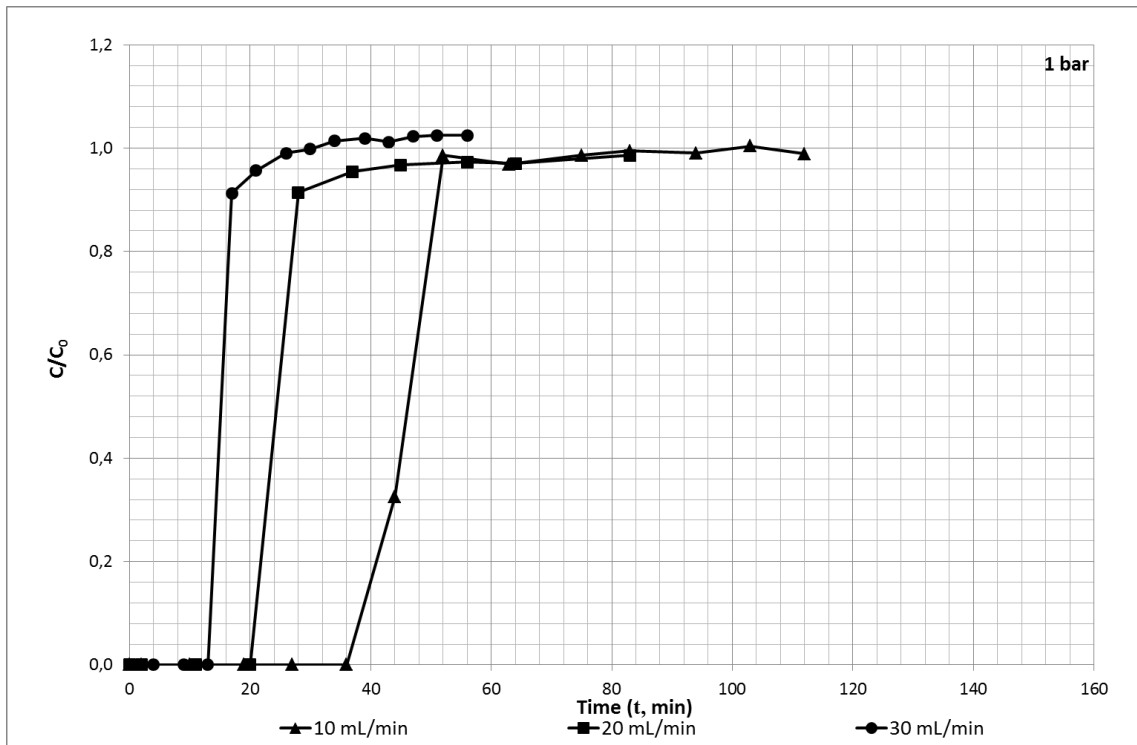


Figure 5.35. Effect of feed flow rate on CO₂ adsorption breakthrough curves in 13X zeolite (P= 1 bar)

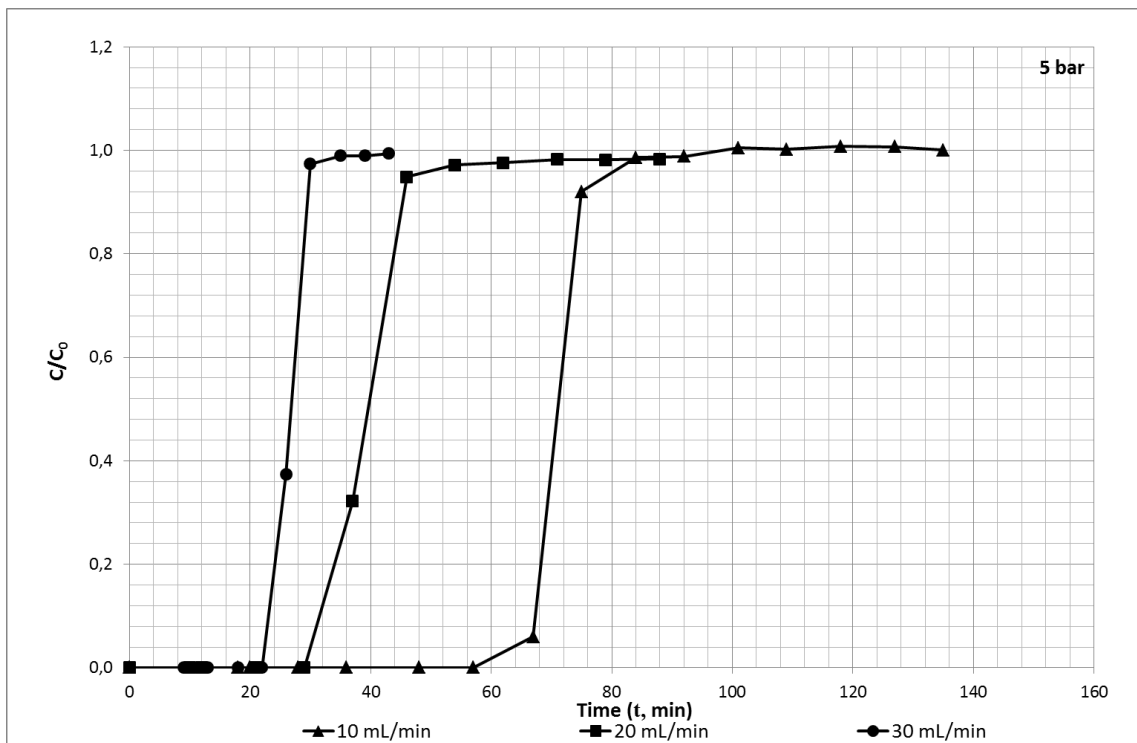


Figure 5.36. Effect of feed flow rate on CO₂ adsorption breakthrough curves in 13X zeolite (P= 5 bar)

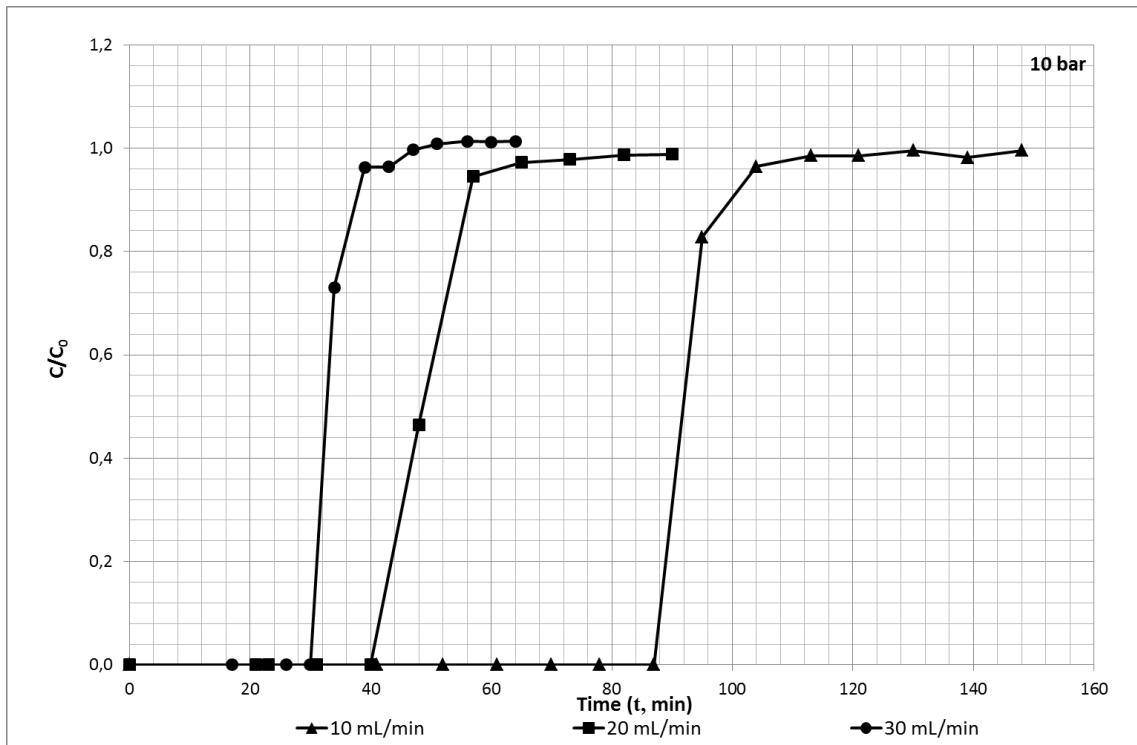


Figure 5.37. Effect of feed flow rate on CO₂ adsorption breakthrough curves in 13X zeolite (P= 10 bar)

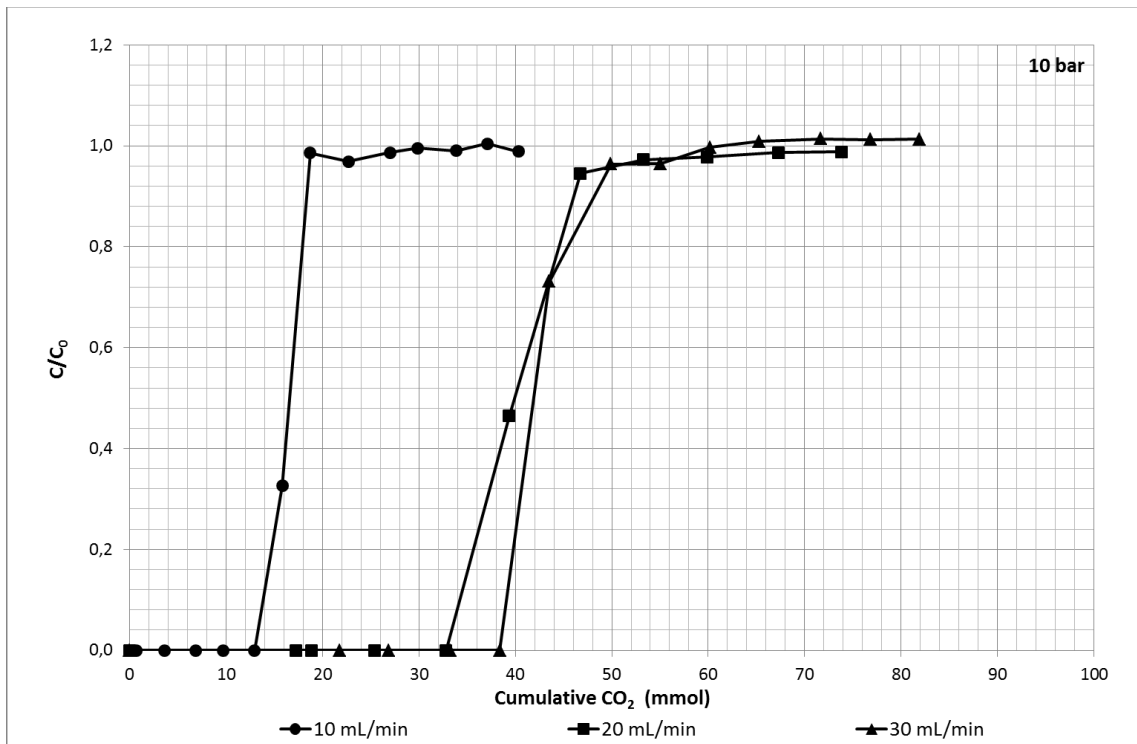


Figure 5.38. Cumulative CO₂ flow in feed versus CO₂ fraction at out flow (P= 10 bar)

The breakthrough curves given in Fig. 5.38 were obtained by replacing time by cumulative CO₂ flow in. The curves obtained for 20 and 30 ml/min are overlapped but that of 10 ml/min don't. This shows that for the adsorption mechanism, controlling mechanism is different in 10 ml/min case. The amount adsorbed was increased (7.01 mmol/g) when flow rate was increased from 10 to 30 mL/min at 10 bars (Table 5.3 and Fig. 5.37). For the flow rate of 20 mL/min, calculated amount adsorbed 4.11 (1 bar) and 5.92 mmol/g (5 bars) are almost same with the literature (Peter et al. 2013). Adsorption isotherms of 13X for different flow rate at 10 bars was given in Figure 5.39.

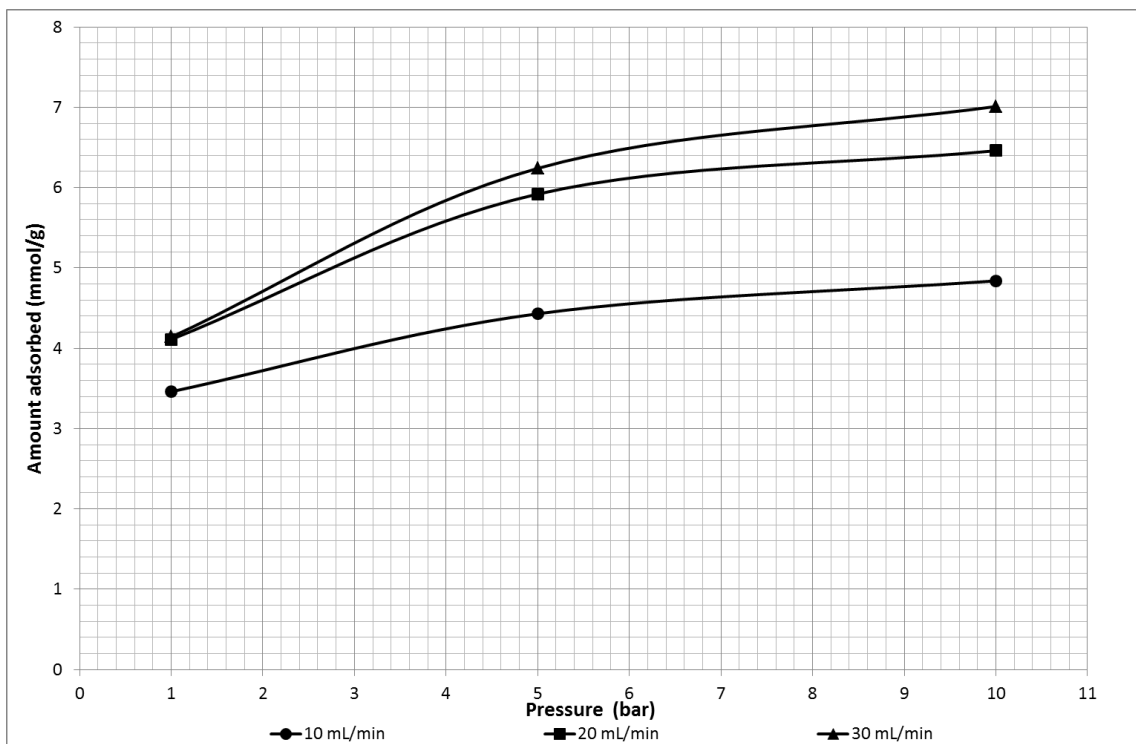


Figure 5.39. Adsorption isotherms of CO₂ in 13X zeolite at different flow rates at 303 K

Table 5.3. CO₂ amount adsorbed by 13X

Total flow rate (mL/min)	Pressure (bar)	τ_a (min)	F_{ao} (mmol/min)	X_a	q_{ads} (mmol/g)
10	1	47.10	0.36	0.48	3.46
	5	71.11	0.36	0.48	4.43
	10	90.88	0.36	0.48	4.84
20	1	24.36	0.82	0.49	4.11
	5	39.70	0.82	0.49	5.92
	10	49.25	0.82	0.49	6.46
30	1	15.70	1.28	0.49	4.14
	5	26.60	1.28	0.49	6.24
	10	33.52	1.28	0.49	7.01

As can be seen from figure 5.41, 5.43, 5.44, 5.45, 5.46 and, 5.47, effect of pressure and total feed flow rate on the CO₂ breakthrough curves from equimolar CO₂/H₂ binary mixture was studied. The amount adsorbed by CuTPA is increased with the increasing pressure. Thus the breakthrough times increased with the increasing pressure (Figures 5.45-5.47). As seen from the Fig.5.47, the breakthrough point is increased from 2 min to 9 min by the decreasing total flow rate from 30 to 10 mL/min at 10 bars. Desorption curves at 303 K for 10 mL/min total flow rate at 1, 5 and, 10 bars were given in figure 5.42.

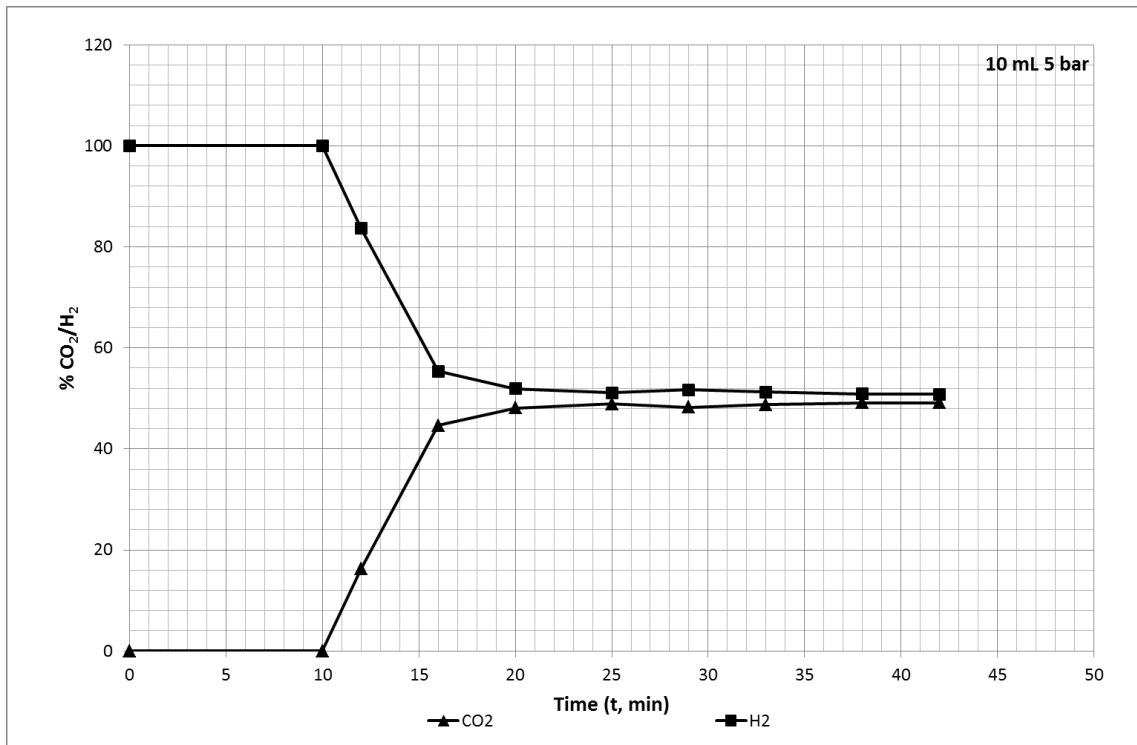


Figure 5.40. Breakthrough curves of CO₂ and H₂ effluent over CuTPA

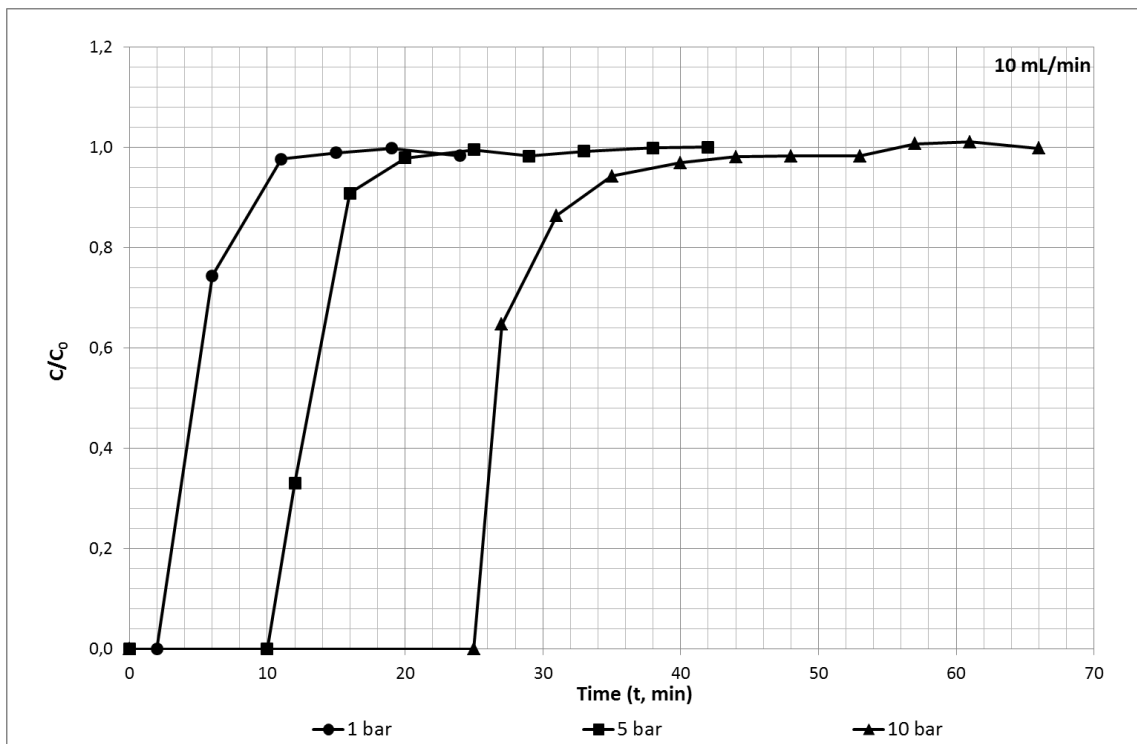


Figure 5.41. Effect of pressure on CO₂ adsorption breakthrough curves in CuTPA (Total flow rate= 10 mL/min)

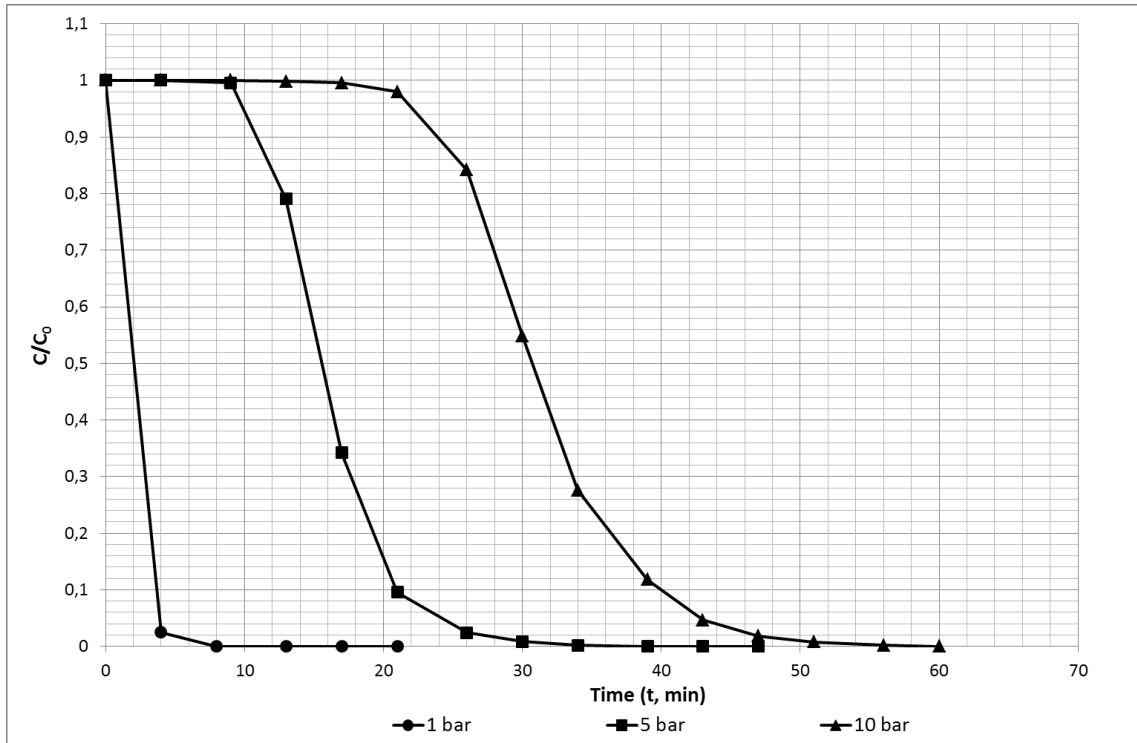


Figure 5.42. CO₂ desorption curves with helium flow over CuTPA (Flow rate (He)= 20 mL/min)

Table 5.4. Breakthrough, adsorption and, desorption times for CO₂ over CuTPA

		Breakthrough time (min)	Adsorption time (min)	Desorption time (min)
10 mL/min	1 bar	2	19	8
	5 bar	10	38	39
	10 bar	25	57	60

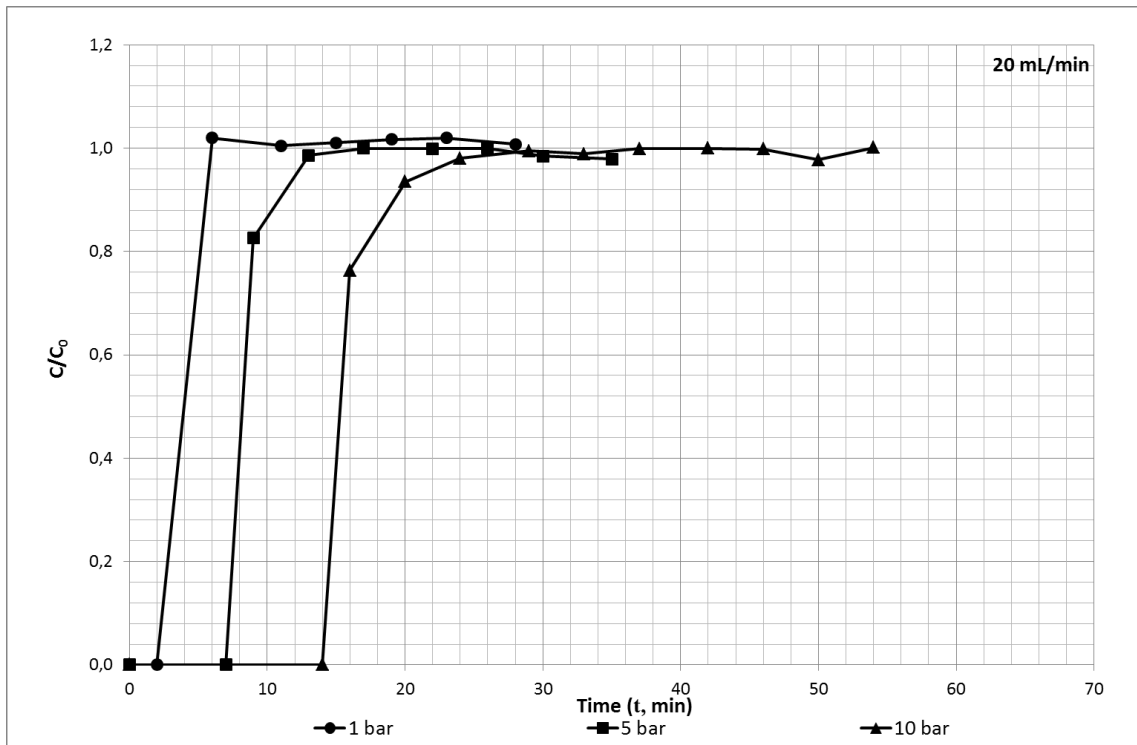


Figure 5.43. Effect of pressure on CO₂ adsorption breakthrough curves in CuTPA (Total flow rate= 20 mL/min)

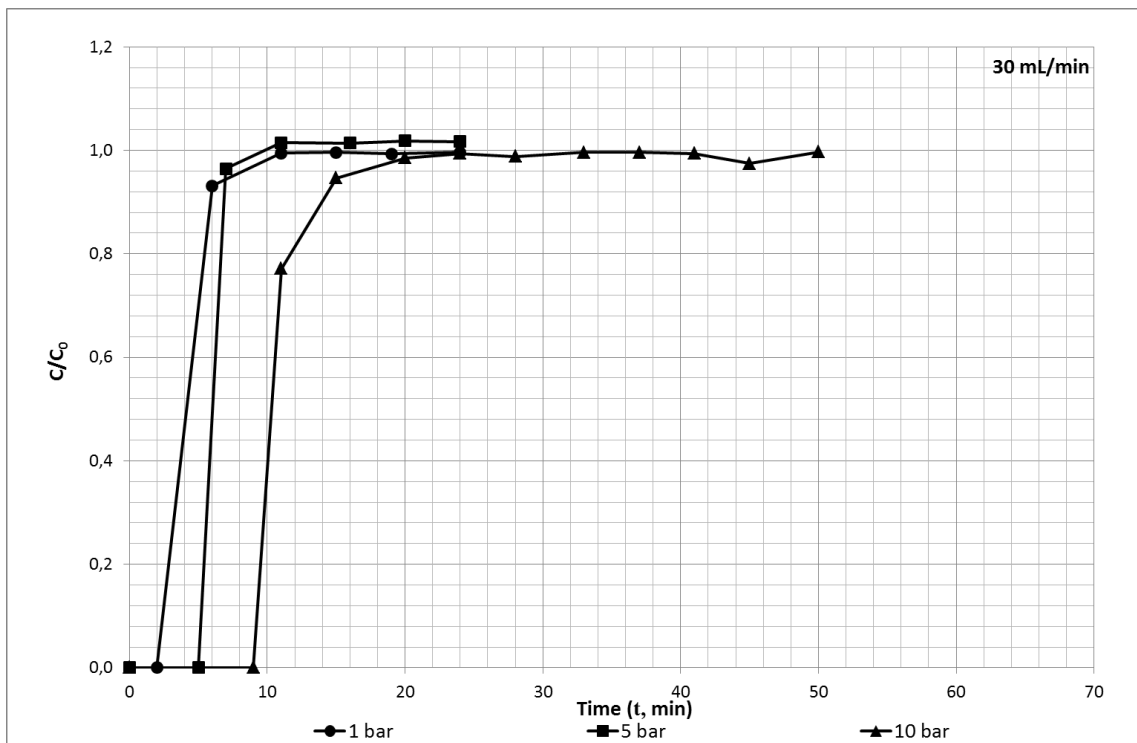


Figure 5.44. Effect of pressure on CO₂ adsorption breakthrough curves in CuTPA (Total flow rate= 30 mL/min)

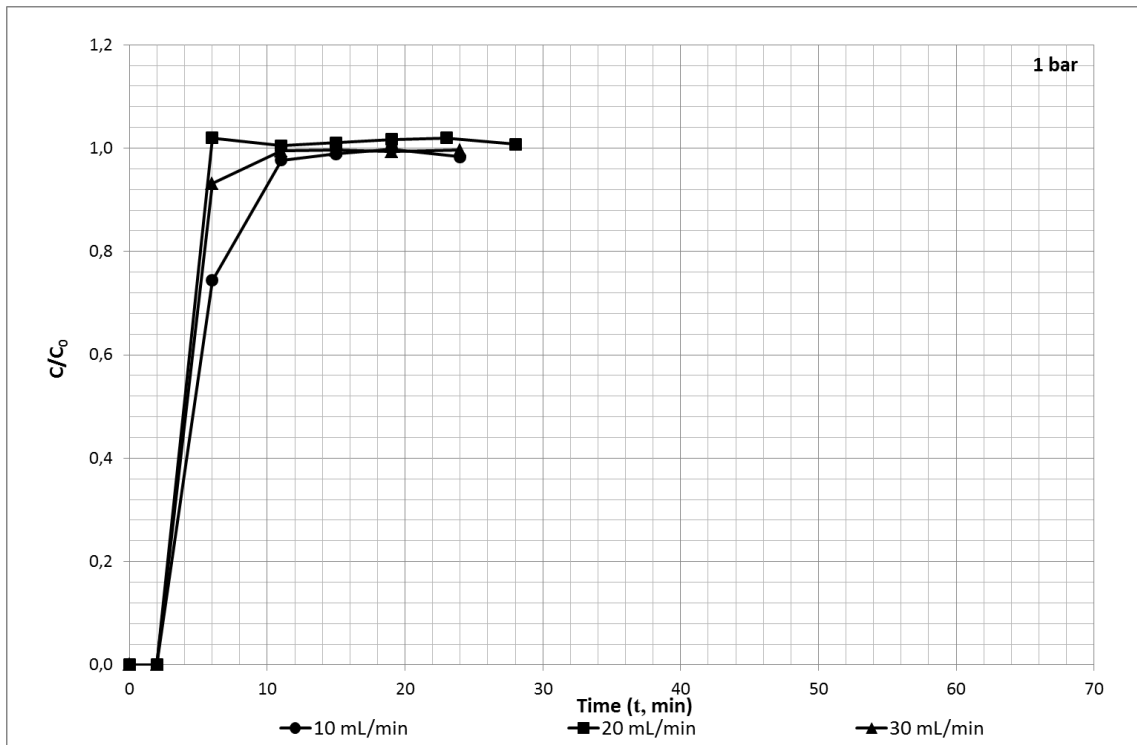


Figure 5.45. Effect of feed flow rate on CO₂ adsorption breakthrough curves in CuTPA (P= 1 bar)

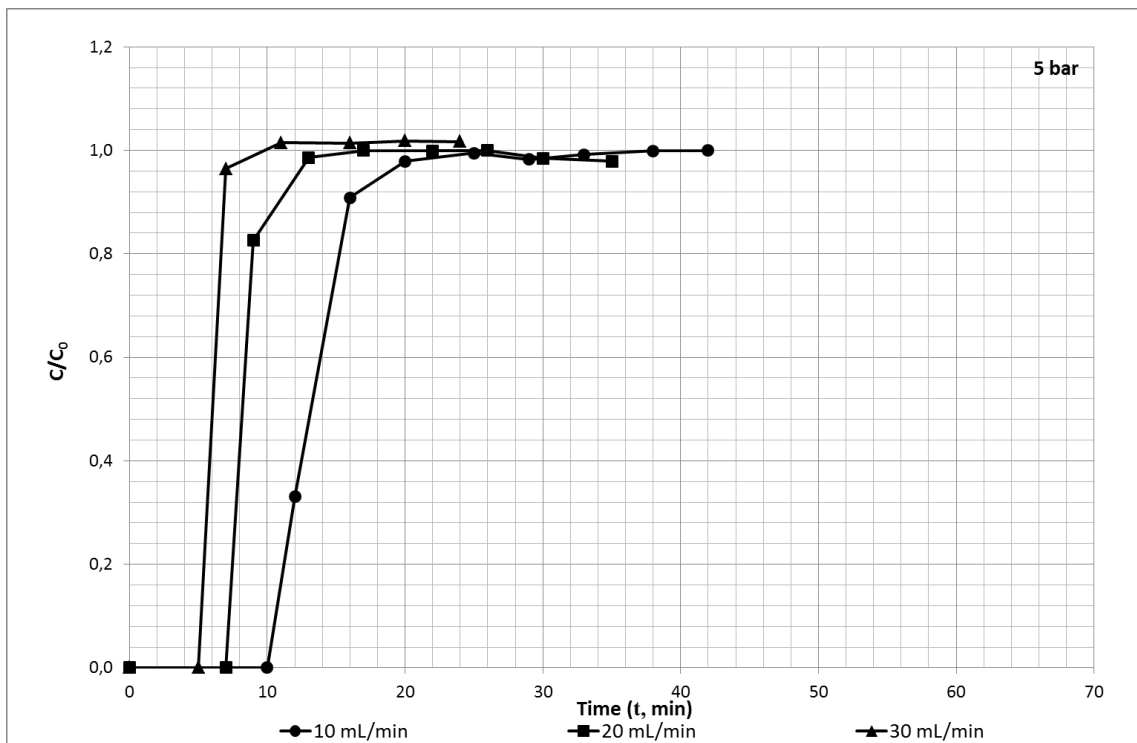


Figure 5.46. Effect of feed flow rate on CO₂ adsorption breakthrough curves in CuTPA (P= 5 bar)

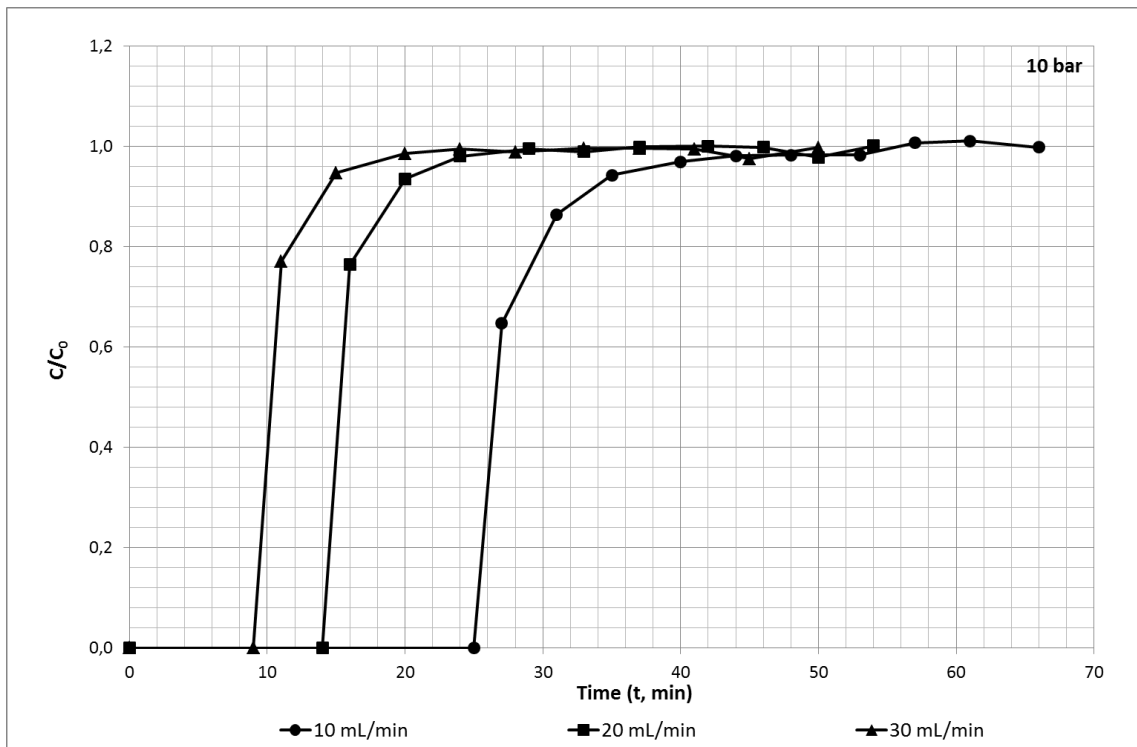


Figure 5.47. Effect of feed flow rate on CO₂ adsorption breakthrough curves in CuTPA (P= 10 bar)

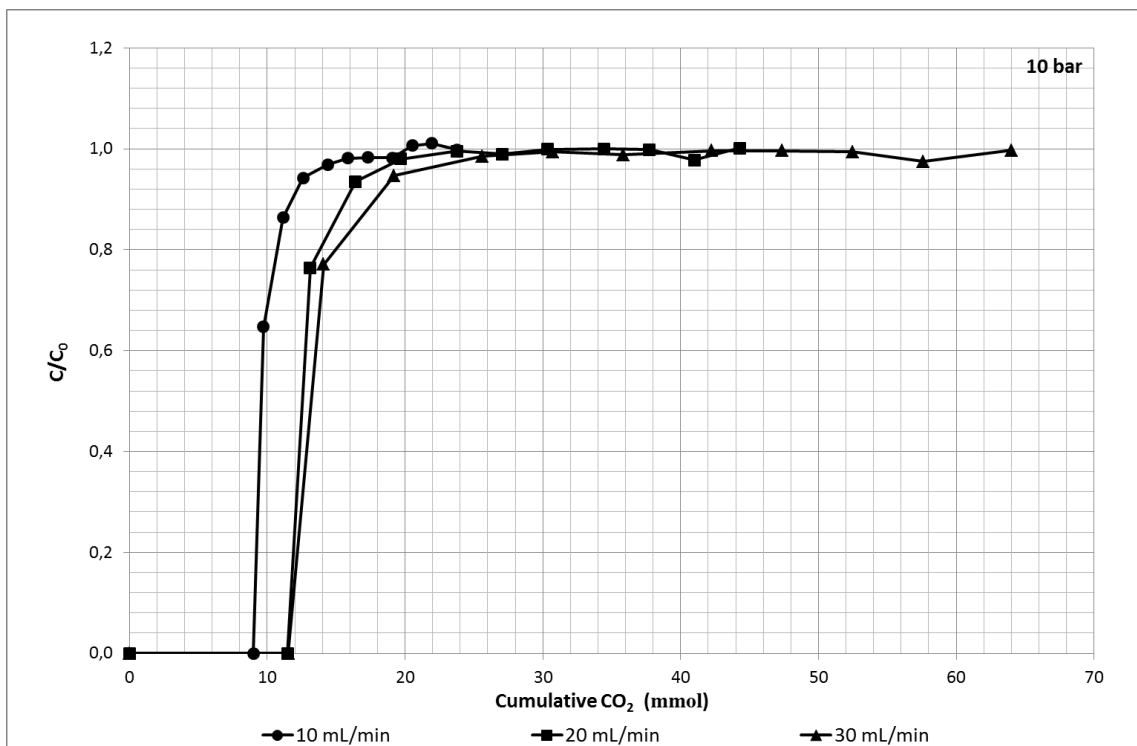


Figure 5.48. Cumulative CO₂ flow in feed versus CO₂ fraction at out flow (P= 10 bar)

As shown in Fig. 5.48, curves are overlapped while flow rate is increasing. Hence, external resistance is not controlling the adsorption. So external resistance is less effective at higher flow rates. Adsorption breakthrough times decreased as 25, 14 and, 9 minutes at increasing flow rate. As a reason of this, saturation of adsorbent required more time due to lower CO₂ concentration in mixture of CO₂/H₂. Up to this breakthrough points pure H₂ observed at the outlet of column. The amount adsorbed was increased (1.64 mmol/g) when flow rate was increased from 10 to 20 mL/min at 10 bars (Table 5.5 and Fig. 5.48). Adsorption isotherm of CuTPA for different flow rate at 10 bars was given in Figure 5.49.

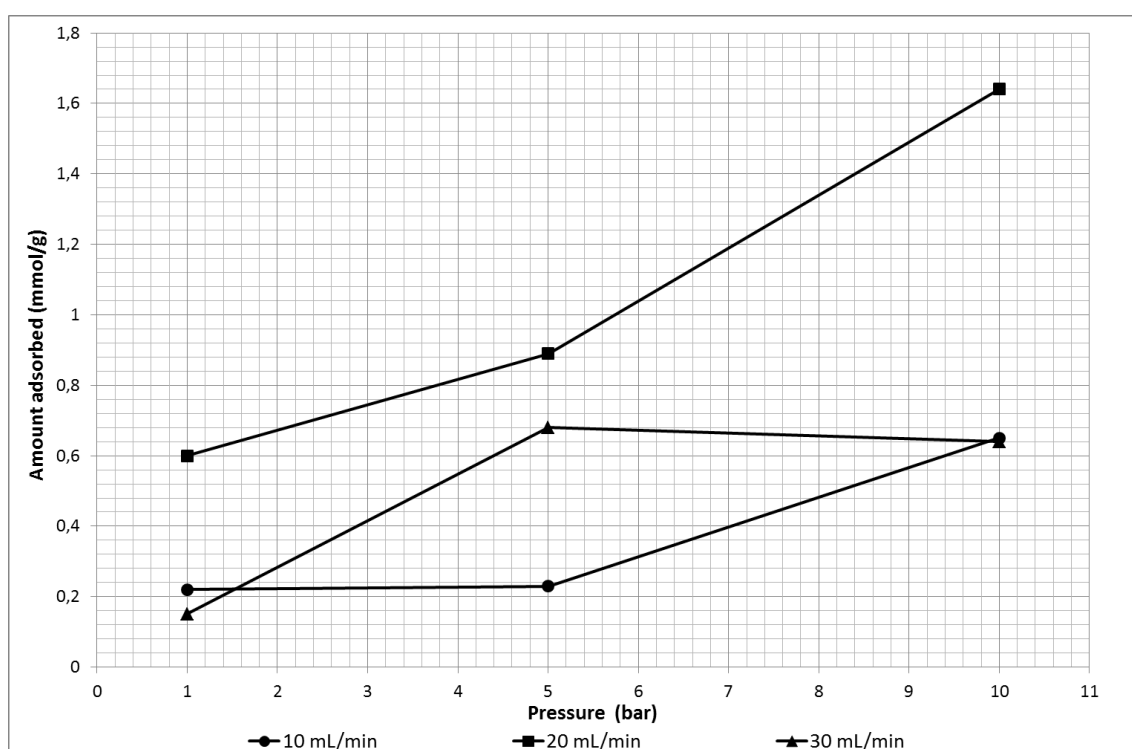


Figure 5.49. Adsorption isotherms of CO₂ in CuTPA for different flow rates at 303 K

In the table 5.6, when compared to adsorption and desorption times of CuTPA and 13X, there are big differences. These differences are resulting from pore sizes. CuTPA synthesized is a biporous material while 13X microporous. That is why adsorption and desorption on CuTPA is becoming faster than 13X.

CO₂ amount adsorbed on 13X also increased with increasing pressure although higher pressure increased the contact time and concentration difference due to driving

force external resistance eliminated. So gas molecules are easily reach to small pores and amount adsorbed increased.

Table 5.5. CO₂ amount adsorbed by CuTPA

Total flow rate (mL/min)	Pressure (bar)	τ_a (min)	F_{ao} (mmol/min)	X_a	q_{ads} (mmol/g)
10	1	4.65	0.36	0.48	0.22
	5	13.45	0.36	0.48	0.23
	10	29.04	0.36	0.48	0.65
20	1	3.88	0.82	0.49	0.60
	5	9.24	0.82	0.49	0.89
	10	17.78	0.82	0.49	1.64
30	1	3.76	1.28	0.49	0.15
	5	4.32	1.28	0.49	0.68
	10	8.14	1.28	0.49	0.64

Table 5.6. Comparison of amount adsorbed and adsorption/desorption times of adsorbents

Total flow rate (mL/min)	Pressure (bar)	t_{ads} (min)	t_{des} (min)	q_{ads} (mmol/g) CuTPA	t_{ads} (min)	t_{des} (min)	q_{ads} (mmol/g) Zeolite 13X
10	1	19	8	0.22	83	211	3.46
	5	38	39	0.23	101	366	4.43
	10	57	60	0.65	130	357	4.84
20	1	6	5	0.60	45	112	4.11
	1						*4.13
	5	17	17	0.89	62	203	5.92
	5						*5.26
	10	29	30	1.64	82	225	6.46
30	1	11	19	0.15	30	74	4.14
	5	11	21	0.68	35	116	6.24
	10	20	30	0.64	47	120	7.01

*Measured amount adsorbed at same conditions (Peter, 2013)

CHAPTER 6

CONCLUSIONS

The aim of this study was to synthesize Copper based metal organic framework (CuTPA) and investigate dynamic CO₂ behavior of the adsorbent packed bed column. The mostly used adsorbent, zeolite 13X also used as adsorbent for reliability of data obtained from the home-made adsorption system.

In the synthesis of CuTPA, Crystallization in schott bottle (F48) was found with high specific Langmuir surface area of 245 m²/g while 119 m²/g in autoclave (A48) and 157 m²/g in parr (P48). When compared to crystallization time for 36 h and 48 h in schott bottle, specific surface areas were found as 228 and 245 m²/g, respectively. Finally, crystallization temperature was investigated in schott bottle for 50 °C and 110 °C and Langmuir surface area of synthesized CuTPA under 50 °C was found as 319 m²/g. Crystallized CuTPAs were purified with different washing methods (soxhlet extraction (Sx) or stirring (St)) by using solvents (dimethylformamide (D) or methanol (M)). Effective washing was achieved with methanol by using under soxhlet extraction. Specific surface area was found as 123 m²/g under MSx while MSt was 95, DSx was 46 m²/g. Purified CuTPAs then thermally activated as last step of synthesis with directly heating up to 160 °C (R160) under vacuum or 225 °C (R225) in oven or 50 °C/h step size heating (R50) up to 200 °C under vacuum oven for 24 hours. Vacuum activation was found appropriate activation method with the highest specific Langmuir surface areas of 776 m²/g heating up to 160 °C compared to R50 activation (228 m²/g).

Dynamic adsorption breakthrough curves was evaluated and maximum amount adsorbed was achieved with 30 mL/min total flow rate in feed under 10 bars of bed pressure for NaX zeolite (13X) adsorbent (7.01 mmol/g for CO₂ adsorption). Amount adsorbed also increased with increasing flow rate and increasing pressure. Same manner was seen for CuTPA, amount adsorbed of CO₂ was increased from 0.60 to 1.64 mmol/g with increasing pressure (from 1 to 10 bars) under 20 mL/min total flow rate of equimolar CO₂/H₂ mixture.

REFERENCES

- Abdelouhab, Sandra, Michel François, Eric Elkaim, and Pierre Rabu. 2005. "Ab initio crystal structure of copper(II) hydroxy-terephthalate by synchrotron powder diffraction and magnetic properties." *Solid State Sciences* 7 (2):227-232. doi: <http://dx.doi.org/10.1016/j.solidstatesciences.2004.10.020>.
- Anbia, Mansoor, and Sara Sheykhi. 2012. "Synthesis of nanoporous copper terephthalate [MIL-53(Cu)] as a novel methane-storage adsorbent." *Journal of Natural Gas Chemistry* 21 (6):680-684. doi: [http://dx.doi.org/10.1016/S1003-9953\(11\)60419-2](http://dx.doi.org/10.1016/S1003-9953(11)60419-2).
- Arul Dhas, N., C. Paul Raj, and A. Gedanken. 1998. "Preparation of Luminescent Silicon Nanoparticles: A Novel Sonochemical Approach." *Chemistry of Materials* 10 (11):3278-3281. doi: 10.1021/cm980408j.
- Arunkumar, Lagashetty, Havanoor Vijayanand, S. Basavaraja, S. D. Balaji, and A. Venkataraman. 2007. "Microwave-assisted route for synthesis of nanosized metal oxides." *Science and Technology of Advanced Materials* 8 (6):484.
- Bastin, Laurent, Patrick S. Bárcia, Eric J. Hurtado, José A. C. Silva, Alírio E. Rodrigues, and Banglin Chen. 2008. "A Microporous Metal–Organic Framework for Separation of CO₂/N₂ and CO₂/CH₄ by Fixed-Bed Adsorption." *The Journal of Physical Chemistry C* 112 (5):1575-1581. doi: 10.1021/jp077618g.
- Beldon, Patrick J., László Fábián, Robin S. Stein, A. Thirumurugan, Anthony K. Cheetham, and Tomislav Friščić. 2010. "Rapid Room-Temperature Synthesis of Zeolitic Imidazolate Frameworks by Using Mechanochemistry." *Angewandte Chemie International Edition* 49 (50):9640-9643. doi: 10.1002/anie.201005547.
- Brunauer, Stephen, P. H. Emmett, and Edward Teller. 1938. "Adsorption of Gases in Multimolecular Layers." *Journal of the American Chemical Society* 60 (2):309-319. doi: 10.1021/ja01269a023.
- Bux, Helge, Fangyi Liang, Yanshuo Li, Janosch Cravillon, Michael Wiebcke, and Jürgen Caro. 2009. "Zeolitic Imidazolate Framework Membrane with Molecular Sieving Properties by Microwave-Assisted Solvothermal Synthesis." *Journal of the American Chemical Society* 131 (44):16000-16001. doi: 10.1021/ja907359t.
- Carson, Cantwell G., Giuseppe Brunello, Seung Geol Lee, Seung Soon Jang, Rosario A. Gerhardt, and Rina Tannenbaum. 2014. "Structure Solution from Powder Diffraction of Copper 1,4-Benzenedicarboxylate." *European Journal of Inorganic Chemistry* 2014 (12):2140-2145. doi: 10.1002/ejic.201301543.
- Carson, Cantwell G., Kenneth Hardcastle, Justin Schwartz, Xiaotao Liu, Christina Hoffmann, Rosario A. Gerhardt, and Rina Tannenbaum. 2009. "Synthesis and Structure Characterization of Copper Terephthalate Metal–Organic

- Frameworks." *European Journal of Inorganic Chemistry* 2009 (16):2338-2343. doi: 10.1002/ejic.200801224.
- Carton, Anne, Adel Mesbah, Thomas Mazet, Florence Porcher, and Michel François. 2007. "Ab initio crystal structure of nickel(II) hydroxy-terephthalate by synchrotron powder diffraction and magnetic study." *Solid State Sciences* 9 (6):465-471. doi: <http://dx.doi.org/10.1016/j.solidstatesciences.2007.04.003>.
- Cerofolini, G. F., and W. Rudziński. 1997. "Chapter 1. Theoretical principles of single- and mixed-gas adsorption equilibria on heterogeneous solid surfaces." In *Studies in Surface Science and Catalysis*, edited by W. A. Steele W. Rudziński and G. Zgrablich, 1-103. Elsevier.
- Chen, Banglin, Liangbo Wang, Fatima Zapata, Guodong Qian, and Emil B. Lobkovsky. 2008. "A Luminescent Microporous Metal–Organic Framework for the Recognition and Sensing of Anions." *Journal of the American Chemical Society* 130 (21):6718-6719. doi: 10.1021/ja802035e.
- Chen, Chao, Dong-Wha Park, and Wha-Seung Ahn. 2014. "CO₂ capture using zeolite 13X prepared from bentonite." *Applied Surface Science* 292 (0):63-67. doi: <http://dx.doi.org/10.1016/j.apsusc.2013.11.064>.
- Cueto, S., V. Gramlich, W. Petter, F. S. Rys, and P. Rys. 1991. "Structure of copper(II) terephthalate trihydrate." *Acta Crystallographica Section C* 47 (1):75-78. doi: doi:10.1107/S0108270190006345.
- Daniel, D., and M.P.G. De. 1964. Process for separating a binary gaseous mixture by adsorption. Google Patents.
- Dasgupta, Soumen, Nabanita Biswas, Aarti, Nilesh G. Gode, Swapnil Divekar, Anshu Nanoti, and Amar N. Goswami. 2012. "CO₂ recovery from mixtures with nitrogen in a vacuum swing adsorber using metal organic framework adsorbent: A comparative study." *International Journal of Greenhouse Gas Control* 7 (0):225-229. doi: <http://dx.doi.org/10.1016/j.ijggc.2011.10.007>.
- Dey, Chandan, Tanay Kundu, Bishnu P. Biswal, Arijit Mallick, and Rahul Banerjee. 2014. "Crystalline metal-organic frameworks (MOFs): synthesis, structure and function." *Acta Crystallographica Section B* 70 (1):3-10. doi: doi:10.1107/S2052520613029557.
- Do, Duong D. 1998. Adsorption Analysis: Equilibria and Kinetics. edited by Duong D. Do: Imperial College Press
- Du, Miao, Cheng-Peng Li, and Xiao-Jun Zhao. 2005. "Metal-Controlled Assembly of Coordination Polymers with the Flexible Building Block 4-Pyridylacetic Acid (Hpya)." *Crystal Growth & Design* 6 (1):335-341. doi: 10.1021/cg0502542.
- Eisenhardt, A., J. Krogmann, E. Leung, U. Mueller, and C. Kiener. 2014. Vacuum insulation units comprising getter materials. Google Patents.

- Erten-Kaya, Y., and F. Cakicioglu-Ozkan. 2012. "Effect of ultrasound on the kinetics of cation exchange in NaX zeolite." *Ultrason Sonochem* 19 (3):701-6. doi: 10.1016/j.ultsonch.2011.10.010.
- Everett, D. H. 1972. "MANUAL OF SYMBOLS AND TERMINOLOGY FOR PHYSICO-CHEMICAL QUANTITIES AND UNITS APPENDIX II." *IUPAC (INTERNATIONAL UNION OF PURE AND APPLIED CHEMISTRY)* 31 (4):577-638. doi: 10.1351/pac197231040577.
- Farha, Omar K., Abraham M. Shultz, Amy A. Sarjeant, SonBinh T. Nguyen, and Joseph T. Hupp. 2011. "Active-Site-Accessible, Porphyrinic Metal–Organic Framework Materials." *Journal of the American Chemical Society* 133 (15):5652-5655. doi: 10.1021/ja111042f.
- Ferey, G., C. Mellot-Draznieks, C. Serre, F. Millange, J. Dutour, S. Surble, and I. Margiolaki. 2005. "A chromium terephthalate-based solid with unusually large pore volumes and surface area." *Science* 309 (5743):2040-2. doi: 10.1126/science.1116275.
- Finsky, V., L. Ma, L. Alaerts, D. E. De Vos, G. V. Baron, and J. F. M. Denayer. 2009. "Separation of CO₂/CH₄ mixtures with the MIL-53(Al) metal–organic framework." *Microporous and Mesoporous Materials* 120 (3):221-227. doi: <http://dx.doi.org/10.1016/j.micromeso.2008.11.007>.
- Friščić, Tomislav, Ivan Halasz, Patrick J. Beldon, Ana M. Belenguer, Frank Adams, Simon A. J. Kimber, Veijo Honkimäki, and Robert E. Dinnebier. 2013. "Real-time and in situ monitoring of mechanochemical milling reactions." *Nat Chem* 5 (1):66-73. doi: <http://www.nature.com/nchem/journal/v5/n1/abs/nchem.1505.html#supplementary-information>.
- Fujita, Makoto, Yoon Jung Kwon, Satoru Washizu, and Katsuyuki Ogura. 1994. "Preparation, Clathration Ability, and Catalysis of a Two-Dimensional Square Network Material Composed of Cadmium(II) and 4,4'-Bipyridine." *Journal of the American Chemical Society* 116 (3):1151-1152. doi: 10.1021/ja00082a055.
- Halper, Sara R., Loi Do, Jay R. Stork, and Seth M. Cohen. 2006. "Topological Control in Heterometallic Metal–Organic Frameworks by Anion Templating and Metalloligand Design." *Journal of the American Chemical Society* 128 (47):15255-15268. doi: 10.1021/ja0645483.
- Hamon, Lomig, Philip L. Llewellyn, Thomas Devic, Aziz Ghoufi, Guillaume Clet, Vincent Guillerm, Gerhard D. Pirngruber, Guillaume Maurin, Christian Serre, Gordon Driver, Wouter van Beek, Elsa Jolimaître, Alexandre Vimont, Marco Daturi, and Gérard Férey. 2009. "Co-adsorption and Separation of CO₂–CH₄ Mixtures in the Highly Flexible MIL-53(Cr) MOF." *Journal of the American Chemical Society* 131 (47):17490-17499. doi: 10.1021/ja907556q.
- Harbuzaru, Bogdan V, Avelino Corma, Fernando Rey, Jose L Jordá, Duarte Ananias, Luis D Carlos, and João Rocha. 2009. "A Miniaturized Linear pH Sensor Based

- on a Highly Photoluminescent Self-Assembled Europium(III) Metal–Organic Framework." *Angewandte Chemie International Edition* 48 (35):6476-6479. doi: 10.1002/anie.200902045.
- Hindelang, Konrad, Sergei I. Vagin, Christian Anger, and Bernhard Rieger. 2012. "Tandem post-synthetic modification for functionalized metal-organic frameworks via epoxidation and subsequent epoxide ring-opening." *Chemical Communications* 48 (23):2888-2890. doi: 10.1039/C2CC16949E.
- Hofmann, K. A., and F. Kuspert. 1897. "Verbindungen von Kohlenwasserstoffen mit Metallsalzen." *Zeitschrift für anorganische Chemie* 15 (1):204-207. doi: 10.1002/zaac.18970150118.
- Horcajada, P., C. Serre, G. Maurin, N. A. Ramsahye, F. Balas, M. Vallet-Regi, M. Sebban, F. Taulelle, and G. Férey. 2008. "Flexible porous metal-organic frameworks for a controlled drug delivery." *J Am Chem Soc* 130 (21):6774-80. doi: 10.1021/ja710973k.
- Horike, Satoshi, Mircea Dincă, Kentaro Tamaki, and Jeffrey R. Long. 2008. "Size-Selective Lewis Acid Catalysis in a Microporous Metal-Organic Framework with Exposed Mn²⁺ Coordination Sites." *Journal of the American Chemical Society* 130 (18):5854-5855. doi: 10.1021/ja800669j.
- Huang, Zhong-Le, Marc Drillon, Norberto Masciocchi, Angelo Sironi, Jing-Tai Zhao, Pierre Rabu, and Pierre Panissod. 2000. "Ab-Initio XRPD Crystal Structure and Giant Hysteretic Effect ($H_c = 5.9$ T) of a New Hybrid Terephthalate-Based Cobalt(II) Magnet †." *Chemistry of Materials* 12 (9):2805-2812. doi: 10.1021/cm000386c.
- Inglezakis, Vassilis J., and Stavros G. Pouloupoulos. 2006. "2 - Adsorption, Ion Exchange, and Catalysis." In *Adsorption, Ion Exchange and Catalysis*, edited by Vassilis J. Inglezakis and Stavros G. Pouloupoulos, 31-56. Amsterdam: Elsevier.
- Jhung, S. H, J. H. Lee, J. W Yoon, C. Serre, G. Férey, and J. S. Chang. 2007. "Microwave Synthesis of Chromium Terephthalate MIL-101 and Its Benzene Sorption Ability." *Advanced Materials* 19 (1):121-124. doi: 10.1002/adma.200601604.
- Jürgen U. Keller, and Reiner Staudt. 2005. "Basic Concepts." In *Gas Adsorption Equilibria*, 17-78. Springer US.
- Keskin, Seda, and Seda Kızılel. 2011. "Biomedical Applications of Metal Organic Frameworks." *Industrial & Engineering Chemistry Research* 50 (4):1799-1812. doi: 10.1021/ie101312k.
- Klinowski, Jacek, Filipe A. Almeida Paz, Patricia Silva, and Joao Rocha. 2011. "Microwave-Assisted Synthesis of Metal-Organic Frameworks." *Dalton Transactions* 40 (2):321-330. doi: 10.1039/C0DT00708K.

- Kondo, Mitsuru, Tomomichi Yoshitomi, Hiroyuki Matsuzaka, Susumu Kitagawa, and Kenji Seki. 1997. "Three-Dimensional Framework with Channeling Cavities for Small Molecules: $\{[M_2(4, 4'\text{-bpy})_3(\text{NO}_3)_4] \cdot x\text{H}_2\text{O}\}_n$ ($M = \text{Co, Ni, Zn}$)." *Angewandte Chemie International Edition in English* 36 (16):1725-1727. doi: 10.1002/anie.199717251.
- Kumar, R., and T. C. Golden. 1991. "Thermal swing adsorption process for removing trace impurities from a multi-component gas mixture: (Landfill gas)." *Gas Separation & Purification* 5 (1):21-24. doi: [http://dx.doi.org/10.1016/0950-4214\(91\)80044-6](http://dx.doi.org/10.1016/0950-4214(91)80044-6).
- Kuppler, Ryan J., Daren J. Timmons, Qian-Rong Fang, Jian-Rong Li, Trevor A. Makal, Mark D. Young, Daqiang Yuan, Dan Zhao, Wenjuan Zhuang, and Hong-Cai Zhou. 2009. "Potential applications of metal-organic frameworks." *Coordination Chemistry Reviews* 253 (23–24):3042-3066. doi: <http://dx.doi.org/10.1016/j.ccr.2009.05.019>.
- Langmi, Henrietta W., Jianwei Ren, Brian North, Mkhulu Mathe, and Dmitri Bessarabov. 2014. "Hydrogen Storage in Metal-Organic Frameworks: A Review." *Electrochimica Acta* 128 (0):368-392. doi: <http://dx.doi.org/10.1016/j.electacta.2013.10.190>.
- Langmuir, Irving. 1918. "THE ADSORPTION OF GASES ON PLANE SURFACES OF GLASS, MICA AND PLATINUM." *Journal of the American Chemical Society* 40 (9):1361-1403. doi: 10.1021/ja02242a004.
- Liang, Weibin, and Deanna M. D'Alessandro. 2013. "Microwave-assisted solvothermal synthesis of zirconium oxide based metal-organic frameworks." *Chemical Communications* 49 (35):3706-3708. doi: 10.1039/C3CC40368H.
- Lincke, J., D. Lässig, J. Moellmer, C. Reichenbach, A. Puls, A. Moeller, R. Gläser, G. Kalies, R. Staudt, and H. Krautscheid. 2011. "A novel copper-based MOF material: Synthesis, characterization and adsorption studies." *Microporous and Mesoporous Materials* 142 (1):62-69. doi: <http://dx.doi.org/10.1016/j.micromeso.2010.11.017>.
- Liu, Yunling, Victor Ch Kravtsov, Randy Larsen, and Mohamed Eddaoudi. 2006. "Molecular building blocks approach to the assembly of zeolite-like metal-organic frameworks (ZMOFs) with extra-large cavities." *Chemical Communications* (14):1488-1490. doi: 10.1039/B600188M.
- Lu, Zhen-Zhong, Rui Zhang, Yi-Zhi Li, Zi-Jian Guo, and He-Gen Zheng. 2011. "Solvatochromic Behavior of a Nanotubular Metal–Organic Framework for Sensing Small Molecules." *Journal of the American Chemical Society* 133 (12):4172-4174. doi: 10.1021/ja109437d.
- MacGillivray, Leonard R. 2010. "Metal-Organic Frameworks: Design and Application." In *Metal-Organic Frameworks*, edited by Leonard R. MacGillivray, 341-349. John Wiley & Sons, Inc.

- Martinez Joaristi, Alberto, Jana Juan-Alcañiz, Pablo Serra-Crespo, Freek Kapteijn, and Jorge Gascon. 2012. "Electrochemical Synthesis of Some Archetypical Zn²⁺, Cu²⁺, and Al³⁺ Metal Organic Frameworks." *Crystal Growth & Design* 12 (7):3489-3498. doi: 10.1021/cg300552w.
- Mérel, J., M. Clause, and F. Meunier. 2006. "Carbon dioxide capture by indirect thermal swing adsorption using 13X zeolite." *Environmental Progress* 25 (4):327-333. doi: 10.1002/ep.10166.
- Mori, Wasuke, Fumie Inoue, Keiko Yoshida, Hirokazu Nakayama, Satoshi Takamizawa, and Michihiko Kishita. 1997. "Synthesis of New Adsorbent Copper(II) Terephthalate." *Chemistry Letters* 26 (12):1219-1220. doi: 10.1246/cl.1997.1219.
- Mori, Wasuke, Tomohiko Sato, Chika Nozaki Kato, Tohru Takei, and Tetsushi Ohmura. 2005. "Discovery and development of microporous metal carboxylates." *The Chemical Record* 5 (6):336-351. doi: 10.1002/tcr.20060.
- Morris, Russell E, and Paul S Wheatley. 2008. "Gas Storage in Nanoporous Materials." *Angewandte Chemie International Edition* 47 (27):4966-4981. doi: 10.1002/anie.200703934.
- Mueller, U., M. Schubert, F. Teich, H. Puetter, K. Schierle-Arndt, and J. Pastre. 2006. "Metal-organic frameworks-prospective industrial applications." *Journal of Materials Chemistry* 16 (7):626-636. doi: 10.1039/B511962F.
- Munusamy, Kuppusamy, Govind Sethia, Dinesh V. Patil, Phani B. Somayajulu Rallapalli, Rajesh S. Somani, and Hari C. Bajaj. 2012. "Sorption of carbon dioxide, methane, nitrogen and carbon monoxide on MIL-101(Cr): Volumetric measurements and dynamic adsorption studies." *Chemical Engineering Journal* 195–196 (0):359-368. doi: <http://dx.doi.org/10.1016/j.cej.2012.04.071>.
- Ni, Zheng, and Richard I. Masel. 2006. "Rapid Production of Metal–Organic Frameworks via Microwave-Assisted Solvothermal Synthesis." *Journal of the American Chemical Society* 128 (38):12394-12395. doi: 10.1021/ja0635231.
- Panella, B., and M. Hirscher. 2013. "FUELS – HYDROGEN STORAGE | Metal–Organic Frameworks." In *Reference Module in Chemistry, Molecular Sciences and Chemical Engineering*. Elsevier.
- Peter, SunilA, GinoV Baron, Jorge Gascon, Freek Kapteijn, and JoeriF M. Denayer. 2013. "Dynamic desorption of CO₂ and CH₄ from amino-MIL-53(Al) adsorbent." *Adsorption* 19 (6):1235-1244. doi: 10.1007/s10450-013-9564-x.
- Pichon, Anne, Ana Lazuen-Garay, and Stuart L. James. 2006. "Solvent-free synthesis of a microporous metal-organic framework." *CrystEngComm* 8 (3):211-214. doi: 10.1039/B513750K.

- Ranocchiari, Marco, and Jeroen Anton van Bokhoven. 2011. "Catalysis by metal-organic frameworks: fundamentals and opportunities." *Physical Chemistry Chemical Physics* 13 (14):6388-6396. doi: 10.1039/C0CP02394A.
- Ribeiro, Ana M., Marta C. Campo, Guler Narin, João C. Santos, Alexandre Ferreira, Jong-San Chang, Young Kyu Hwang, You-Kyong Seo, U. Hwang Lee, José M. Loureiro, and Alírio E. Rodrigues. 2013. "Pressure swing adsorption process for the separation of nitrogen and propylene with a MOF adsorbent MIL-100(Fe)." *Separation and Purification Technology* 110 (0):101-111. doi: <http://dx.doi.org/10.1016/j.seppur.2013.03.009>.
- Rosi, Nathaniel L., Juergen Eckert, Mohamed Eddaoudi, David T. Vodak, Jaheon Kim, Michael O'Keeffe, and Omar M. Yaghi. 2003. "Hydrogen Storage in Microporous Metal-Organic Frameworks." *Science* 300 (5622):1127-1129. doi: 10.1126/science.1083440.
- Ruthven, D.M., S. Farooq, and K.S. Knaebel. 1993. *Pressure Swing Adsorption*: Wiley.
- Ruthven, Douglas Morris. 1984. *Principles of adsorption and adsorption processes*: New York: John Wiley and Sons, c1984. Book.
- Sherif, Fawzy G. 1970. "Heavy Metal Terephthalates." *Product R&D* 9 (3):408-412. doi: 10.1021/i360035a026.
- Silva, Bruna, Ioan Solomon, Ana M. Ribeiro, U. Hwang Lee, Young Kyu Hwang, Jong-San Chang, José M. Loureiro, and Alírio E. Rodrigues. 2013. "H₂ purification by pressure swing adsorption using CuBTC." *Separation and Purification Technology* 118 (0):744-756. doi: <http://dx.doi.org/10.1016/j.seppur.2013.08.024>.
- Silva, José A. C., Kristin Schumann, and Alírio E. Rodrigues. 2012. "Sorption and kinetics of CO₂ and CH₄ in binderless beads of 13X zeolite." *Microporous and Mesoporous Materials* 158 (0):219-228. doi: <http://dx.doi.org/10.1016/j.micromeso.2012.03.042>.
- Sips, Robert. 1948. "On the Structure of a Catalyst Surface." *The Journal of Chemical Physics* 16 (5):490-495. doi: [doi:http://dx.doi.org/10.1063/1.1746922](http://dx.doi.org/10.1063/1.1746922).
- Skarstrom, C.W. 1966. Oxygen concentration process. Google Patents.
- Son, W. J., J. Kim, J. Kim, and W. S. Ahn. 2008. "Sonochemical synthesis of MOF-5." *Chemical Communications* (47):6336-6338. doi: 10.1039/b814740j.
- Sun, Chun-Yi, Xin-Long Wang, Chao Qin, Jun-Ling Jin, Zhong-Min Su, Peng Huang, and Kui-Zhan Shao. 2013. "Solvatochromic Behavior of Chiral Mesoporous Metal-Organic Frameworks and Their Applications for Sensing Small Molecules and Separating Cationic Dyes." *Chemistry – A European Journal* 19 (11):3639-3645. doi: 10.1002/chem.201203080.

- Tedds, Steven, Allan Walton, Darren P. Broom, and David Book. 2011. "Characterisation of porous hydrogen storage materials: carbons, zeolites, MOFs and PIMs." *Faraday Discussions* 151 (0):75-94. doi: 10.1039/C0FD00022A.
- Toth, J. 1971. "State equations of the solid-gas interface Layers." *Acta Chim. Acad. Sci. Hung.* 69:311.
- Webb, Paul A. 2003. "Introduction to Chemical Adsorption Analytical Techniques and their Applications to Catalysis." *MIC Technical Publications*:1-12.
- Yaghi, Omar M., and Qiaowei Li. 2009. "Reticular Chemistry and Metal-Organic Frameworks for Clean Energy." *MRS Bulletin* 34 (09):682-690. doi: doi:10.1557/mrs2009.180.
- Yaghi, Omar M., Michael O'Keeffe, Nathan W. Ockwig, Hee K. Chae, Mohamed Eddaoudi, and Jaheon Kim. 2003. "Reticular synthesis and the design of new materials." *Nature* 423 (6941):705-714.
- Zdravkov, BorislavD, Jiří Čermák, Martin Šefara, and Josef Janků. 2007. "Pore classification in the characterization of porous materials: A perspective." *Central European Journal of Chemistry* 5 (2):385-395. doi: 10.2478/s11532-007-0017-9.
- Zhao, Dan, Daqiang Yuan, and Hong-Cai Zhou. 2008. "The current status of hydrogen storage in metal-organic frameworks." *Energy & Environmental Science* 1 (2):222-235. doi: 10.1039/B808322N.
- Zhou, Hong Cai Joe , and Susumu Kitagawa. 2014. "Metal–Organic Frameworks (MOFs)." *Chemical Society Reviews* 43 (16):5415-5418. doi: 10.1039/C4CS90059F.
- Zornoza, Beatriz, Alberto Martinez-Joaristi, Pablo Serra-Crespo, Carlos Tellez, Joaquin Coronas, Jorge Gascon, and Freek Kapteijn. 2011. "Functionalized flexible MOFs as fillers in mixed matrix membranes for highly selective separation of CO₂ from CH₄ at elevated pressures." *Chemical Communications* 47 (33):9522-9524. doi: 10.1039/C1CC13431K.